(2)

Approved for public release; distribution unlimited

SCATTERING AND RADIATION BY SHELLS AND NONLINEAR ACOUSTICS OF PARTICLE SUSPENSIONS

Philip L. Marston
Department of Physics
Washington State University
Pullman, Washington 99164-2814

Final Technical Report for Grant N00014-89-J-3088

October 1992

REPORT DOCUMENTATION PAGE

Form Approved
OMB No. 0704-0188

1. AGENCY USE ONLY (Leave blank)	2. REPORT DATE	3. REPORT TYPE AND DATES COVERED
	23 Oct 92	Final Technical 15 Jul 89 - 30 Sep 92

4. TITLE AND SUBTITLE
SCATTERING AND RADIATION BY SHELLS AND NONLINEAR ACOUSTICS OF PARTICLE SUSPENSIONS

5. FUNDING NUMBERS
PE 61153N
G N0001489J3800
TA uri5004

6. AUTHOR(S)
Philip L. Marston

7. PERFORMING ORGANIZATION NAME(S) AND ADDRESS(ES)
Department of Physics
Washington State University
Pullman, WA 99164-2814

8. PERFORMING ORGANIZATION REPORT NUMBER
N00014-89-J-3800-FR

9. SPONSORING / MONITORING AGENCY NAME(S) AND ADDRESS(ES)
Office of Naval Research
Physics Division - Code 1112
800 North Quincy Street
Arlington, VA 22217-5000

10. SPONSORING / MONITORING AGENCY REPORT NUMBER

11. SUPPLEMENTARY NOTES
Research proposed in "Scattering and Radiation by Shells and Nonlinear Acoustics," P. L. Marston principal investigator. Telephone (509) 335-5343.

12a. DISTRIBUTION / AVAILABILITY STATEMENT
Approved for public release: Distribution unlimited.

12b. DISTRIBUTION CODE

13. ABSTRACT *(Maximum 200 words)*

The research reported concerns three main areas: (A) Surface Guided Wave Contributions to the Scattering of Sound by Elastic Shells in Water -- Quantitative ray representations described for the scattering by shells give insight into the coupling of sound with structures. A backscattering enhancement near the coincidence frequency was observed, modeled, and shown to be due to a subsonic wave. Aspects of a high-frequency enhancement were investigated along with time-frequency spectrograms of the impulse response. (B) Radiation Mechanisms for Evanescent Tone Bursts on Fluid Loaded Membranes and Plates -- Subsonic flexural waves on unbounded plates ordinarily produce evanescent wavefields in the surrounding fluid that are trapped to the plate. Two mechanisms for radiating sound were investigated experimentally: (a) diffraction by a rigid barrier in an evanescent field in air and (b) transition radiation produced when a wave packet travels down a vertical plate through a water surface. (C) Acoustical Four-Wave Mixing in Suspensions -- Sound is shown to interact with sound in a suspension of microspheres. The spheres are attracted to pressure nodes of counter-propagating pump waves. The banded suspension acts as a diffraction grating and scatters a probe-wave when a Bragg condition is satisfied.

14. SUBJECT TERMS	15. NUMBER OF PAGES
Acoustical Scattering, Ray Methods, Elastic Shells, Evanescent Waves, Plates, Suspensions, Nonlinear Acoustics, Radiation Pressure	67
	16. PRICE CODE

17. SECURITY CLASSIFICATION OF REPORT	18. SECURITY CLASSIFICATION OF THIS PAGE	19. SECURITY CLASSIFICATION OF ABSTRACT	20. LIMITATION OF ABSTRACT
UNCLASSIFIED	UNCLASSIFIED	UNCLASSIFIED	

Approved for public release; distribution unlimited

SCATTERING AND RADIATION BY SHELLS AND NONLINEAR ACOUSTICS OF PARTICLE SUSPENSIONS

Philip L. Marston
Department of Physics
Washington State University
Pullman, Washington 99164-2814

Final Technical Report for Grant N00014-89-J-3088

October 1992

Prepared for: Office of Naval Research
Physics Division - Code 1112
800 North Quincy Street
Arlington, VA 22217-5000

ABSTRACT

The research reported in this Final Technical Report may be grouped into three main areas as follows:

A. **Surface Guided Wave Contributions to the Scattering of Sound by Elastic Shells in Water** -- Quantitative ray representations for the scattering by shells should be generalizable to shells having various shapes and give insight into the coupling of sound with the structure. The research was concerned with frequencies above the breathing resonance or ring frequency of spheres and cylinders and also with the impulse and tone burst responses. A midfrequency backscattering enhancement near the coincidence frequency was observed, modeled, and shown to be due to a subsonic wave. Aspects of a high-frequency enhancement were investigated along with calculations of time-frequency spectrograms of the impulse response.

B. **Radiation Mechanisms for Evanescent Tone Bursts on Fluid Loaded Membranes and Plates** -- Ordinarily flexural waves with subsonic phase velocities on unbounded plates produce evanescent wavefields in the surrounding fluid that are trapped to the plate. Inhomogeneities as well as curvature cause energy to be radiated. Two such mechanisms were investigated experimentally: (a) diffraction by a rigid barrier in the evanescent field of a membrane in air and (b) transition radiation produced when a wave packet travels down a vertical plate through a free water surface. Low-frequency EMAT transducers were used to generate the tone bursts.

C. **Acoustical Four-Wave Mixing in Suspensions** -- A novel mechanism was investigated for the interaction of sound with sound that relies on the slow response of the acoustic medium to the radiation pressure of a pump wave. Counter propagating 800 kHz pump waves establish a standing wave in a saline suspension of Latex microspheres. In response, the spheres are attracted to pressure nodes and form bands. The banded suspension acts as a diffraction grating for a higher frequency probe-wave tone burst giving rise to coherent scattering from the suspension when the Bragg condition is satisfied. Theories for the scattering amplitude using different methods of analysis were found to be mutually consistent and in general agreement with the measured amplitudes of steady-state Bragg scattering. The temporal development of the scattering as the grating initially forms was also calculated and measured.

TABLE OF CONTENTS

I. INTRODUCTION AND ORGANIZATION OF THIS REPORT

This Final Technical Report is organized as follows. Section II lists the personnel involved in the research. Section III gives a bibliography of publications, reports, dissertations, and communications resulting from the sponsored research. The items are listed to facilitate easy reference in the main body of the report. Section IV reviews selected research results grouped according to the three principal task areas originally proposed: (A) surface guided wave contributions to scattering of sound by elastic shells in water, (B) radiation mechanisms for evanescent tone bursts on fluid loaded membranes and plates, and (C) acoustical four-wave mixing in suspensions. Summarized in the final subsection is (D) supplemental scattering research. Section V summarizes facilities improvements that facilitated the sponsored research and other ongoing research. Section VI lists references not included in Section III that pertain to the discussion of results.

II. PERSONNEL

The following persons participated in the research.

Graduate students

1. H. J. Simpson: completed Ph.D. in 1992 on ultrasonic four-wave mixing mediated by a suspension.

2. T. J. Matula: awarded M. S. degree in 1990 with project supported research. Continuing as a Ph.D. candidate on research pertaining to the radiation and scattering by flexural waves on plates.

3. G. Kaduchak: awarded M.S. degree in 1992 with project related research. Working as a Ph.D. candidate (since 1991) on scattering by elastic shells.

4. D. H. Hughes: Ph.D. candidate working (since 1990) on theoretical and computational problems pertaining to scattering by elastic shells.

5. L. G. Zhang: awarded M.S. degree for project related thesis on scattering in 1991.

6. S. P. Parry: contributed to testing and initial experimentation in the water-tank scattering facility prior to leaving the program for other scientific employment.

Other personnel

1. P. L. Marston: principal investigator

2. N. H. Sun: postdoctoral researcher who contributed to scattering theory and computations in 1990-1991.

3. J. R. Filler: postdoctoral engineering support pertaining to the development of the scattering facility in 1990. While on appointment, Filler also completed a publication on previous research pertaining to fluid-structure interactions.

III. BIBLIOGRAPHY OF PUBLICATIONS AND REPORTS FOR GRANT N00014-89-J-3088

Research publications, pending publications, dissertations, technical and internal reports, and abstracted oral presentations are listed below according to category. Also listed for reference in the body of the report is a letter code. Thus, for example, J1 refers to the first journal publication. Each list is roughly chronological. Items supported in part by other sources are so indicated.

Code J: Refereed Journal Publications. Items that have been accepted for publication are so indicated while items submitted and under review are listed only as "submitted."

J1. S. G. Kargl and P. L. Marston, "Ray synthesis of the form function for backscattering from an elastic spherical shell: Leaky Lamb waves and longitudinal resonances," J. Acoust. Soc. Am. **89**, 2545-2558 (1991). [Supported in part by N00014-85-C-0141.]

J2. J. R. Filler, P. L. Marston, and W. C. Mih, "Response of the shear layers separating from a circular cylinder to small-amplitude rotational oscillations," Journal of Fluid Mechanics **231**, 481-499 (1991). [Supported in part by N00014-85-C-0141.]

J3. N. H. Sun and P. L. Marston, "Ray synthesis of leaky Lamb wave contributions to backscattering from thick cylindrical shells," J. Acoust. Soc. Am. **91**, 1398-1402 (1992).

J4. L. G. Zhang, N. H. Sun, and P. L. Marston, "Midfrequency enhancement of the backscattering of tone bursts by thin spherical shells," J. Acoust. Soc. Am. **91**, 1862-1874 (1992).

J5. C. K. Frederickson and P. L. Marston, "Transverse cusp diffraction catastrophes produced by the reflection of ultrasonic tone bursts from a curved surface in water: Observations," J. Acoust. Soc. Am. **92**, 2869-2877 (1992). [Supported in part by N00014-85-C-0141.]

J6. P. L. Marston and N. H. Sun, "Resonance and interference scattering near the coincidence frequency of a thin spherical shell: an approximate ray synthesis." J. Acoust. Soc. Am. (accepted for publication).

J7. G. Kaduchak and P. L. Marston, "Observation of the midfrequency enhancement of tone bursts backscattered by a thin spherical shell in water near the coincidence frequency," J. Acoust. Soc. Am. (accepted for publication).

J8. T. J. Matula and P. L. Marston, "Electromagnetic acoustic wave transducer for the generation of acoustic evanescent waves on membranes and an optical wave-number selective detector," J. Acoust. Soc. Am. (submitted in 1992).

J9. T. J. Matula and P. L. Marston, Diffraction of evanescent wave tone bursts on a membrane in air," J. Acoust. Soc. Am. (accepted for publication).

Code B: Chapters in Books.

B1. P. L. Marston, S. G. Kargl, and N. H. Sun, "Elastic resonance amplitudes described by generalized GTD and by product expansions of the S-matrix," in Acoustic Resonance Scattering edited by H. Uberall (Gordon and Breach, New York, 1992) pp. 305-333. [Supported in part by N00014-85-C-0141.]

B2. P. L. Marston, "Geometrical and Catastrophe Optics Methods in Scattering," in High Frequency and Pulsed Scattering, Physical Acoustics, Vol. XXI, edited by R. N. Thurston and A. D. Pierce (Academic Press, Boston, 1992) pp. 1-234. [Supported in part by N00014-85-C-0141.]

B3. P. L. Marston, "Quantitative Ray Methods for Scattering," Handbook of Acoustics, edited by M. J. Crocker, (John Wiley Press), submitted.

B4. P. L. Marston, "Introductory Chapter - Ultrasonics, Quantum Acoustics and Physical Effects of Sound," Handbook of Acoustics, edited by M. J. Crocker, (John Wiley Press), submitted.

Code T: Thesis, Dissertations, or Technical Reports.

T1. Ligang Zhang, "Scattering of tone burst from spherical shells: computations based on Fourier transform method," M.S. thesis, Department of Physics, Washington State University (1991), 154 pages. Grant Technical Report Number 1; DTIC report number A240642.

T2. Harry J. Simpson, "Interaction of Sound with Sound by Novel Mechanisms: Ultrasonic four-Wave Mixing Mediated by a suspension and Ultrasonic Three-Wave Mixing at a Free Surface," Ph.D. dissertation, Department of Physics, Washington State University (1992), 318 pages. Grant Technical Report Number 2; DTIC report number A254657.

Code P: Papers In Conference Proceedings.

P1. P. L. Marston and S. G. Kargl, "Scattering from hollow shells: Quantitative ray representations of amplitudes," in Proceedings of the International Congress on Recent Developments in Air and Structure Bourne Sound and Vibration, edited by M. J. Crocker (Auburn University, 1990) pp. 565-69. [Supported in part by N00014-85-C-0141.]

P2. *Invited paper:* P. L. Marston, L. Zhang, N. Sun, G. Kaduchak, D. H. Hughes, "Ray representations of the backscattering of tone bursts by shells in water: Calculations and related experiments," in Proceedings of the Second International congress on

Recent Developments in Air - and Structure-Borne Sound and Vibration, edited by M. J. Crocker and P. K. Raju (Auburn University, 1992), pp. 1203-1210.

P3. L. Zhang, N. Sun, and P. L. Marston, "Mid-frequency enhancement of the backscattering of tone bursts by thin spherical shells: ray approximation and exact Fourier synthesis," in Proceedings of the 14th International Congress on Acoustics, edited by Li Peizi (Beijing, 1992), pp. A-7-9.1, 2.

Code I: Internal Reports. These include various reports on file that were not widely distributed. Copies will be available for a limited time form the principal investigator. Some of these have been superseded by other manuscripts that were submitted for publication.

I1. T. J. Matula, "Electromagnetic Generation of Plane Waves on Membranes for the Production of Acoustic Evanescent Waves," M.S. degree project report, Department of Physics, Washington State University (1990).

I2. T. J. Matula, "Diffraction of evanescent wave tone bursts on a membrane in air and related observations of bursts guided by plates in water," March, 1992. Note: This paper (and associated presentation) by Matula resulted in the Second Place Award for a student paper on Structural Acoustics and Vibration, Salt Lake City Meeting of the Acoustical Society of America, April, 1992.

I3. G. Kaduchak, "Observation of the midfrequency enhancement of tone bursts backscattered by a thin spherical shell in water," March, 1992.

I4. D. H. Hughes, "Impulse response for backscattering by a thin spherical shell displayed in time and frequency," March, 1992.

I5. G. Kaduchak, "Observation of the E_6 Diffraction Catastrophe by Optical Scattering from Levitated Drops in the Rainbow Region," M.S. degree project report, Department of Physics, Washington State University. [Supported in part by N00014-85-C-0141.]

Code M: Oral Presentations at Professional Meetings. Presentations at meetings having published proceedings are listed in code P (above). Unless otherwise

noted presentations listed below were at national meetings of the Acoustical Society of America and an abstract was published. Various invited research presentations at government research centers or universities are not listed.

M1. P. L. Marston, "Applications to radiation and scattering of a wavefront construction using the involute of circular virtual caustics," J. Acoust. Soc. Am. **87**, 50 (1990).

M2. S. G. Kargl and P. L. Marston, "Anomalies in the ray synthesis of backscattering from hollow elastic spherical shells," J. Acoust. Soc. Am. **88**, 15 (1990). [Supported in part by N00014-85-C-0141.]

M3. T. J. Matula and P. L. Marston, "Novel electromagnetic generation of subsonic waves on a membrane and a wave-number-selective differential optical detector," J. Acoust. Soc. Am. Suppl. **88**, 167-168 (1990).

M4. N. H. Sun and P. L. Marston, "Ray synthesis of backscattering by thin cylindrical shells," J. Acoust. Soc. Am. **89**, 949 (1991).

M5. P. L. Marston and N. H. Sun, "Ray synthesis of the angular dependence and backscattering by thick cylindrical shells," J. Acoust. Soc. Am. **89**, 1949 (1991).

M6. P. L. Marston, N. H. Sun, S. P. Parry, and D. H. Hughes, "Scattering by thick cylindrical shells: Ray methods for shell reverberations and experiments," J. Acoust. Soc. Am. **89**, 1949 (1991).

M7. *Invited Paper:* P. L. Marston and C. K. Frederickson, "Aberrated foci in the time and frequency domains and experiments with acoustical diffraction catastrophes," J. Acoust. Soc. Am. **90**, 2288 (1991). [Supported in part by N00014-85-C-0141.]

M8. H. J. Simpson and P. L. Marston, "Ultrasonic four-wave mixing mediated by a suspension of polymer microspheres in water," J. Acoust. Soc. Am. **90**, 2244 (1991).

M9. P. L. Marston, N. H. Sun, and L. Zhang, "Backward-wave model of the high-frequency enhancement or quasiresonance in the backscattering from spherical shells," J. Acoust. Soc. Am. **90**, 2341 (1991).

M10. L. Zhang, N. H. Sun, and P. L. Marston, "Mid-frequency enhancement of the backscattering of tone bursts from thin elastic shells: Fourier synthesis and ray model," J. Acoust. Soc. Am. **90**, 2342 (1991).

M11. H. J. Simpson and P. L. Marston, "Ultrasonic four-wave mixing mediated by a suspension of microspheres in water: Scattering analysis and temporal response," J. Acoust. Soc. Am. **91**, 2351 (1992).

M12. P. L. Marston, "Mid-frequency enhancement of the impulse response of a thin spherical shell: Ray approximation and a related frequency-domain analysis," J. Acoust. Soc. Am. **91**, 2385 (1992).

M13. P. L. Marston, "Uncoupling supersonic Lamb waves on plates and shells from the surrounding fluid: Approximate condition on the phase velocity," J. Acoust. Soc. Am. **91**, 2438 (1992).

M14. D. H. Hughes and P. L. Marston, "Generalized Lamb waves near mode thresholds of spherical shells," J. Acoust. Soc. Am. **91**, 2439 (1992).

M15. T. J. Matula, "Diffraction of evanescent wave tone bursts on a membrane in air and related observations of bursts guided by plates in water," J. Acoust. Soc. Am. **91**, 2401 (1992). [Second Place Award for Student Paper in Structural Acoustics and Vibration, Salt Lake City Meeting of the Acoustical Society of America.]

M16. G. Kaduchak, "Observation of the midfrequency enhancement of tone bursts backscattered by a thin spherical shell in water,"J. Acoust. Soc. Am. **91**, 2400 (1992).

M17. D. H. Hughes, "Impulse response for backscattering by a thin spherical shell displayed in time and frequency," J. Acoust. Soc. Am. **91**, 2401 (1992).

M18. *Invited Pater:* P. L. Marston, "Using Acoustic Levitation and Radiation Pressure to Study the Dynamics of Drops and Bubbles and Optical Diffraction Catastrophes," International Workshop on Physical Acoustics, Nanjing University, September, 1992. [Supported in part by N00014-85-C-0141 and N00014-91-J-1374.]

IV RESEARCH PROJECTS

This discussion summarizes the research results in the context of previous work by others and by Marston and associates. The reader should see the various publications and reports listed in Section III for theoretical and technical details.

A. Surface Guided Wave Contributions to the Scattering of Sound by Elastic Shells in Water.

1. Ray Methods for Leaky Waves on Spheres and Cylinders.

An important advance in the development of ray methods for scattering by shells was the realization that the coupling of the acoustic field with guided wave amplitudes could be expressed in a simple form.[1] The application of that analysis to leaky Lamb waves on spherical shells was confirmed with tone burst measurements by Kargl and Marston.[2] The relevant coupling coefficient G_l for the lth class of guided waves was expressed in terms of the radiation damping of the guided wave β_l and geometric factors associated with the location of the internal virtual caustics from which the outgoing wave appeared to radiate.[1] The ray method also facilitates the identification of elastic contributions by their arrival time when short tone bursts are used. Extensions should be possible for shells with slowly varying curvature and internal structure. Furthermore, since G_l appears to be well approximated directly in terms of guided wave parameters, it becomes unnecessary to analytically and numerically evaluate it from the Sommerfeld-Watson transform as was done by Williams and Marston[3] for Rayleigh waves on solid spheres. Kargl and Marston[4,5,J1] completed other computations, tests, and extensions of the method for forward and backward scattering by spherical shells. While the emphasis was on resonances associated with leaky Lamb waves, the earlier experiments[2] were also extended to forward scattering[4] and some aspects of thickness resonance were modeled.[5,J1] In related work a ray model for the backscattering contribution due to repeated reverberation (or bouncing) of normally incident longitudinal waves was developed and tested by comparison with exact partial-wave series calculations for a hollow fluid shell. This was first achieved by Kargl and Marston[6] for a sphere and was later extended with support from this grant by Marston and Sun (Section IV D) for a circular cylinder.

An important result from this grant concerns backscattering contributions by subsonic waves on shells. It is appropriate to review the ray picture for leaky and subsonic cases. Figure 1 illustrates the usual ray picture for backscattering contributions by the lth

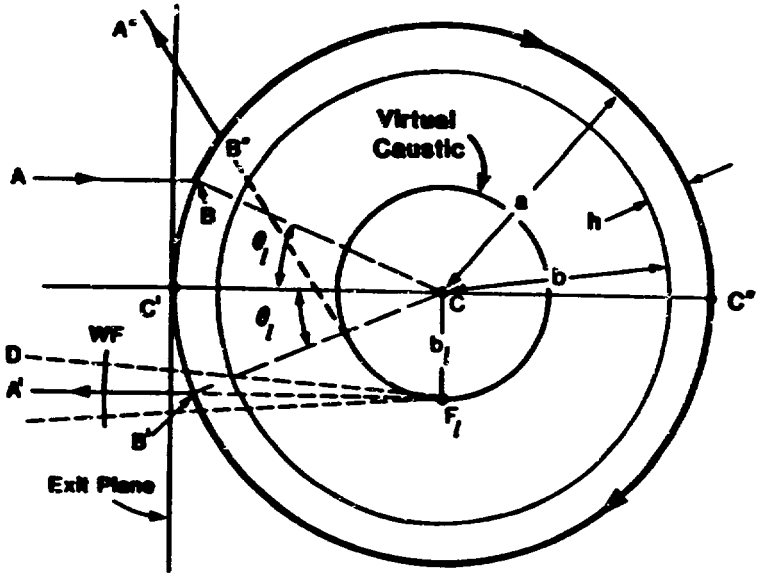

Figure 1 -- Ray diagram for sound backscattered due to a leaky Lamb wave of type *l* excited near B traveling repeatedly sound a spherical or circular cylindrical shell. Simple approximations for the outgoing wave amplitudes were given by Marston (Ref. 1). In the proposed work, the analysis would be generalized to cylinders of variable curvature and tested.

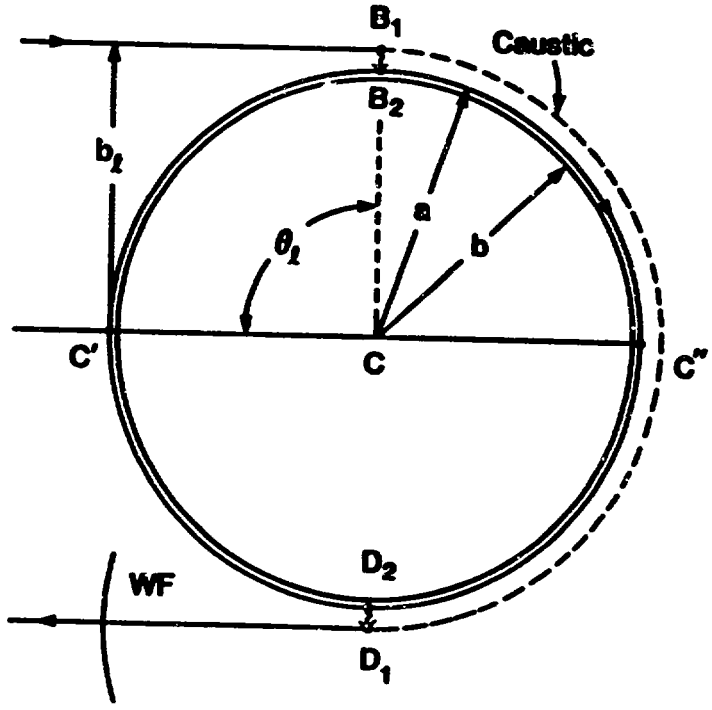

Figure 2 -- Like Fig. 1 but for a guided wave whose phase velocity along the outer surface of the shell is subsonic with respect to the surroundings. WF denotes a section of wavefront that appears to be radiated from an external caustic of radius b*l*. Near the coincidence frequency a ray of the class shown gives a very large backscattering contribution.

guided wave where the phase velocity of the wave along the outer surface of the shell c_l exceeds the speed of sound c in the surrounding water.[1,2] Such supersonic waves usually continuously leak or radiate sound at an angle $\theta_l = \arcsin(c/c_l)$ relative to the local shell normal as determined by the trace velocity matching condition (see however, discussion below). To facilitate the extension of midfrequency ray methods to thin shells, it is necessary to allow for subsonic guided waves where $c_l < c$. Figure 2 shows the modified ray picture [7,8,J4] where the coupling is through an evanescent region having a thickness $(b_l - a) = (ac/c_l)(1 - c_l/c)$ that diverges as the outer radius a of the shell diverges. Apparent from truncations or other inhomogeneities, the subsonic waves considered would not radiate in this flat plate limit and are sometimes described as "trapped". The existence of such waves for plates in water has long been known.[9-11] The radiation and coupling with acoustic fields introduced by curvature is analogous with the bending losses of fiber-optic waveguides.[B2] The sponsored analysis and experiments (Publications J4, J6, J7, T1, P2, and P3) give quantitative scattering amplitudes based on the modified ray picture in Fig. 2 and are summarized below.

2. Midfrequency Enhancement of the Backscattering of Tone Bursts Near the Coincidence Frequency.

The contribution of a subsonic guided wave to the backscattering by thin spherical shells is especially significant when ka is in the general vicinity of a/h where $h = a - b$ is the shell thickness and $k = \omega/c$. [This corresponds to kh close to unity which for a metallic plate or shell in water is close to the "coincidence condition." Here the phase velocity of the flexural wave (without fluid loading) coincides to that of sound in the surrounding water. Some authors call this the critical coincidence frequency.] For the purpose of illustrating a ray model for such contributions,[J4] consider the example of a stainless steel 304 shell with $a/h = 40$. The relevant guided wave properties are computed by finding the complex ν roots of $D_\nu(ka) = 0$ as previously described[2,4,5] where D_n is the denominator of the nth term of the exact partial wave series for the form function. (The method is based on the Watson transform.) The resulting properties for the case under consideration are shown in Fig. 3. The wave labeled with long and short dashes, designated by $l = a_{0-}$, is subsonic throughout the region of interest but displays a noticeable rise in the radiation damping parameter β_l as c_l approaches c. This rise in coupling appears to be associated with the decrease in the thickness of the evanescent region near coincidence[J4,J7] and causes an enhanced backscattering as may be seen from the ray analysis summarized below. Extension of the analysis of guided wave scattering contributions by distinct leaky waves[1,2] to the present case of subsonic waves is possible by appreciating the importance

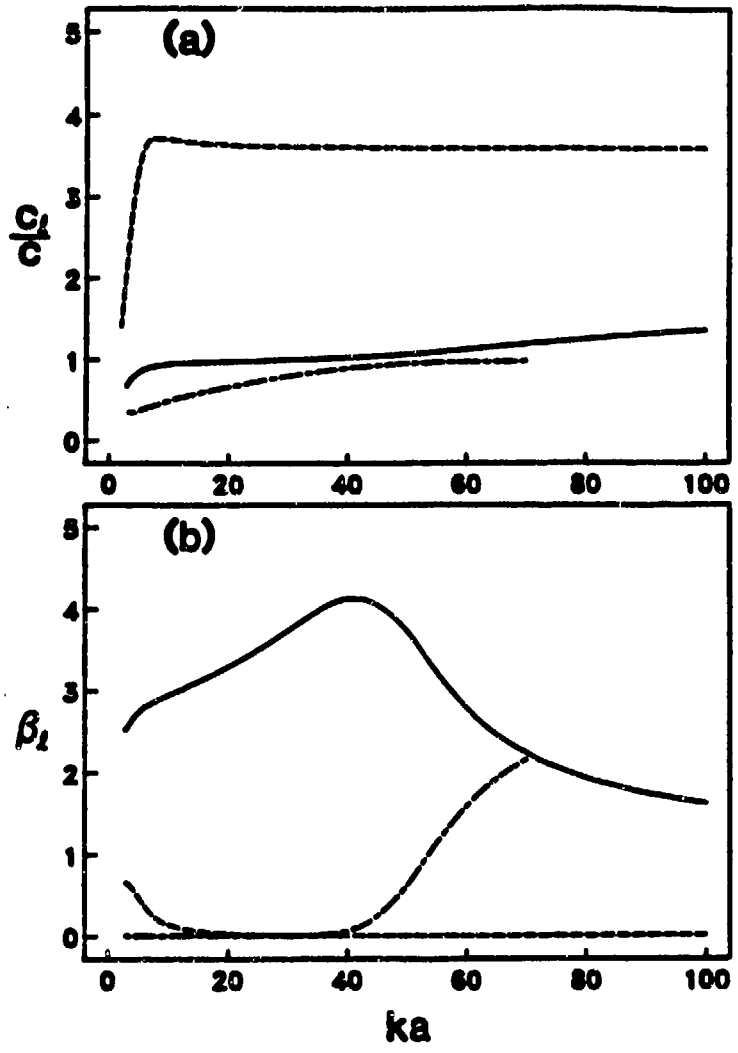

Figure 3 -- Normalized phase velocity (a) and radiation damping (b) of surface guided waves on a 304 stainless steel shell in water with $h/a = 0.025$. The curves are identified as follows: long and short dashes ($l = a_{0-}$), dashes ($l = s_0$), and solid ($l = a_0$).

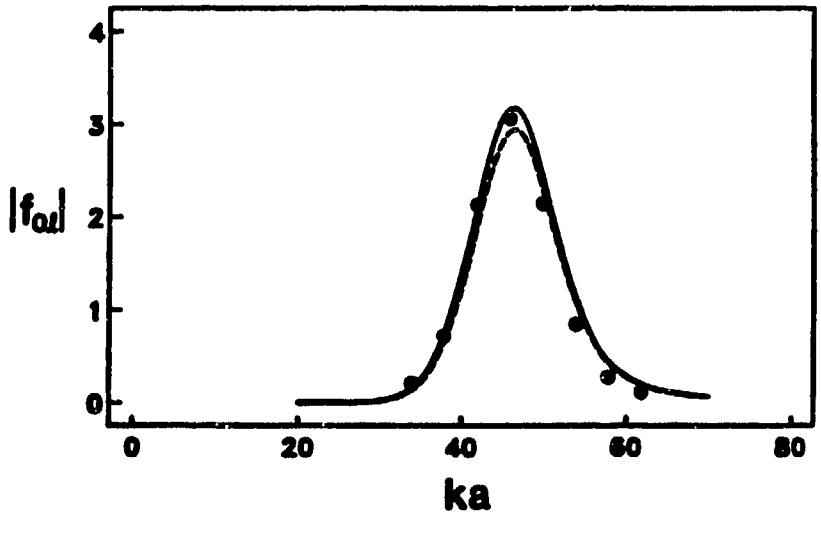

Figure 4 -- The solid curve gives the ray model in Eq. (1) for the a_0 guided wave echo amplitude in the region of the enhancement near $ka = 46$. The points are from the exact echo amplitude determined by a Fourier synthesis as illustrated in Fig. 5.

of the caustic radius b_l to the backscattering amplitude.[J4] The resulting contribution of the mth circumnavigation to the form function f has the magnitude

$$|f_{ml}| \approx 8\pi\beta_l (c/c_l) \exp(-\pi\beta_l - 2\pi m\beta_l), \quad (1)$$

where for m = 0, the wave has traveled only around the backside of the sphere as shown in Fig. 2. The solid curve in Fig. 4 gives $|f_{0l}|$ for $l = a_0$- while the dashed curve omits the factor c/c_l ; $|f_{0l}|$ for the a_0- wave shows a strong enhancement that peaks near $ka = 46.3$ where the value of $|f_{0l}| \approx 3.17$. It may be shown[J4] that the value of $|f_{0l}|$ at such a peak depends only weakly on the shell thickness and material parameters since the ka dependance is dominated by that of β_l. The peak $|f_{0l}|$ occurs close to where β_l is $1/\pi$.

Equation (1) is directly applicable to the calculation of the enhanced backscattering by tone bursts that are sufficiently short that the echoes associated with different values of m don't overlap. The incident burst must be sufficiently long that the effects of dispersion are weak. The time domain echoes for such tone bursts were calculated by a Fourier synthesis that used the exact partial wave series.[J4,T1] This was done for several bursts of different ka. Figure 5 shows the resulting calculated amplitude for a 20 cycle burst with $ka = 46$. The dimensionless time units are $T = ct/a$. The normalization is such that specular reflection by a fixed rigid sphere of radius a has a unit amplitude. The earliest contribution from the shell in Fig. 5 is a specular reflection of close to unit amplitude. This is followed by the m = 0 and m = 1 contributions of the $l = a_0$- wave where the amplitude of the m = 0 echo of 3.07 is close to the aforementioned predicted enhancement. The identity of these echoes was also confirmed by comparison of their arrival times with ray theory. The amplitude of the m = 0, $l = a_0$- echo was similarly determined for several other values of ka and are plotted as the points in Fig. 4. The comparison with Eq. (2) gives strong support for the ray model of the enhancement. It is noteworthy that the later (m = 1) echo in Fig. 5 is weaker by a factor close to the expected value of $\exp(-2\pi\beta_l) \approx \exp(-2) \approx 0.135$. Furthermore, the predicted amplitudes are weak for the distinct ray contributions of the $l = a_0$ and s_0 guided waves whose properties are also shown in Fig. 3. Consequently those contributions only weakly affect the time record in Fig. 5. The enhanced contribution to the backscattering by the a_0- wave may be especially useful for inverse problems.[J4] The echo is generally much larger than leaky wave echoes previously studied.[2,3]

3. Laboratory Observations of the Midfrequency Enhancement.

The existence and general magnitude of the enhancement described above was confirmed with experiments in a large redwood tank of water.[J5] [See Section V for a description of the facility.] The volume of water available, approximately 6500 gallons,

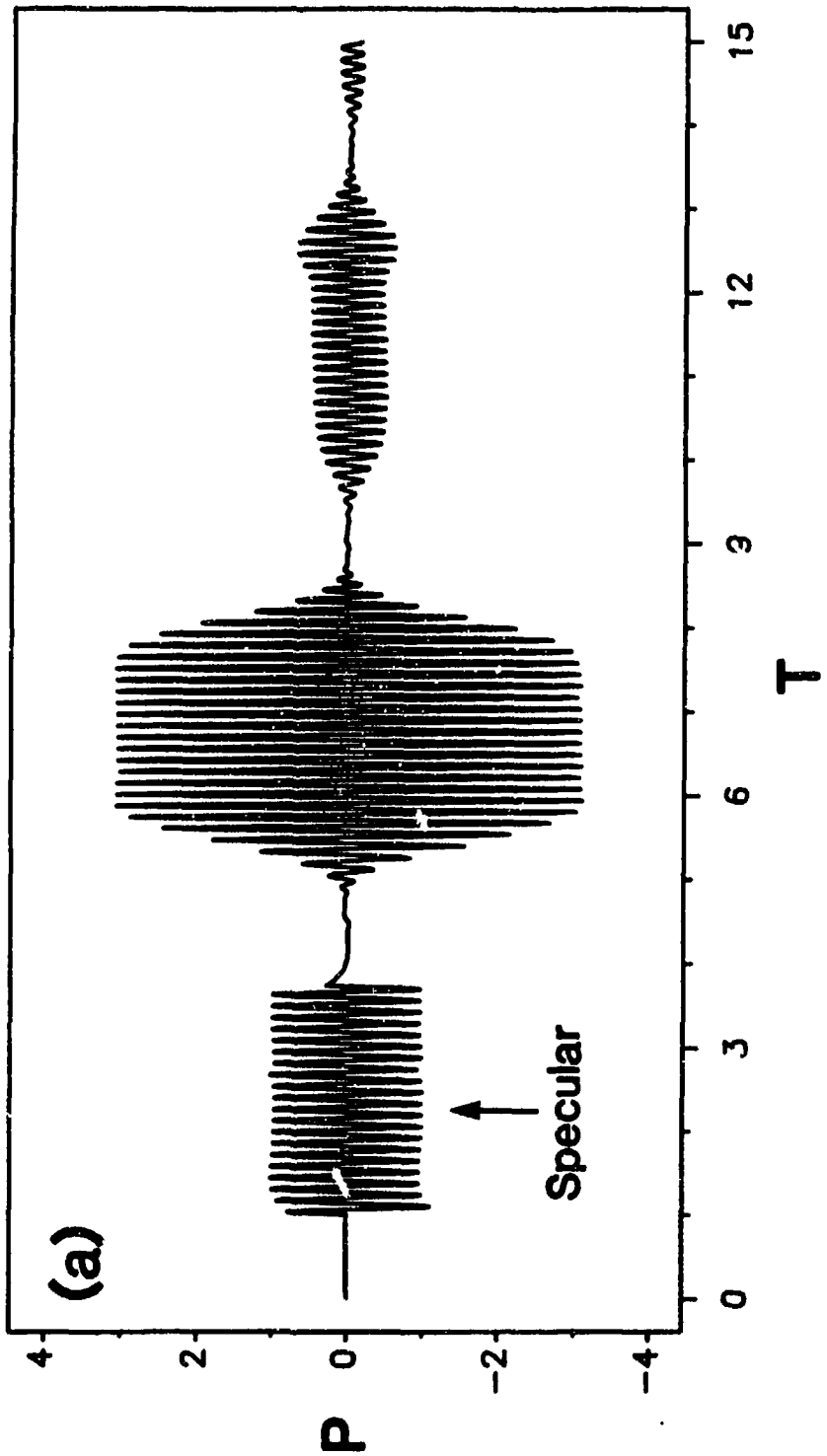

Figure 5 -- Farfield scattered normalized pressure P(T) calculated by Fourier synthesis from the exact of partial-wave series for 20 cycle incident burst with a carrier ka of 46 for the shell considered in Fig. 3. The large second echo is enhanced as predicted in Fig. 4.

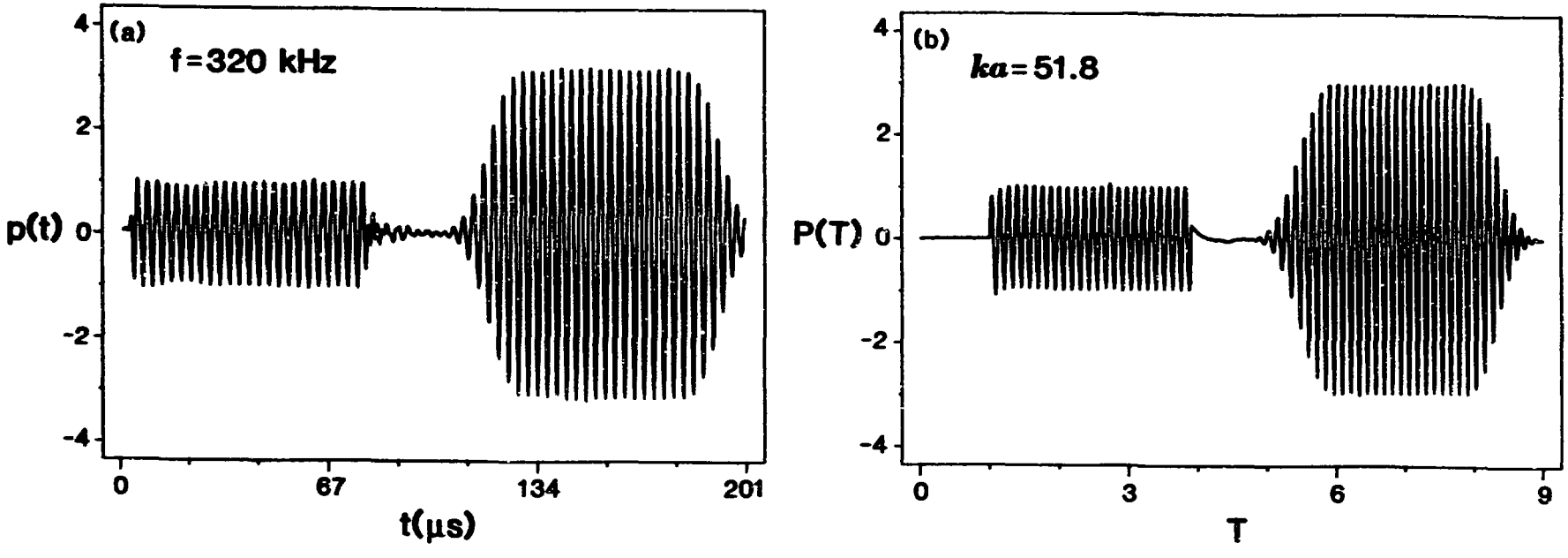

Figure 6 -- (a) Experimental time record with an arbitrary pressure normalization where the first echo is the specular echo followed approximately 108 μs later by the first guided wave contribution. The horizontal axis represents time in microseconds referenced just prior to the specular return. The delay relative to the transmitted tone burst is 3.32 ms. (b) Time records computed by Fourier synthesis from the exact form function. The horizontal axis represents time where one T unit is equal to 25.8 μs.

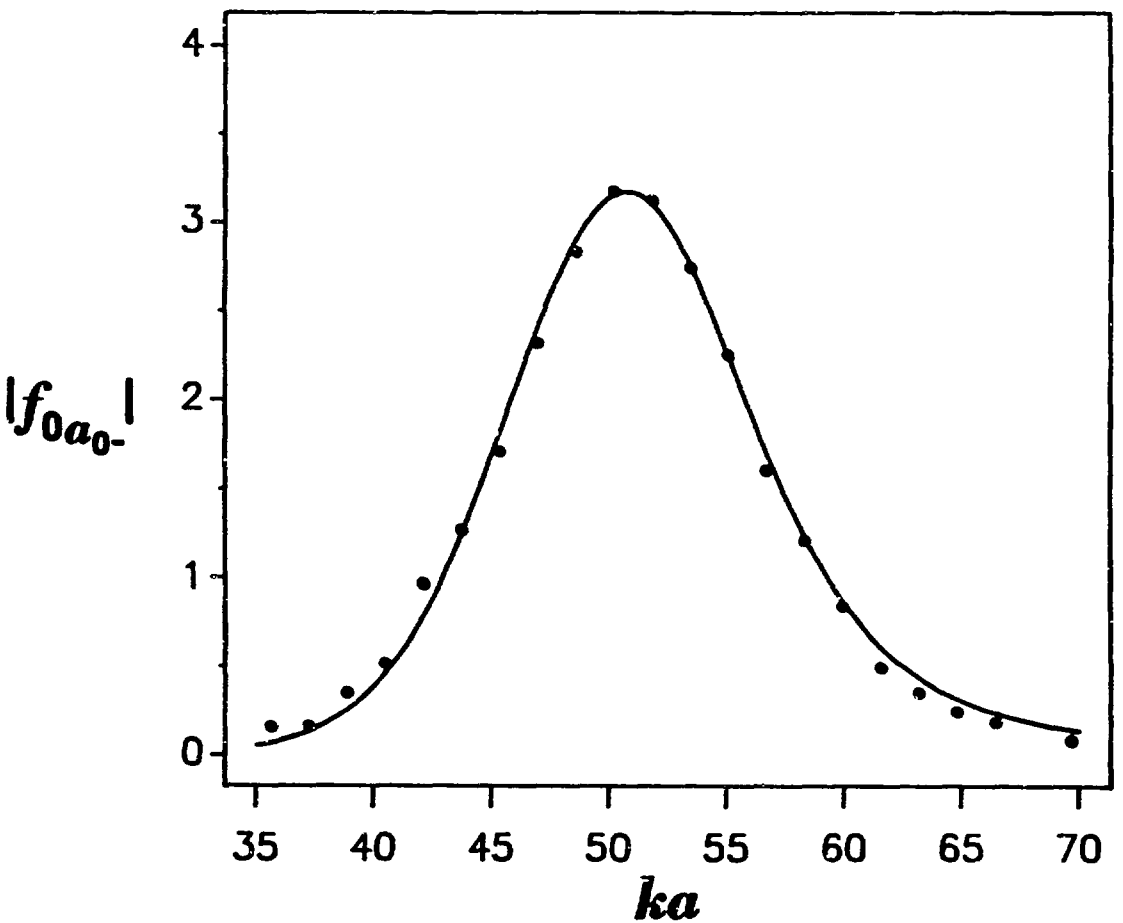

Figure 7 -- The solid line represents the magnitude of the form function contribution for the a_{0-} wave for the $m = 0$ circumnavigation. It is calculated from Eq. (1) and has a maximum near $ka \approx 50.8$. The solid circles represent the a_{0-} response for $m = 0$ found by taking the ratio of the measured a_{0-} echo magnitude to that of the specular echo.

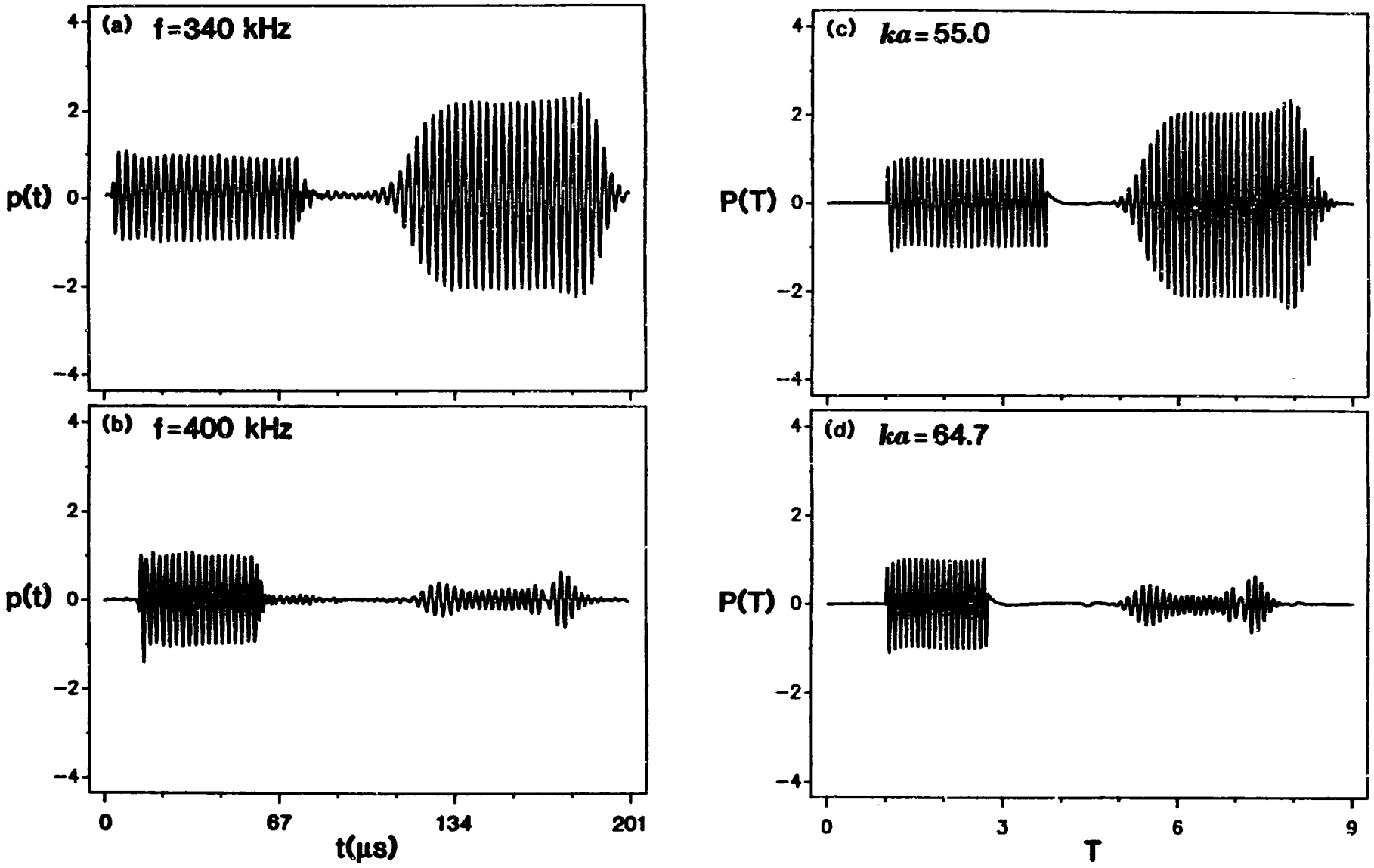

Figure 8 – (a) and (b) represent experimental time records like in Fig. 6(a) except the carrier frequency is raised. (c) and (d) correspond to the respective Fourier synthesis calculations.

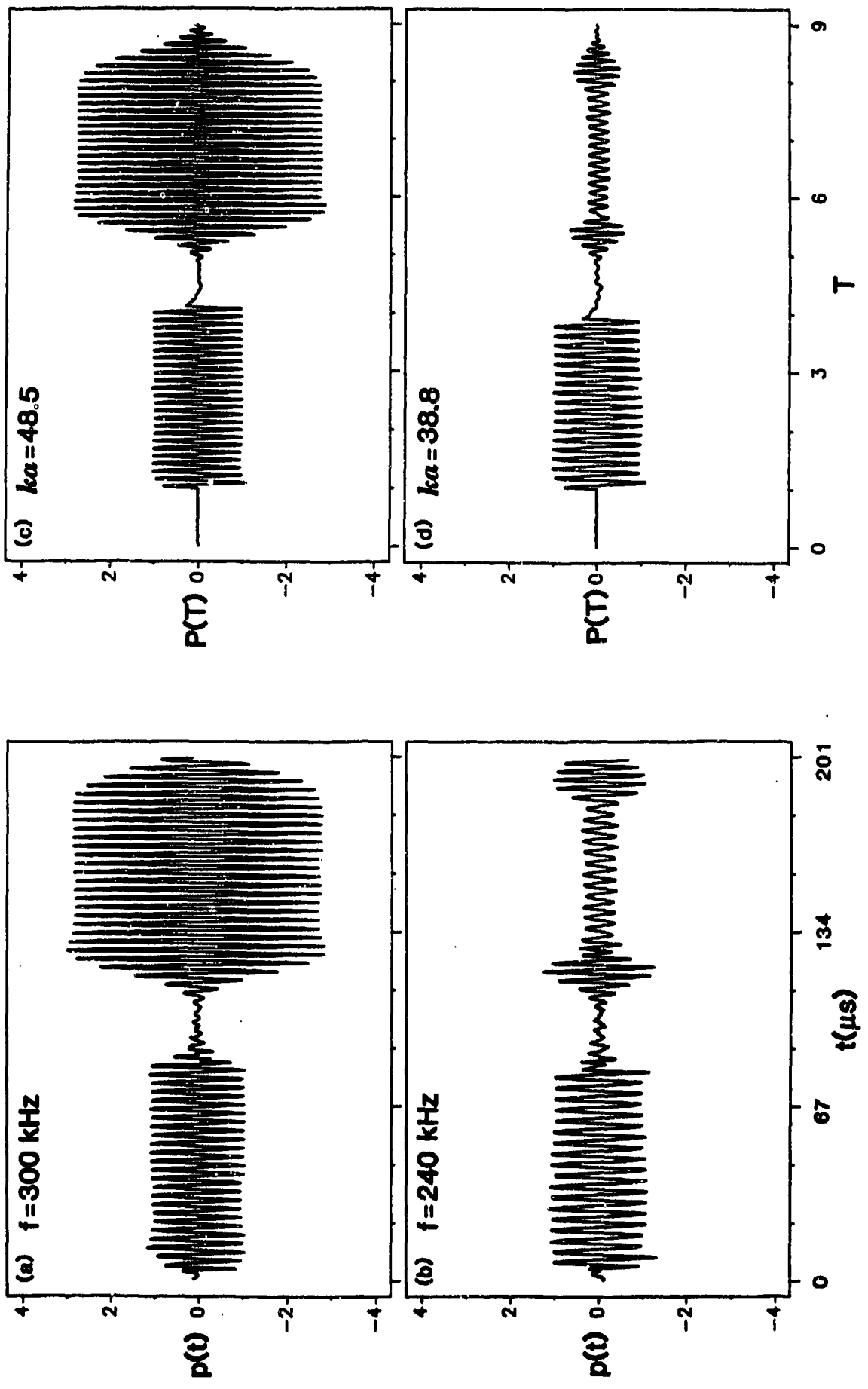

Figure 9 -- Same as Fig. 8 except that carrier frequency has been lowered.

was such that reflections from the sides, top, and bottom of the tank did not occur in the time region of interest. The target was a stainless steel 304 shell with a radius a = 38.1 mm and a radius-to-thickness ratio a/h= 43.8. The predicted enhancement is for frequencies near 310 kHz. Figure 6(a) shows a representative time record in the region of greatest enhancement of the guided wave echo which is the second of the echoes. This record, which is for 320 kHz manifests the important features of the Fourier synthesis for this shell shown in Fig. 6(b). A substantial shift of the carrier frequency was observed to cause a reduction in the guided wave echo magnitude relative to that of the specular reflection and the observed behavior is in at least qualitative agreement with the shape of $|f_{0l}|$ as is evident from the comparison shown in Fig. 7. The results are supportive of the ray model.[J7] Figures 8 and 9 show how the echoes are in detailed agreement with predictions at other frequencies.

4. Midfrequency Enhancement of the Form Function.

The ray model was also used to synthesize the exact form function f for steady-state backscattering in the region of the midfrequency enhancement for the spherical shell considered in Fig. 3 with a/h = 40. The dashed curve in Fig. 10 shows the |f| from the exact partial wave series and the solid curve shows $|f_{ray}|$ where[J6]

$$f_{ray} = f_{sp} + f_{a_{0-}} + f_{s_0} + f_{a_0} \tag{2}$$

where f_{sp} is the specular contribution (here neglecting a small curvature correction) and f_l for $l = s_0$ and a_0 are leaky wave contributions computed as discussed previously.[5,J1] In the region shown $|f_l|$ is negligible for $l = a_0$ but for $l = s_0$ it gives rise to the vary narrow resonance spikes. The enhancement is associated with the $l = a_{0-}$ term which is computed by summing ray terms of the form f_{ml} as in Eq. (1) but including phase information. The result reduces to

$$f_l = \frac{-G_l \exp\left[-\pi\beta_l + i\eta_l\right]}{\left[1 + \exp\left(-2\pi\beta_l + i2\pi xc/c_l\right)\right]}, \quad G_l = \frac{8\pi\beta_l c \exp(i\phi_l)}{c_l}, \tag{3,4}$$

where $\eta_l = \pi xc/c_l - (\pi/2)$, $x = ka$, and except for the expression for $\arg(G_l) = \phi_l$, the generalization to this case of a subsonic wave follows from the ray geometry in Fig. 2 and related considerations.[1,J4] The approximation for ϕ_l used in Fig. 10 was obtained by assuming that ϕ_l varies linearly with c_l as c_l approaches c,

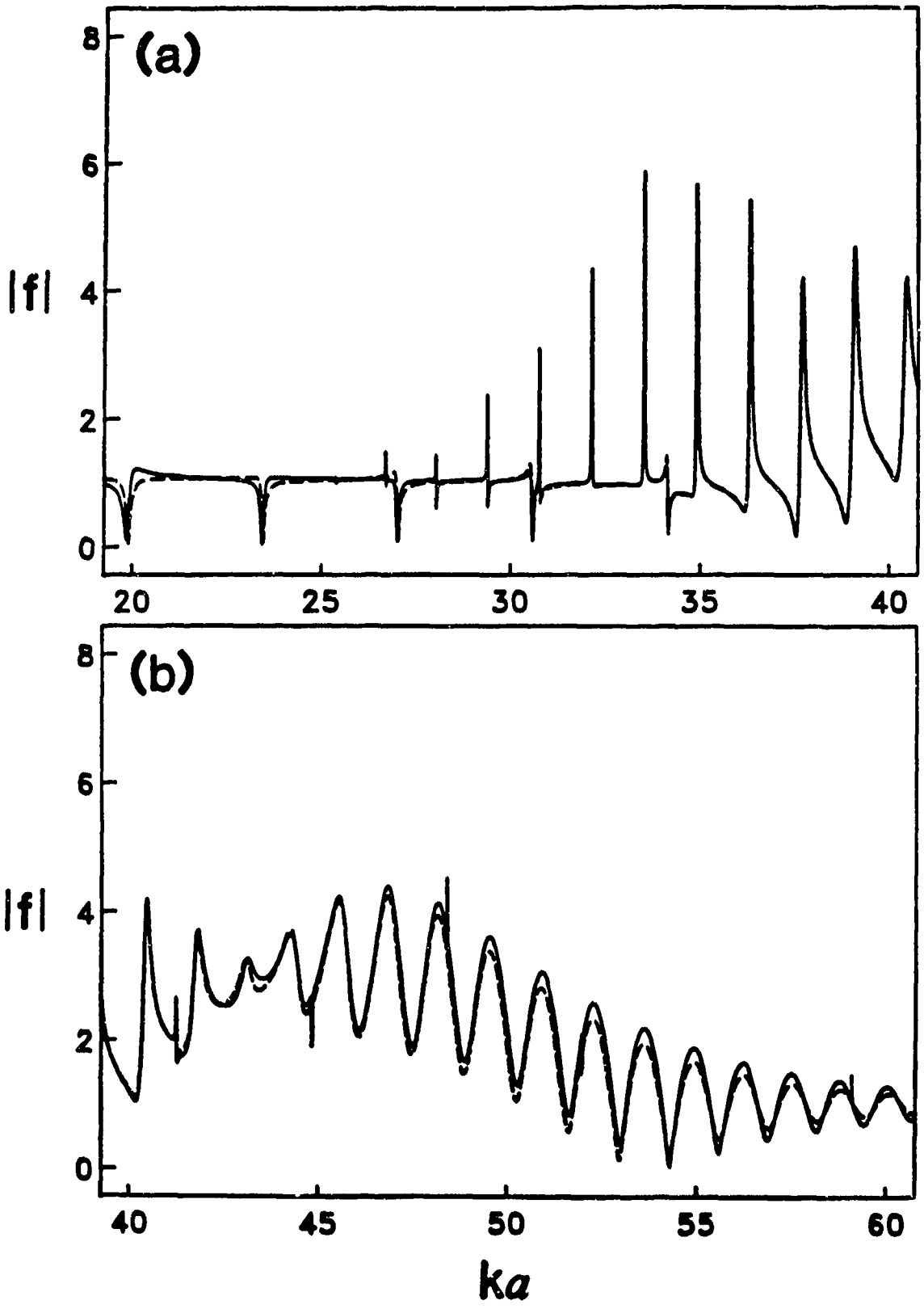

Figure 10(a) and (b) -- The dashed curve gives the exact form function |f| for the empty 2.5% thick shell considered in Figs. 3-5. The solid curve gives the approximate ray synthesis $|f_{ray}|$ from Eq. (2) and manifests an enhancement in (b).

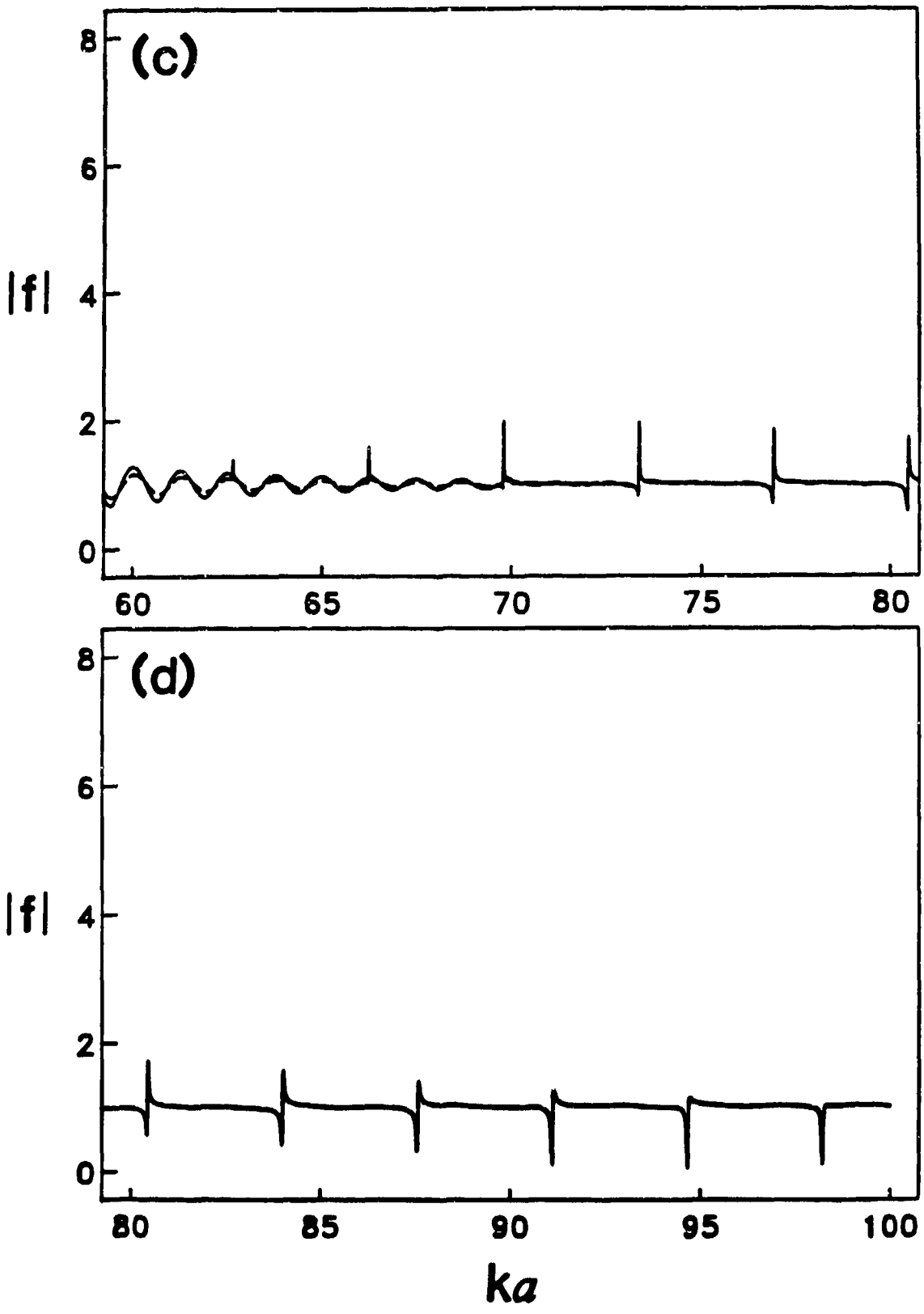

Figure 10(c) and (d) -- As in (a) and (b) but for the high frequency region. In (d) the synthesis and exact curves completely overlap. The shape of the interference structure from the s_0 wave changes with ka in a way predicted by ray theory.

$$\phi_l \left(Rc < c_l < c\right) \approx \pi\left[(3/2) - (2F/3)\right], \quad F = \left[\left(c_l/c\right) - V\right]/(1 - V), \qquad (5,6)$$

but that ϕ_l becomes constant for c_l/c below a particular value of $V < 1$ so that $\phi(c_l < Vc) = 3\pi/2$. Note that F varies from 0 to 1 in the domain of Eq. (5). Results of Ho and Felsen were used as a guide for formulating the limiting values of ϕ_l though the value of $V = 0.91$ used for the synthesis in Fig. 10 was determined empirically. Inspection of Fig. 3(b) shows that for ka near 40, β_l is sufficiently small for the a_0 wave that contributions from repeated circumnavigations are important giving rise to a distinct resonance structure. With increasing ka there is an enhancement in $|f_l|$ associated primarily with the $m = 0$ contribution plotted in Fig. 4. For $ka \gtrsim 50$, β_l is so large that repeated circumnavigations are no longer important and the gradual periodic variations in |f| shown in Fig. 10 are due to the interference with the specular reflection. This was verified with a simple ray calculation of the quasiperiod $\Delta ka \approx 2\pi[2 + (\pi c/c_l)]^{-1} \approx 1.2$. A ray synthesis was also demonstrated for backscattering from a circular cylindrical stainless steel shell also with $a/h = 40$ and the agreement with the exact result was slightly improved over that of Fig. 10.[M4] The magnitude of the enhancement relative to the strength of the specular contribution is weaker for cylinders than for spheres due to the absence of axial focusing in the cylinder case.[1,J4]

It is noteworthy that there has been considerable attention by other groups given to the enhancement of |f| near coincidence as calculated directly from the exact partial-wave series as in the dashed curve in Fig. 10. (See e.g. Refs. 12-14 and other publications cited therein.) The approach usually taken to understand the broad enhancement is to first locate resonances in the complex frequency plane for different partial waves n. From the trajectory of resonances an attempt is made to infer the existence and phase velocities of the various surface guided waves. It is noteworthy that phase velocity curves found from the complex ν roots such as shown in Fig. 3(a) are consistent with results for a flat plate near the coincidence frequency and are perhaps clearer than some of the published dispersion curves based on complex frequency plane roots. (The results of Sammelmann et al.[12] exhibit the same behavior for c_l as Fig. 3(a).) The point here is that in the region of the coincidence anomaly, the locus of complex-ν roots used in ray theory are easy to interpret since $\beta_l(ka)$ is given directly. Another advantage of complex-ν plane ray theory is evident from the simplicity of Eqs. (2)-(4). The ray approach provides a natural mathematical basis for describing the wavefield in the region of rapidly varying damping β_l (Fig. 3(b)) and that, at least in principle, the ray approach can be generalized to other shapes for which no partial wave series exists. There are advantages of ray approaches based on complex-ν roots both for the time domain envelopes, Fig. 4, and for the frequency responses, Fig. 10.

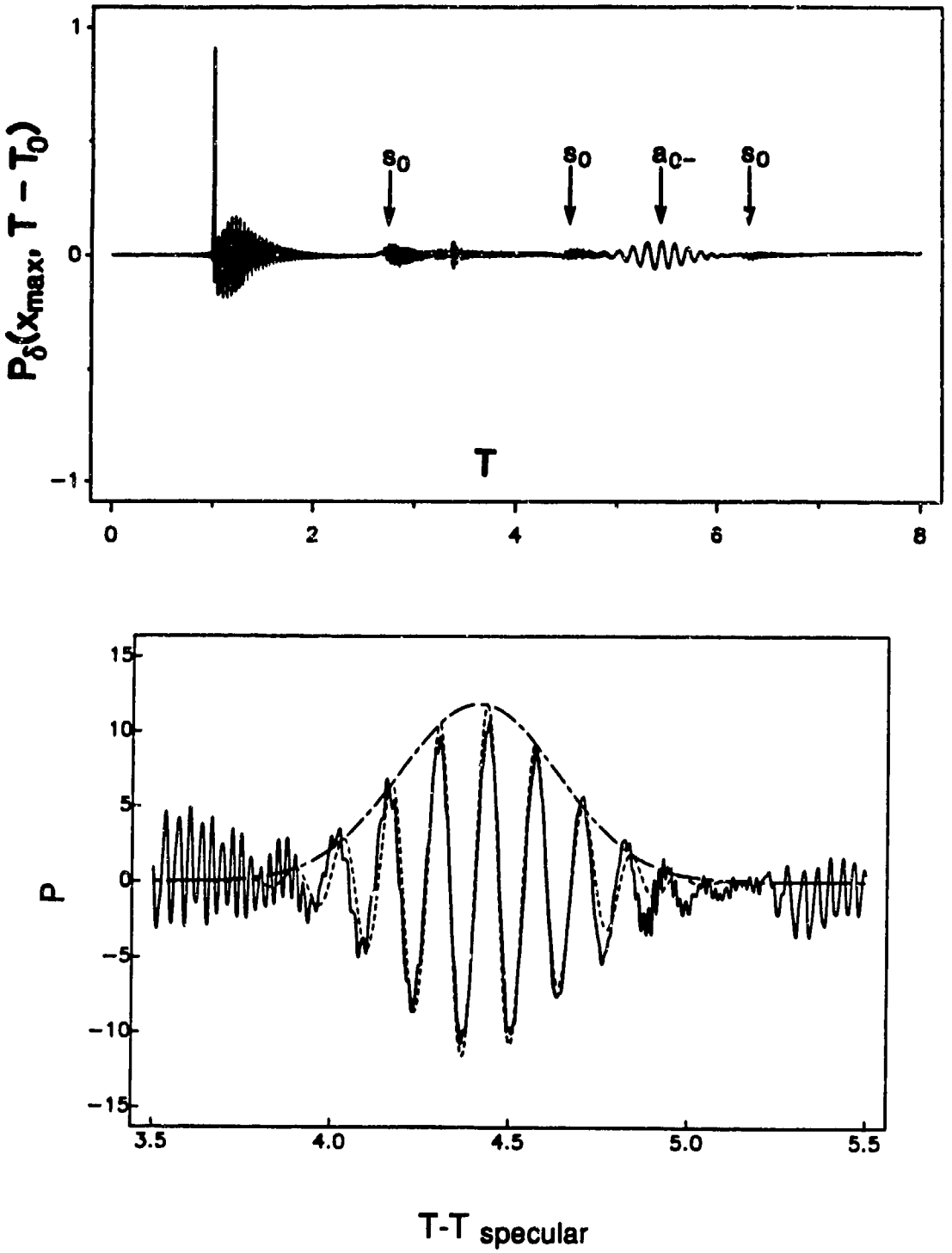

Figure 11(a) -- Impulse response from an FFT of the form function. (b) Solid curve is an expanded version of (a) near the a_{0-} wave packet. The dashed curve is a ray approximation.

5. Impulse Response of a Thin Spherical Shell and a Significant Wave Packet at the Coincidence Frequency.

It is well known that for linear systems, the response to an arbitrary "input" may be expressed as a convolution of the input with the system's impulse response. It follows that an understanding and analysis of a shell's farfield scattering in response to a δ-function pressure impulse will give insight into the scattered pressure for an arbitrary incident wave. This method of approach to scattering from shells appears to be underutilized. Figure 11(a) shows the farfield impulse response for the thin shell considered in Figs. 2-5 computed by Zhang, Sun, and Marston[J4] from a numerical Fourier transform of the exact partial wave series. The size of the initial specular spike and the relative normalization to the subsequent guided wave contributions are discused in Ref. J4. What is important to the present discussion is the prominent feature labeled a_{0-} that has a frequency close to the coincidence frequency of the shell. The other guided wave contributions are lower in amplitude and relatively chirped. The large magnitude of the a_{0-} guided wave echo in Fig. 5 can be understood as the convolution of that wave packet with the incident tone burst. A weaker subsequent (m = 1) wave packet for the a_{0-} wave yields the lower amplitude late echo in Fig. 5.

It is worth considering the earliest wave packet's large contribution to the impulse response from an approximate analytical Fourier transform of the associated contribution to the form function as predicted by ray theory. This is because such a calculation is a sensitive test of ray methods and may in principle be extended to complicated objects. (The initial specular spike may be predicted from ray theory as discussed by Zhang, Sun, and Marston.[J4]) To obtain an approximate analysis of the a_{0-} wave packet Marston[M12] used a stationary phase approximation to analytically approximate the Fourier transform of the relevant spectral contribution, $f_{m=0,l}$. First it was noted that $|f_{m=0,l}|$ as shown in Fig. 4 could be well approximated by a Gaussian function centered at the peak $ka = x_l \approx 46.4$. The width of the Gaussian was expressed in terms of ray parameters evaluated at that ka. Then the approximate phase from Eqs. (5) and (6) and the propagation delay were introduced. Only the leading effect of dispersion (the dependence of c_l on ka) could be introduced and certain other simplifications were made which led to a narrow range of possible parameters for the scattered wave packet. The resulting approximate analytical wave packet may be reduced to the simple form for the a_{0-} wave

$$P_\delta(T) \approx \frac{A}{(T')^{1/2}} f_{m=0,l}(x) \cos(x_l \Delta T + \Psi), \qquad x = x_l + (\Delta T/T'), \tag{7}$$

where the time shift relative to the center of the packet at T_l is $\Delta T = T - T_l$. The amplitude

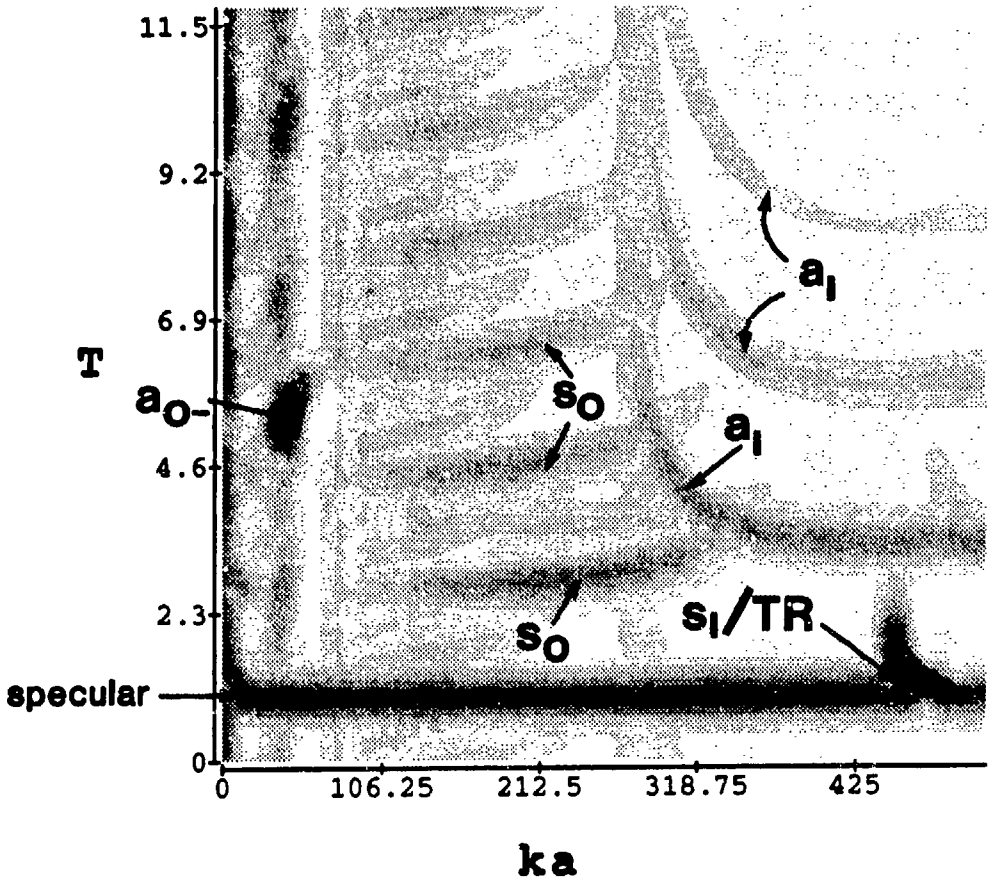

Figure 12 -- Time- frequency analysis of the impulse response for backscattering by the 2.5% thick shell considered in Figs. 3-5. The dynamic range is such that the darkest regions correspond to signals that are orders-of-magnitude larger than the light regions. The earliest and strongest of a sequence of a_0- wave packets is labeled as is the prompt large thickness-resonance/s_1-wave-threshold feature, both of which are stronger in this plot than the specular reflection. Features associated with circumnavigations of dispersive leaky Lamb waves are also evident.

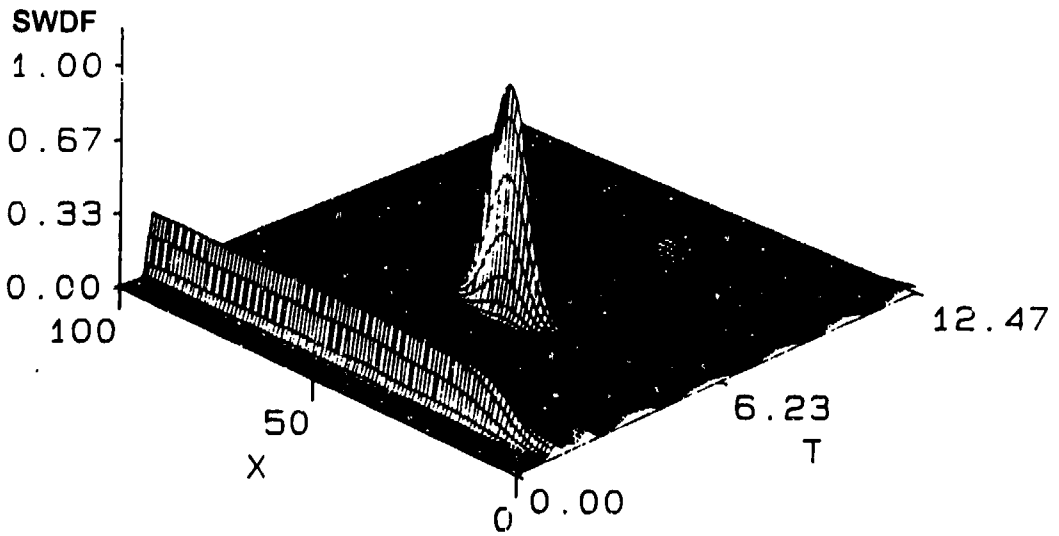

Figure 13 -- Plot of the Gaussian smoothed Wigner distribution function (SWDF) of the impulse response for the same shell as Fig. 12 but for x = ka from 0 to 100. The SWDF is normalized to the maximum value which is the peak from the a_0- wave packet. The ridge at T = 1 is due to the specular reflection.

factor A is predicted by the analysis as are estimates for T_l, T', and Ψ. Figure 11(b) compares an exact impulse response (the solid curve) on an expanded scale with the approximate analytical form given by Eq. (7). The exact response was computed as in Fig. 11(a) but with a different offset T_0 so that the dimensionless time T is relative to the specular spike that is outside of the range of Fig. 11(b). Also shown is the envelope of the wave packet as predicted by ray theory. The important result is that the simple ray approximation describes moderately well the exact packet. One shortcoming of the theory (in addition to the imprecision of the wave packet parameters) is that the exact packet displays a weak low-frequency to high-frequency chirp not analyzed for the degree of dispersion retained in the approximation. (The wave packet in Eq. (7) has a fixed frequency.) Nevertheless, there is no doubt as to the basic cause of this feature of the impulse response.

6. Time-Frequency Analysis of Backscattering by Spherical Shells and Applications.

Yen et al.[15] explored the use of a modified version of the Wigner distribution function (WDF) for displaying a time-frequency analysis of transients scattered by elastic objects. In our research D. H. Hughes applied methods of smoothing the WDF discussed by Nuttall[16] to scattering by spherical shells. The example considered below is that of backscattering by the same shell considered in Figs. 3-5. The response to an impulse is computed for the time domain in Fig. 11(a) where it is shown that, in addition to the specular reflection, there is a large wave packet associated with the $l = a_0$. wave with the m = 0 ray path shown in Fig. 2. The impulse response in the time-frequency domain displays the spectral evolution of this and other wave packets. Figure 12 shows the smoothed WDF for the impulse response based on the exact f from the partial-wave series.[P2,M17,I4] The axes are in dimensionless ka and $T = tc/a$ where the time offset used is the same as that of Fig. 5 so that the earliest contribution is the specular reflection at T = 1 in the narrow time resolution limit. Various contributions can be identified by comparing the time of the contribution with predictions from ray theory as discussed e.g. in Ref. 2 and J4. The dark bar centered on T = 1 is the specular reflection and the dark patch centered near $T \approx 5.5$ and $ka \approx 46$ is from the $l = a_0$., m = 0 wave packet associated with the midfrequency enhancement. The central frequency is close to the coincidence frequency and the timing of the packet follows from the ray analysis. Leaky wave contributions that can be easily identified include those due to the $l = s_0$ and a_1 generalizations of Lamb waves to the present case of a hollow fluid-loaded shell. Figure 13 shows another way of plotting the smoothed WDF that also reveals the features discussed above.[17]

Figure 12 shows that there is a large prompt contribution to the backscattering for ka in the region from approximately 455 to 485. This enhancement is in the vicinity of the threshold for the s_1 Lamb wave as well as the longitudinal resonance discussed in Ref. 6 and J1 that, for the present shell [Eq. (9), below], is at $(ka)_{LR} = 482$. Since Fig. 12 shows that this contribution is close in time to the specular reflection, a surface guided wave does not have sufficient time to travel around the backside of the sphere A novel alternative prompt guided-wave mechanism is from rays with the group velocity directed opposite to the phase velocity[M9,M14] and Fig. 12 is generally supportive of such a mechanism. This mechanism is examined below in Section IV A10.

7. Ray Synthesis of Leaky Lamb Wave Contributions to Backscattering from Thick Cylindrical Shells.

A ray synthesis as indicated in this subtitle was carried out by Sun and Marston[J3,M5] to test Marston's earlier analysis[1,18] of the approximate phase of the coupling coefficient G_l for leaky Lamb waves on a cylindrical shell. It is noteworthy that subsequent analysis by Felsen et al.[8] reduces to the same approximate phase and amplitude for G_l in this case so that the synthesis can also be taken as a test of their results. The ray picture is as shown in Fig. 1. Attention here is restricted to the case of a stainless steel 440 C shell with $h/a = 0.162$. Figure 14 compares the resulting synthesis (the solid curve) with the form function $|f|$ from the exact partial wave series. The agreement is good down to $ka \approx 7$. The synthesis is quite analogous to the discussion for shells given by Kargl and Marston.[J1] For future reference the relevant phase velocity and dispersion curves are shown in Fig. 15 as given by the complex-ν plane method.

8. Weakly-or-Non-Radiating Supersonic Lamb Waves on Fluid-Loaded Plates and Shells.

Consider again the conventional leaky ray picture for backscattering by spheres and cylinders shown in Fig. 1. The associated contributions have been used to synthesize the exact f for thick hollow spherical[J1] and cylindrical[J5] shells. In those ray calculations, the leaky lamb wave properties $c_l(ka) > c$ and $\beta_l(ka)$ are calculated from the exact elastic equations as discussed above in conjunction with Fig. 3. One curious result of those calculations is that for certain leaky rays, the function $\beta_l(ka)$ can exhibit a minimum where β_l can be as small as 10^{-4} Np/rad which means that the supersonic guided wave only weakly leaks energy. In the region of ka where β_l is small, the resonances associated with that leaky wave are narrow.[1] For the example of a thick stainless steel shell with $h/a = 0.162$ considered in Fig. 15, such a minimum β_l occurs at $ka \approx 18$ for the $l = s_0$ wave. Marston[M13,P2] showed that insight into the cause of such minima can be found by first

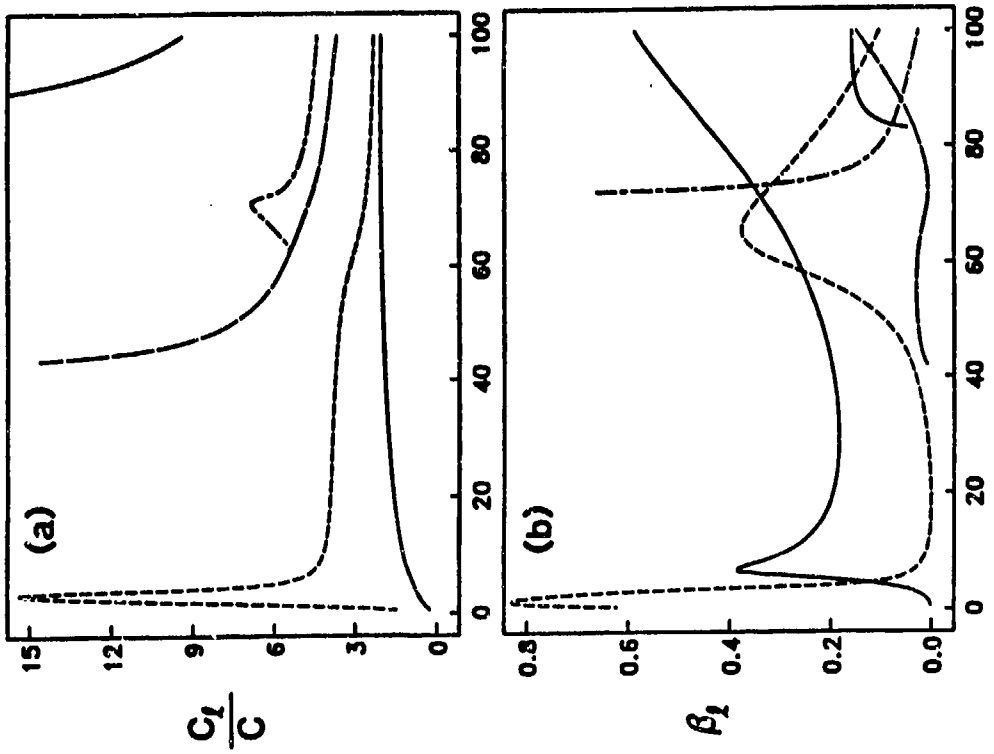

Figure 15 – Velocity and damping parameters of leaky Lamb waves for thick stainless steel shell in Fig. 14 with h/a = 0.162.

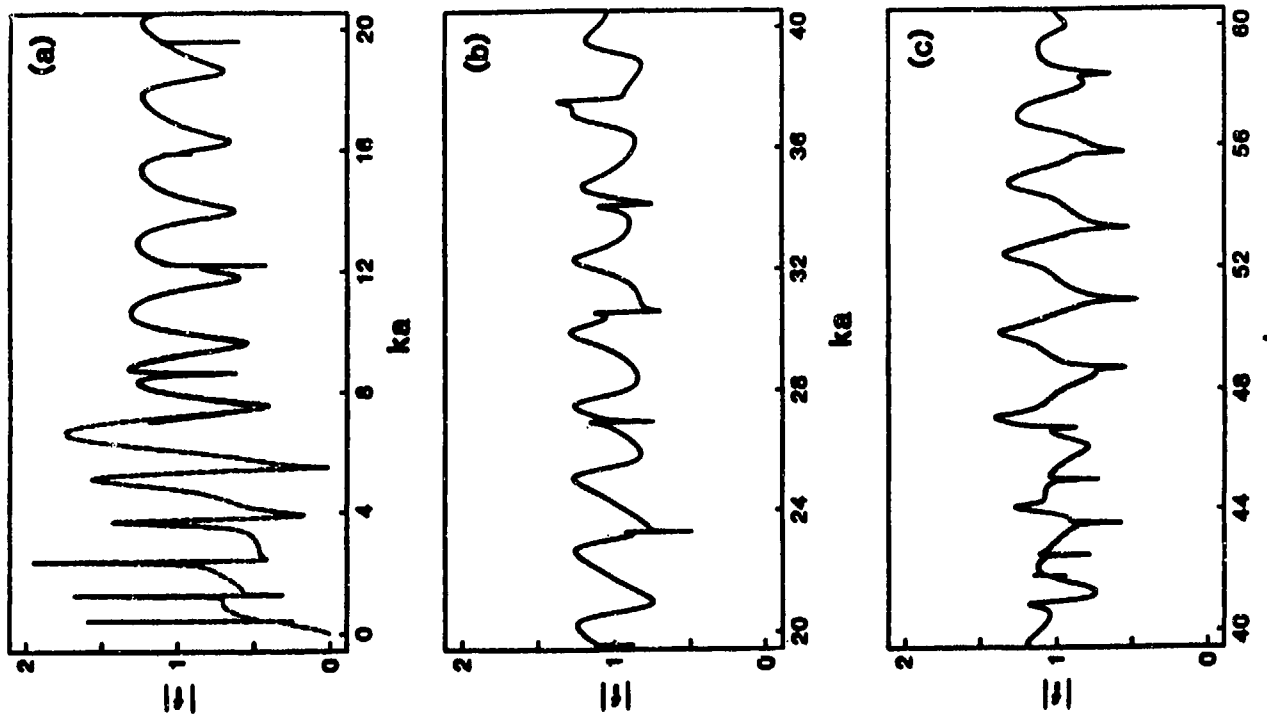

Figure 14 – Confirmation of the ray approximation (solid curve) including leaky Lamb wave contributions to backscattering. The dashed curve is exact. From Sun and Marston (Publication J3).

considering the particle displacement at the surface of a flat plate in a vacuum. Worlton[19] has shown that when the phase velocity c_{lP} of the lth symmetric Lamb mode of the plate is equal to the longitudinal wave speed c_L of the bulk material, then there is no normal displacement at the plate's surface. For a supersonic wave to radiate or leak sound into the surrounding inviscid fluid, it is essential that surface displacements occur perpendicular to the plate. Consequently, it is to be expected that the radiation damping vanishes exactly when $c_{lP} = c_L$ for symmetric waves on fluid loaded plates. Inspection of the exact dispersion equations given in Ref. 11 and 10 for the case of (inviscid) fluids on one or both sides, respectively, shows that is indeed the case: when $c_{lP} = c_L$, there is no radiation damping of the lth symmetric Lamb wave and c_{lP} does not depend on the density of the fluid! A corresponding analysis of the exact displacements at the (curved) surface of a shell has not been carried out, however, it is to be anticipated on physical grounds that locally normal surface displacements are essential either for radiation by a given mode or for excitation of that mode by an incident sound wave. For leaky waves with $ka >> 1$ on shells with $h/a << 1$, the effects of curvature should be small so that β_l should be small for symmetric waves when $c_l \approx c_L$. If curvature is neglected in Fig. 15, the prediction becomes that $\beta_l(ka)$ should be small for $c_l(ka)$ such that $c_l/c \approx c_L/c \approx 3.98$. Comparison of Fig. 15(a) with 15(b) for the aforementioned s_0 wave at $ka \approx 18$ confirms the usefulness of this criteria. It is noteworthy that the existence of supersonic waves with little or no radiation is contrary to conventional wisdom.

9. Leaky Lamb Wave Contributions to Backscattering of Tone Bursts by Thick Cylindrical Shells: Experiments.

During the early use of the 6500 gallon tank facility, S. P. Perry (with some assistance from D. H. Hughes) carried out various novel experiments pertaining to the backscattering by an empty thick cylindrical shell for situations where the incident tone burst was sufficiently short that contributions from different reflected and guided waves were separate in time.[M6] The experiment was analogous to Kargl and Marston's previous observations of the backscattering of tone bursts by a thick spherical shell[2] except that now a circular cylinder was used. The relevant ray diagram for the guided wave contributions studied is shown in Fig. 1. The empty cylindrical shell used in the experiments was made of stainless steel 304. The thickness-to-outer radius ratio was $h/a = 0.17$. Figure 16(a) shows the backscattered short tone burst echo at a frequency of 160 kHz which corresponds to $ka = 14.2$. The backscattering of the a_0 leaky Lamb wave is delayed in time relative to the specular and corresponds to the earliest or $m = 0$ circumnavigation.

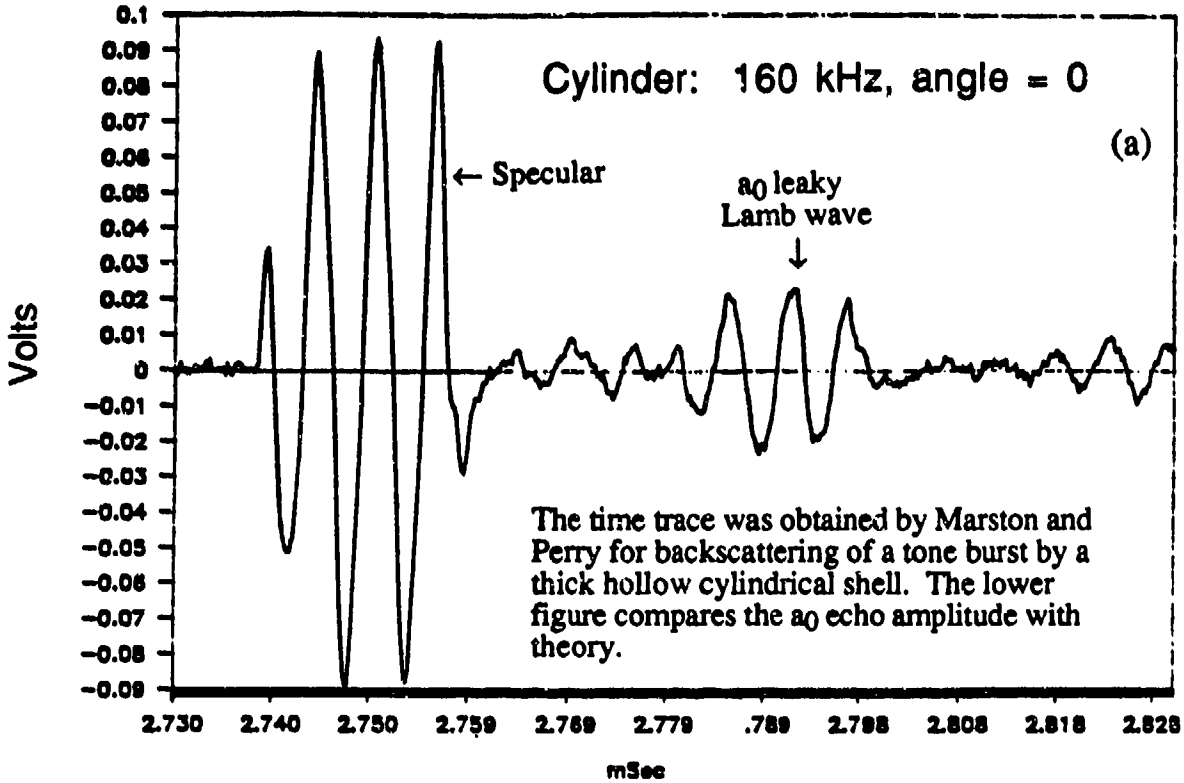

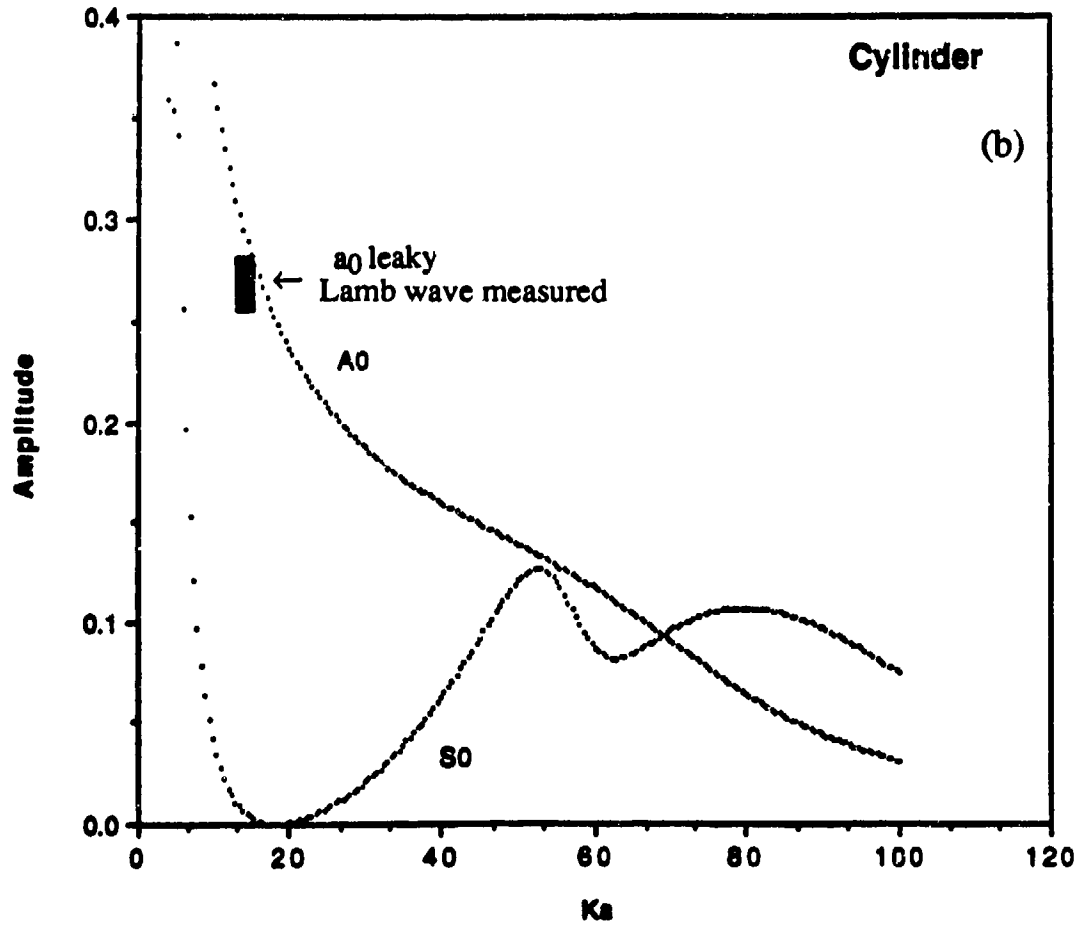

Figure 16 -- Backscattering by a hollow stainless steel cylinder.

Marston's approximation for $|G_l|$ for cylinders[1] predicts that the contribution to the form function for backscattering is

$$|f_{ml}| \approx \left[\frac{8\pi\beta_l}{(\pi ka)^{1/2}}\right] \exp\left[-2(\pi - \theta_l)\,\beta_l - m2\pi\beta_l\right], \tag{8}$$

where $\sin\theta_l = c/c_l < 1$. Figure 16(b) shows the predicted $|f_{ml}|$ contributions of the $m = 0$ circumnavigations of the a_0 and s_0 waves for the cylindrical shell under consideration. Also shown in the experimental result obtained from Fig. 16(a) by taking the ratio of the guided wave and specular echo amplitudes. According to the arrival time, the guided wave is for $m = 0$ and $l = a_0$. The agreement with the theory supports the applicability of Marston's approximation of $|G_l|$. A noteworthy aspect of the experiment is that the frequency was such that all $|f_{ml}|$ for the s_0 wave are predicted to be small. The reason is that close to this frequency β_l is small for $l = s_0$ as a consequence of poor coupling discussed in Sec. IV A8 above. This results in a situation that is experimentally advantageous since interference due to s_0 wave echoes is predicted to be weak. In addition to this experimental result, there is other evidence supporting the correctness of Eq. (8) since when phase information is included and summations over the indices m and l are preferred the resulting guided wave contribution to the steady state scattering is the one verified by the comparison shown in Fig. 14.[J3]

10. High-Frequency Scattering Enhancement by Shells: Negative-Group Velocity Leaky Wave giving Enhanced Prompt Radiation.

Calculations of the steady-state form function $|f|$ for empty spherical shells in water having thicknesses h of less than approximately 10% of the radius a display a prominent enhancement in a region at high frequencies. This enhancement has been noted in discussions of computations by a few authors and there has been some speculation as to the cause. Figure 17 gives calculations by Kargl and Marston[5,J1] for the case of an aluminum shell with $h/a = 0.04$. The solid curve shows $|f|$ which displays a pronounced peak near $ka = 302$. The dashed curve shows the specular contribution calculated from ray theory[6] for the case of a fluid shell having the same thickness and longitudinal sound speed c_L as the aluminum shell. Both curves show evidence of a broad minimum in the specular backscattering contribution near the frequency of the lowest longitudinal resonance which is at[2,J1]

$$(ka)_{LR} = \pi(c_L/c)\, a/h. \tag{9}$$

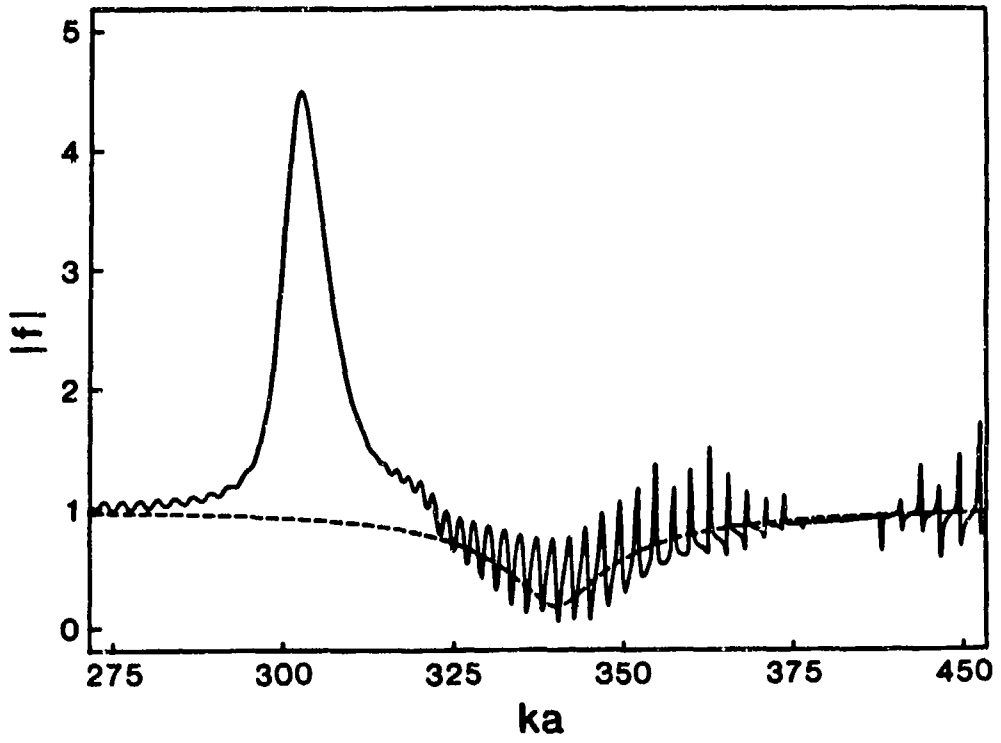

Figure 17 -- Form function for a 4% thick hallow aluminum shell showing a large high-frequency enhancement at ka = 302.

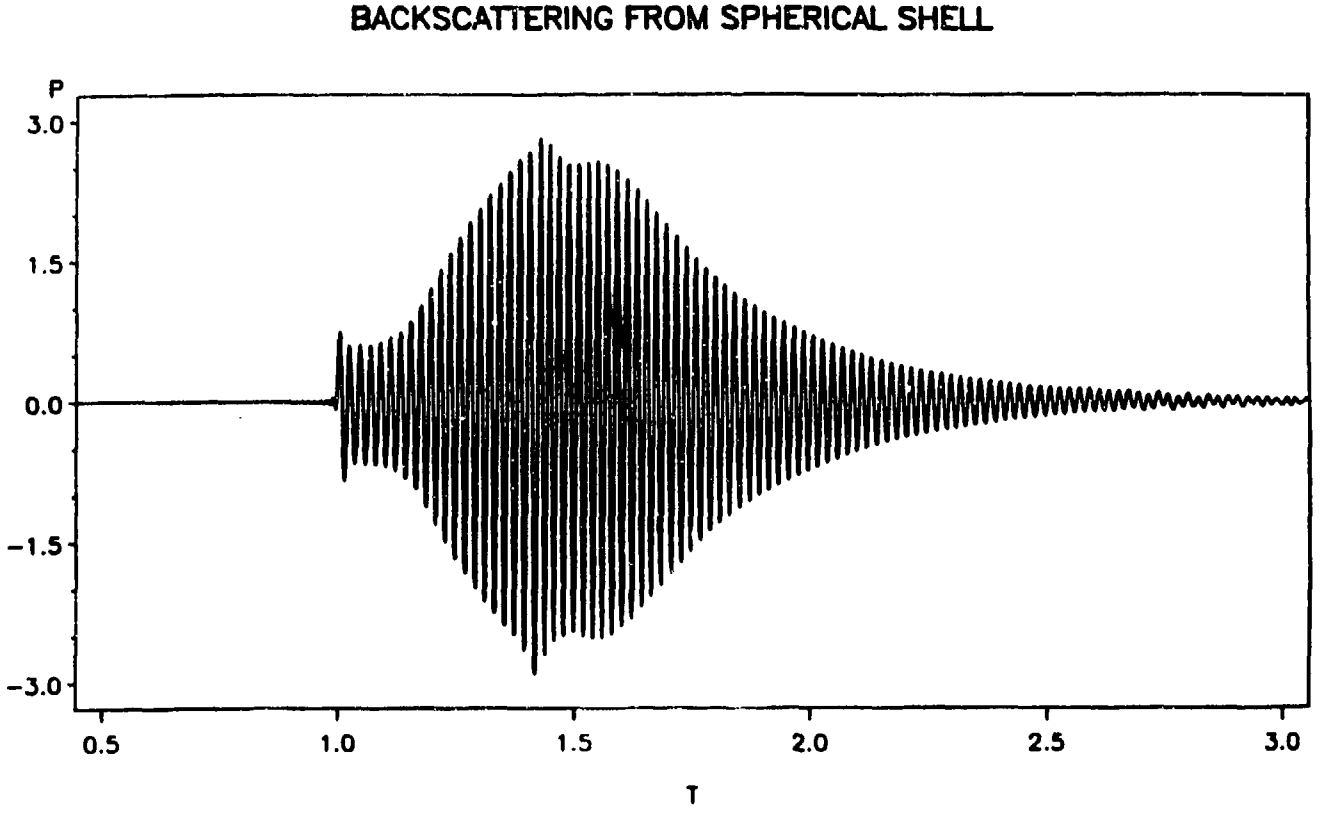

Figure 18 -- Computed backscattering of a 20 cycle sine wave burst with the carrier frequency at ka = 302, the large peak in Fig. 17. The specular reflection at T = 1 is followed by a prompt backscattering enhancement associated with the large peak.

For the aluminum shell in water, c_L = 6.42 km/s and Eq. (9) predicts $(ka)_{LR}$ = 340. The high frequency enhancements predicted in computations by other authors are also at frequencies close to but below the longitudinal resonance condition of Eq. (9).

To gain insight into the mechanism for the enhancement, in Zhang's M.S. degree thesis,[T1] the backscattering of tone bursts having carrier frequencies in the enhanced region were calculated by the exact method of Fourier synthesis. (While the computational method is summarized in Ref. J4, the results for this aspect of the investigation are shown in Ref. T1.) Figure 18 shows an example of the results for the aluminum shell considered in Fig. 17 when the carrier $ka = x_0$ is taken to be 302 corresponding to the peak value of the enhancement. The amplitude and time normalization is the same as that discussed in conjunction with Fig. 5 and there are 20 sine wave cycles in the incident burst. The echo contributions caused by guided waves that travel around the back side of the shell do not arrive until after $T \approx 2.5$. Inspection of Fig. 18 (and similar results for other burst lengths) shows that the high frequency enhancement is associated with a build up beginning by $T \approx 1.2$ that is nearly saturated by about T = 1.5. Consequently the enhancement is not associated with guided waves that travel around the back side of the shell. This conclusion was previously noted in conjunction with the discussion of Fig. 12.

A plausible ray diagram that explains the promptness of the high frequency enhancement was suggested by Marston.[M9] The diagram, Fig. 19, should apply to situations where the sign of the group velocity of the guided wave is negative relative to the phase velocity. The enhancement occurs in the general frequency region where a leaky wave on the shell has a negative group velocity. Such a reversal of group velocity was previously known for waves on plates in a vacuum[20,21] at a frequency slightly below that predicted by Eq. (9). [It is necessary to convert to the units of Eq. (9) that pertain to scattering calculations for a shell of the same thickness as the plate.] The ray diagram in Fig. 19 is based on the usual trace velocity matching condition $0 < \sin\theta_l = c/c_l < 1$ and the energy flow follows the group velocity which is in the backward direction. The contribution to the scattering is expected to be prompt since the energy does not need to flow around the backside of the sphere. Indeed, the backside of the target is seen to be irrelevant to the high frequency enhancement. The enhancement may be relevant to the sonar detection of objects whose backside is buried, floating, or otherwise obscured to sound in water.

Support for the negative-group velocity mechanism diagramed in Fig. 19 was evident when a graduate student working in this project, D. H. Hughes, discovered a previously unknown class of complex-ν plane poles for fluid loaded shells that become relevant in the frequency range of the high-frequency enhancement.[M14] Here ν is the complex partial wave index and the poles correspond to roots of $D_\nu(ka) = 0$ where $D_n(ka) = 0$ is the denominator

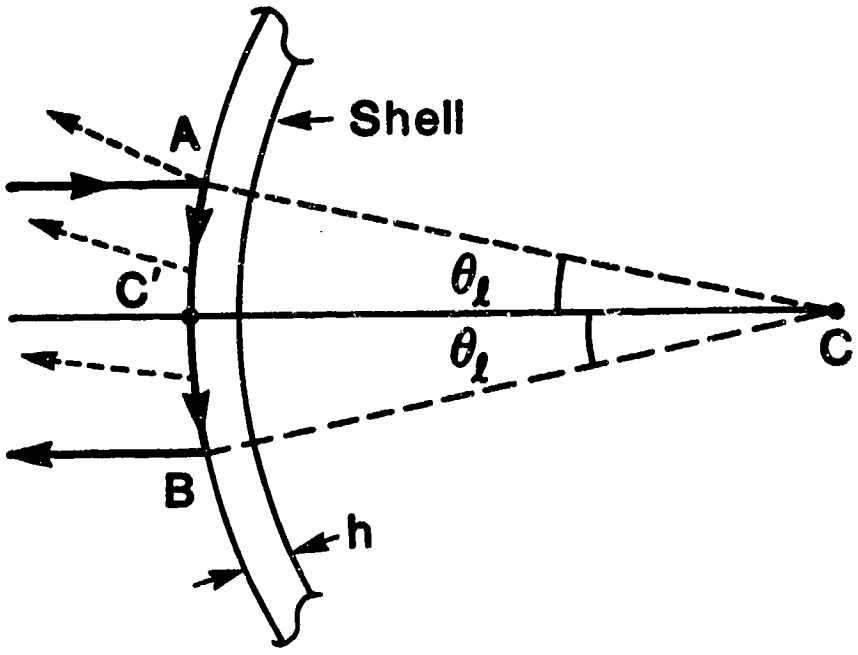

Figure 19 -- Possible mechanism for the prompt enhanced backscattering calculated in Figs. 17 and 18 to occur for a narrow range of ka at high-frequencies. It is necessary for there to exist leaky Lamb waves having negative group velocities with only moderate damping. The phase velocity of the wave coupled at A is clockwise but the energy flux is counterclockwise. The trace velocity condition is matched for backscattering at B. From symmetry there is superposed ray directed from B to A.

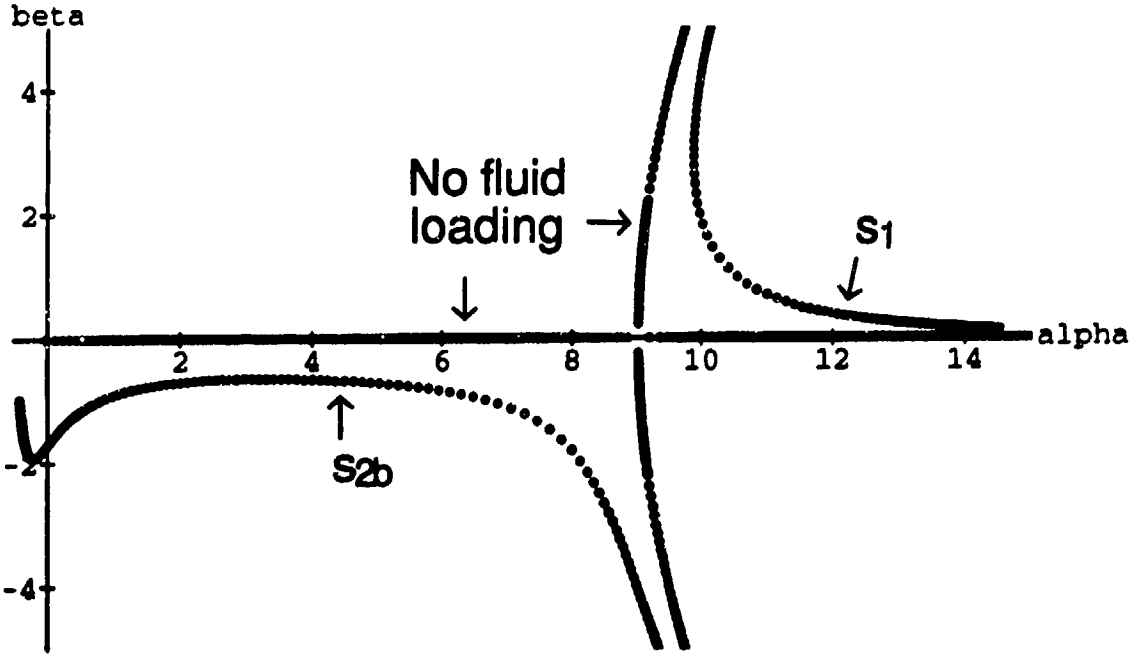

Figure 20 -- The mechanism described in Fig. 19 may be facilitated by a new class of complex-ν plane poles generally lying in the 4th (or 2nd) quadrants of $\nu_l = \alpha_l + i\beta_l$. This figure shows the loci of such poles for a thick stainless steel shell (with and without fluid loading) as ka is varied close to the s_1 mode threshold near ka of $(ka)_{LR}$ 76.8.

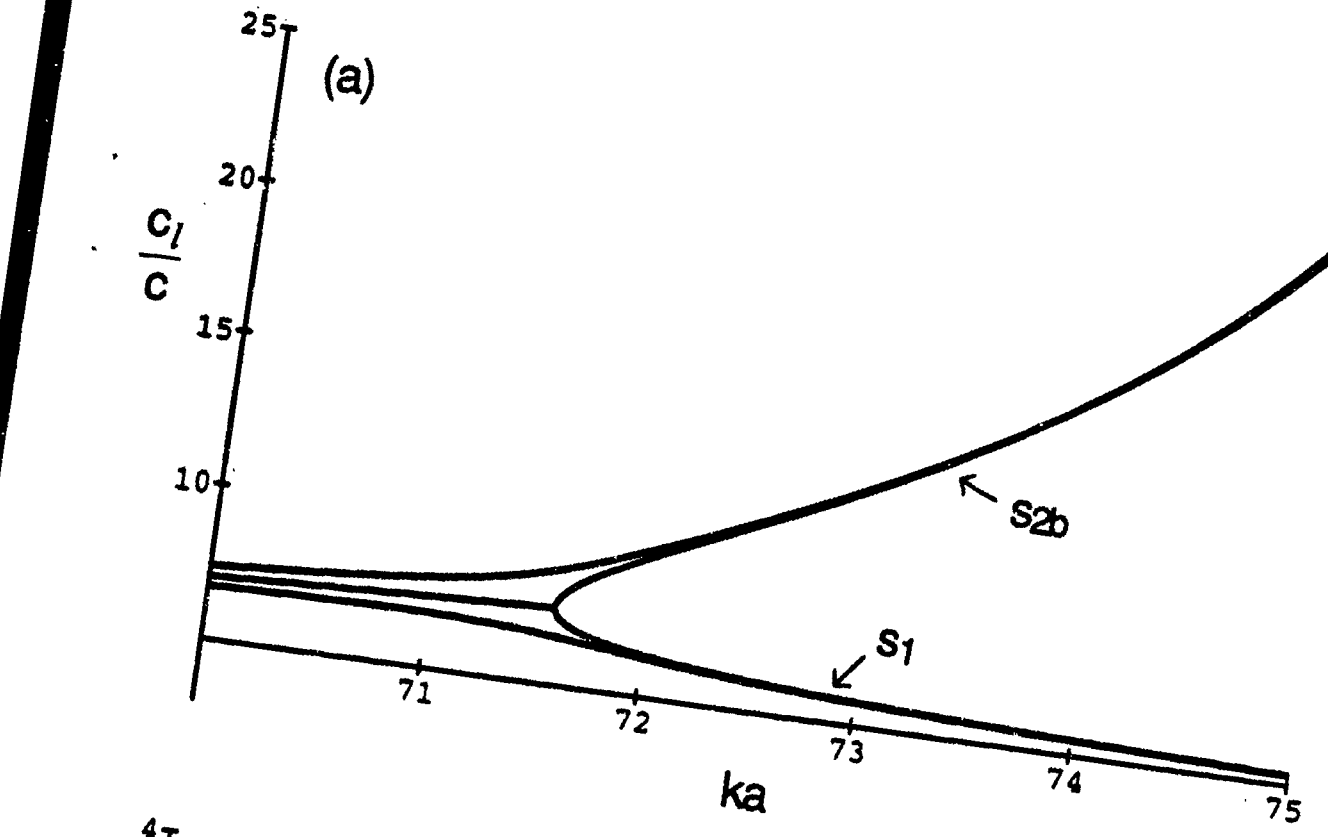

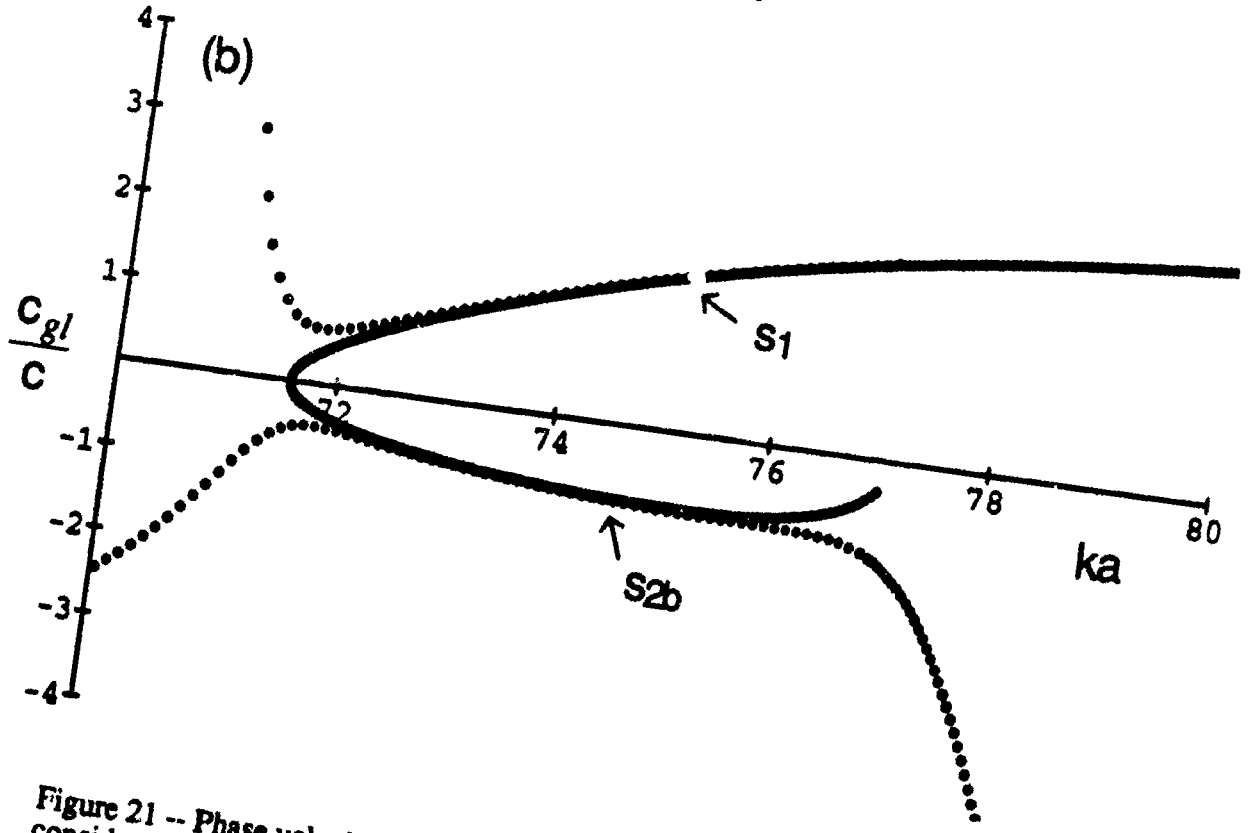

Figure 21 -- Phase velocity c_l(a) and group velocity c_{gl}(b) for the thick stainless steel shell considered in Fig. 20 with and without fluid loading. The curves are shown for the frequency range in ka where the root labeled $l = s_{2b}$ propagates with $c_{gl} < 0$ in the unloaded case. For the fluid loaded case the s_{2b} is shown to propagate with $c_{gl} < 0$ over a wider range of ka.

of the nth term of the partial wave series. (See the discussion of Fig. 3 and the relationship between roots and wave properties reviewed in Refs. 2, 4, J1, and J4.) To appreciate Hughes's discovery it is necessary to summarize these relationships for spheres. For the lth class of guided wave at a frequency ka, the root of $D_\nu(ka) = 0$ is denoted by $\nu_l = \alpha_l + i\beta_l$ where the phase and group velocities are

$$c_l/c = x/(\alpha_l + 1/2), \quad c_{gl}/c = (d\alpha_l/dx)^{-1}, \tag{10,11}$$

where $x = ka$. For the usual class of leaky waves considered ν_l lies in the first quadrant of the complex plane and c_l and c_{gl} are both positive. Hughes discovered a previously unknown class of roots generally lying in the second and fourth quadrants of the complex ν planes. The root trajectories are such at c_l and c_{gl} have opposite signs. For example, the fourth quadrant roots have $\beta_l < 0$, $c_l > 0$, and $c_{gl} < 0$. (Note that a negative value of β_l does not actually imply a growth of the wave with propagation around the shell since the ray direction is reversed in Fig. 19 from the usual situation in Fig. 1. Since c_l diverges as α_l approaches - 1/2, the actual mode threshold for this root lies outside the fourth quadrant. Poles exhibit a reflection symmetry about $\alpha_l = -1/2$, $\beta_l = 0$ so that fourth quadrant poles are mirrored in the second quadrant.) Unfortunately there are computational difficulties in tracking the new complex ν poles over the entire ka interval of interest for thin shells though the existence of such poles has been verified.

For the purposes of the present summary, the numerical results will be illustrated by considering an empty spherical shell of 440C stainless steel having $h/a = 0.162$ so that Eq. (9) gives $(ka)_{LR} = 76.8$. This is the same shell for which the pole trajectories for ν in the first quadrant were previously studied by Kargl and Marston.[2,4,5,J1] Computations for this shell exhibit a high frequency enhancement anomaly near ka = 72 (see Fig. 7 of Ref. J1.). Figure 20 illustrates the relevant root loci including the new fourth-quadrant root. These waves are designated by $l = s_1$ and $l = s_{2b}$ though the reader is cautioned that in the related problem of Lamb waves on a plate in a vacuua, the notations used to denote the wave branch with $(c_l/c_{gl}) < 0$ differ widely among various authors.[19-22] Figure 21 shows the resulting calculation of c_l and c_{gl} for the relevant class of surface guided waves. Prior to examining the trajectories for the fluid loaded shell, the trajectories are examined for a shell in a vacuum by letting the density ρ for the outer fluid (water) vanish. Then the consequences of taking ρ = water = 1.0 g/cm^3 are examined. In both cases the frequency units are taken to be $x = ka$ where $k = \omega/c$ and c is fixed at 1.479 km/s, the speed of sound in (real) water. For the shell in a vacuum the loci of the s_1 and s_{2b} trajectories are such that the locus of the c_l gives the smooth connected curves with a pitch-fork bifurcation at $x \approx 71.6$ shown in Fig. 21(a). The corresponding c_{gl} curves, the solid curves in Fig. 21(b), show the curve with $c_{gl} > 0$ with $l =$

s_1 connects smoothly with curve with $c_{gl} < 0$ for $l = s_{2b}$. The lower curve loops back to $c_{gl} \approx 0$ when $x \approx (ka)_{LR}$. The loop in the group velocity curve with $c_{gl} < 0$ is like the one predicted for waves on a plate in a vacuum[21] and the calculations for shells by Sammelmann and Hackman[22] based on complex-ka plane poles (presumably with negligible fluid loading). When fluid loading corresponding to water is included in our calculation the dotted curves in Fig. 21(b) are obtained where only the lower curve has $c_{gl} < 0$ and (from the locus in Fig. 20) $\beta_l < 0$. This branch corresponds to the upper continuous curve for c_l in Fig. 21(a). Associated with this branch (that is novel for fluid loaded shells) will be a backward propagating wave as diagramed in Fig. 19. There may be complications in assignment of the amplitude for such ray contributions that are currently being investigated though an approximation suggested by Marston[9] appears to be sufficient for explaining the order of magnitude and general position of the enhancement.

It is appropriate to note that Kargl[5] found a different class of negative group velocity first-quadrant poles present only in a more restricted range of ka that for the present example corresponds $ka < 70.5$. There is computational evidence for thinner shells that the fourth (and second) quadrant class of complex-ν poles relevant to Fig. 20 are the ones associated with the high-frequency backscattering enhancement.

B. Radiation Mechanisms for Evanescent Tone Bursts on Fluid Loaded Membranes and Plates.

This line of experiments was started to investigate various mechanisms for radiation by subsonic flexural wave tone bursts on membranes and plates. Ordinarily the evanescent wavefield of a subsonic flexural wave would be trapped to an infinite flat plate. In the presence of curvature, tunneling leads to radiation as diagramed in Fig. 2 for a guided wave that is only slightly subsonic near the coincidence frequency. Radiation is possible for a flat plate or membrane in response to a perturbation of the wavefield. This is diagramed in Fig. 22 for the case of an external obstruction.[B2] Radiation into the fluid may similarly result when a subsonic wave impinges on internal structures such as a rib or at a sudden transition in fluid loading such as when a wave on a plate crosses an interface into water.

Since the problems of interest concerns subsonic flexural waves, it was decided to excite such waves directly with an electromagnetic acoustic wave transducer (EMAT) rather than by driving the reciprocal of the process to be studied with an external sound wave. When such transducers are used for surface waves, the typical application is for frequencies above ~ 1 MHz.[23] In the present application the typical frequency is ~ 100 kHz or less and the width of the region to be excited exceeds ~ 5 inches. The initial

experiments for this aspect of Marston's research program involved the proof of principal for the use of meanderline EMATs to excite low frequency flexural waves. The experiments were done on a stretched aluminized Mylar membrane in air.[J8,I1,M3] The resulting tone bursts driven on the membrane were then used to develop wave-number selective optical and electrical displacement transducers for detecting such bursts.[J8] Some of those transducers were subsequently found useful for detecting flexural wave tone bursts on plates.

Flexural tone bursts on aluminized Mylar that were subsonic relative to the surrounding air were used to confirm one of the radiation processes illustrated in Fig. 22. The tone bursts had a frequency f = 4 kHz, a wavelength along the Mylar λ_f = 1.5 cm, and a phase velocity c_f = 62 m/s. The predicted evanescent pressure field near the membrane is[24,B2,J9]

$$p = p_0 \exp(-k_y y) \exp(ik_x x - i\omega t), \qquad k_y = (k_x^2 - (\omega/c))^{1/2} \tag{12,13}$$

where here c = 340 m/s becomes the speed of sound in air, $k_x = 2\pi/\lambda_f$, and k_y = 1/(2.43 mm). The problem of diffraction of an evanescent sound wave by a (rigid) sharp edge has been considered for the corresponding optics problem by Felsen[24] and others. The analysis should apply to the present situation when the wave scattered by the edge is only weakly rescattered by the membrane. The two-dimensional result may be put in the form

$$|p_{scat}| \approx p_0 \, A r^{-1/2} \exp(-k_y h), \tag{14}$$

where h is the distance of the edge from the membrane, r is the distance of the field point from the edge, and A is a constant. To test this result, a sharp metal blade was used as a barrier and a probe microphone was mounted a small distance away as shown in Fig. 23(b). Tone bursts were used that typically exceeded 10 cycles in length but were sufficiently short to discriminate in time certain background noise sources. (In addition, certain repeatable background noises were subtracted from all of the temporal records.) The blade distance from the membrane h was varied while the microphone was held fixed. It was not possible to achieve acceptable signal-to-noise levels with the microphone in the true farfield of the barrier ($\omega r/c >> 1$). The microphone was sufficiently distant, however, that variations in r had a negligible effect on the received signal for a gap h up to about 1 mm. The observations, Fig. 23(a), confirm that the scattered signal is largest when the blade is close to the membrane but not in contact with it. Furthermore, the signal decreases with increasing h roughly in proportion to $\exp(-k_y h)$ as predicted from a theory that neglects rescattering by the thin membrane. The experiment confirms that perturbations of an evanescent acoustic wavefield do indeed result in scattering.[J9,I2,M15]

Figure 22 -- Radiation to the farfield can occur if objects are placed in the evanescent wavefield of a subsonic wave packet (from Marston, Publication B2).

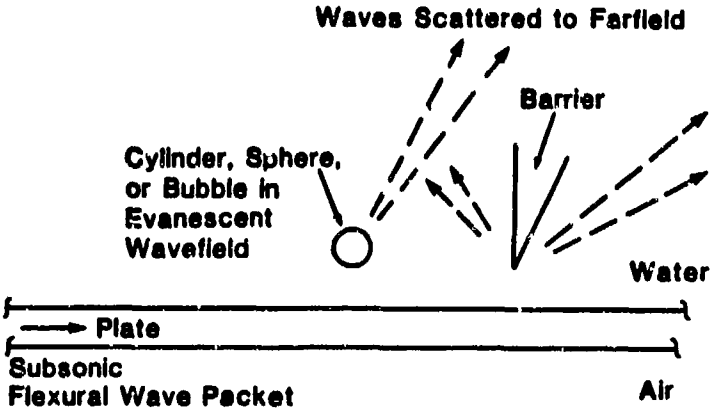

Figure 23 -- Confirmation of the diffraction process illustrated in Fig. 22 but for a subsonic wave packet on a membrane in air.

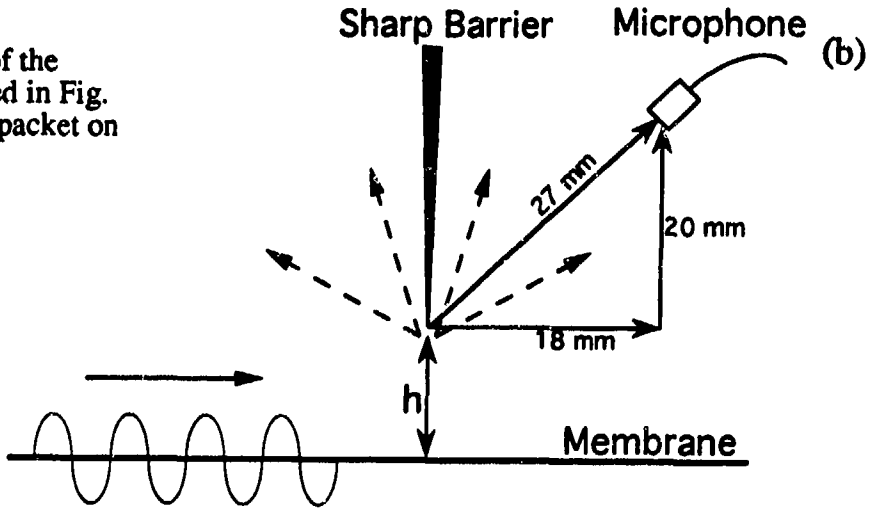

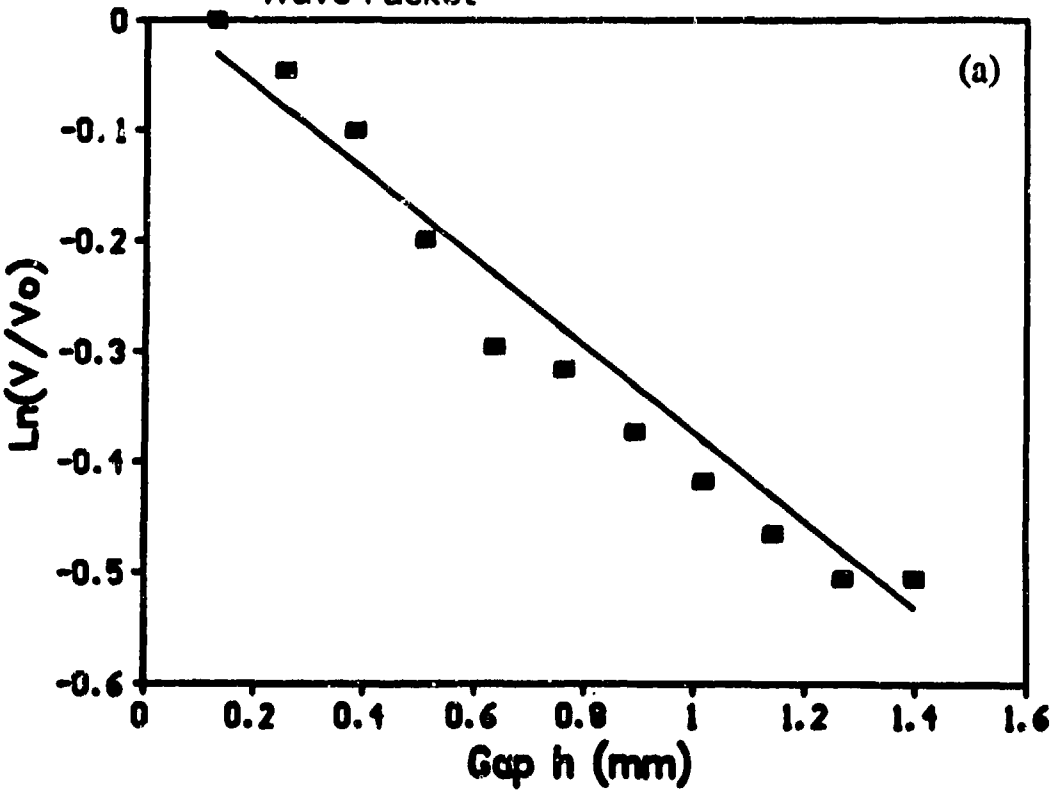

The principal recent effort has been to establish a technical capability of exciting tone bursts of waves on metal plates near and below the coincidence frequency with water on both sides of the plate and to probe the pressure field near the plate. Some of the motivations for establishing this capability will be evident from the discussion below and from the research proposed in Sec. III. The approach has three technical aspects: (a) water tank facility, (b) mode selective EMAT source, and (c) probes of the acoustics field in the water. Progress is summarized as follows: (a) *Tank:* to avoid interference with scattering experiments carried out in the large 12 ft diameter × 8 ft deep tank mentioned earlier, a second wooden tank, 8 ft diameter by 8 ft deep was assembled adjacent to the large one. The tanks use a common metal platform to facilitate access to the experimental region and each is mechanically isolated from adjacent structures. See Section V. (b) *EMAT Sources:* The source was developed in cooperation with Dr. Bruce W. Maxfield (Industrial Sensors and Actuators, San Leandro, CA) drawing upon his previous experience.[23] A functional diagram is shown in Fig. 24. (The transducer is mounted above the water and the plate bends down into the water in a manner to be described subsequently.) A tone burst of current is applied to antisymmetric coils adjacent to the plate but not in contact with it. (The actual coils used differ in detail from the meander coils diagramed.) The plate thickness (1/8 inch) is much thicker than the skin depth for the typical frequencies used (~ 30 kHz and ~ 100 kHz). The coils induce opposing currents on each side of the plate such that current loops are completed near the edges of the plate. Those currents result in oppositely directed Lorentz forces, which if properly balanced produce a pure couple (or torque) that cause the plate to bend. The coils are periodic with a period 2b = 1.5 cm. Consequently, counter propagating antisymmetric Lamb waves are excited having a wavelength of 2b. (Wavelengths that are multiples or certain rational fractions of 2b have also been excited.) When the frequency is selected so that 2b matches the wavelength of a mode, the waves are reinforced by adjacent coils such that the amplitude of the radiated wave is increased by the number N = 8 of complete coil cycles. The magnetic field strength B is 4 kGauss and with the available current source, the displacement amplitude of the radiated Lamb wave tone burst is about 10^{-9} m. The amplitude was inferred by using a differential wavenumber selective capacitor microphone as originally proposed. (c) *Probes of the Acoustic Field:* The wave packets propagate from the plate in air to the portion of the plate in water. This can result in a superposition of leaky and evanescent wavefields near the plate. Hydrophones are used to probe this wavefield which are positioned by a two-dimensional stepper motor positioning system. Figure 36(b) of Section V is a photograph of the EMAT and plate and positioning system as mounted above the tank.

Figure 25 illustrates one of the experimental configurations studied for a flexural wave on a 0.125 inch thick aluminum plate. (By setting the phase velocity in a vacuum of

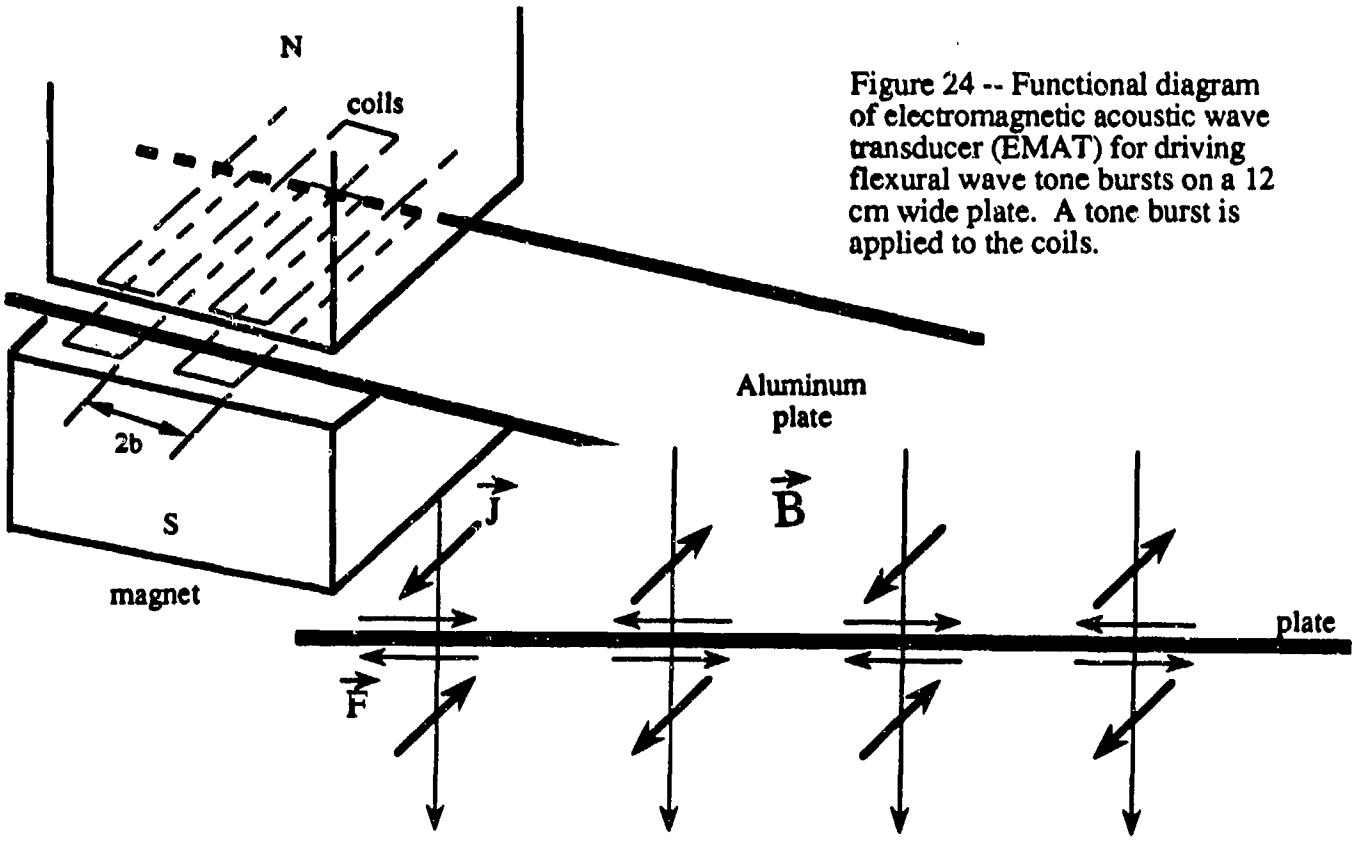

Figure 24 -- Functional diagram of electromagnetic acoustic wave transducer (EMAT) for driving flexural wave tone bursts on a 12 cm wide plate. A tone burst is applied to the coils.

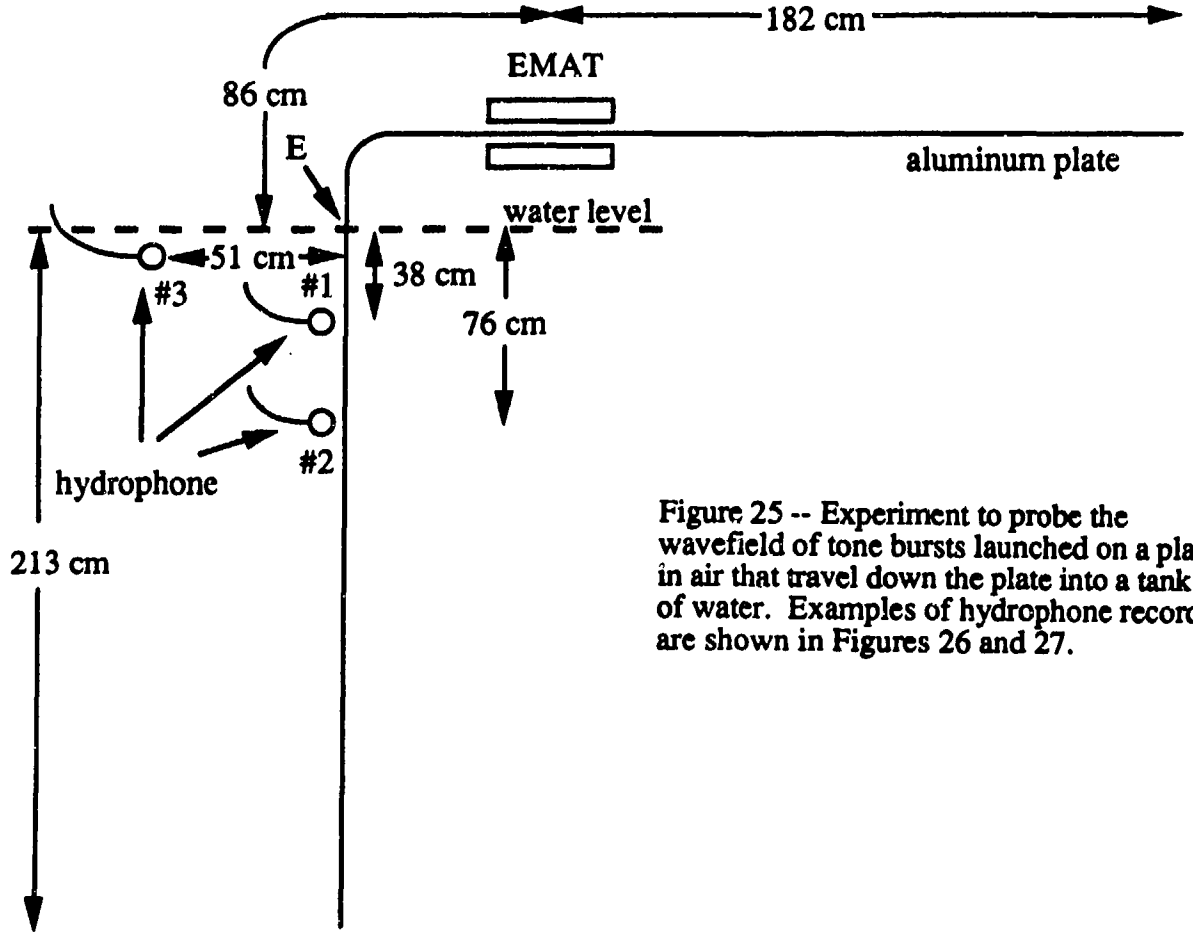

Figure 25 -- Experiment to probe the wavefield of tone bursts launched on a plate in air that travel down the plate into a tank of water. Examples of hydrophone records are shown in Figures 26 and 27.

the a_0 Lamb wave to the speed of sound c in water, the coincidence frequency f_c is estimated to be 89 kHz.) Figure 26(a), (b), and (c) illustrates representative time records with the hydrophone located respectively in the positions labeled 1, 2, and 3 in Fig. 25. The hydrophone separation from the plate for positions 1 and 2 was about 3 mm. The records are for 12 cycles of drive to the EMAT with a carrier frequency of 32 kHz where the phase velocity c_l is subsonic with respect to the velocity of sound c in water. The early time signal on the left is due to direct electrical pickup of current tone burst that drives the EMAT. The larger of the bursts near the center and right of (a) and (b), respectively, are primarily from pressure variations in water resulting from the passage of a flexural wave packet on the fluid-loaded plate. Its group velocity c_g is 1.6 mm/μs as determined from the time shift and difference in propagation distances between (a) and (b) and agrees with predictions. The signal near the left side of (c) has a delay time characteristic of propagation directly from where the plate enters the water, E in Fig. 25, to the hydrophone at position 3. (The calculation of the arrival time includes the delay for the wave packet to propagate from the EMAT to point E.) The decay of amplitude with the distance y from the plate is weaker than predicted by Eq. (12) which is to be expected if the signal is radiated from a line source at E instead of decaying as an evanescent wave. This radiation mechanism is described below. It is remarkable that the signal in Fig. 26, as well as those for Fig. 27 described below, confirm that the properly aligned EMAT is highly selective in the plate mode excited so that only the a_0 mode is driven.

Figure 27 displays records for excitation of the EMAT with 16 cycles at 106 kHz. The hydrophone positions for (a) and (b) are positions 1 and 2 of Fig. 25 and the wave packets again are primarily from pressure variations in water resulting from the passage of a flexural wave packet on the fluid-loaded plate. The wave packet in (c) corresponds to direct radiation form a line source at E but the hydrophone position is not shown in Fig. 25 being at a depth of 50 cm and a horizontal distance from the plate y of 50 cm.

From the delay times for the wave packets shown in Figs. 26 and 27 (and other records not shown) the following is evident: when the hydrophone is far from the plate, the signal is dominated by direct radiation from where the plate enters the water. We call this radiation transition radiation because of a similar terminology used to describe the electromagnetic radiation from relativistic charged particles when they cross the surface of a dielectric. A detailed inspection of the records in (a) and (b) of Figs. 26 and 27 suggests that those records also contain a transition radiation component. That the wavefield consists of a superposition is in agreement with the following considerations.

First consider the wavefield near an infinite plate for which the pressure vanishes on an unbounded perpendicular plane corresponding to the free water surface in Fig. 25.

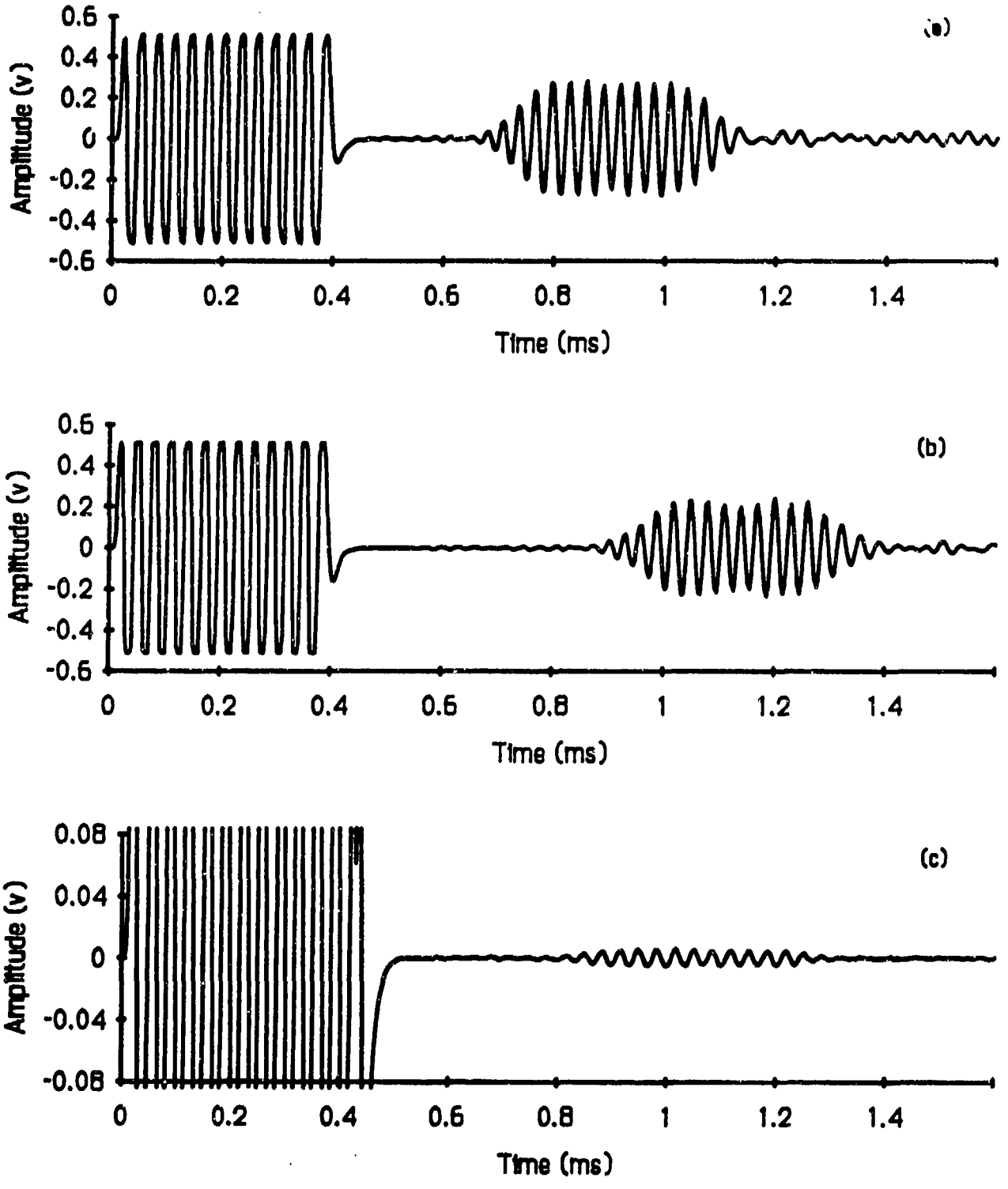

Figure 26 -- Hydrophone records for 32 kHz flexural-wave tone burst on a plate.

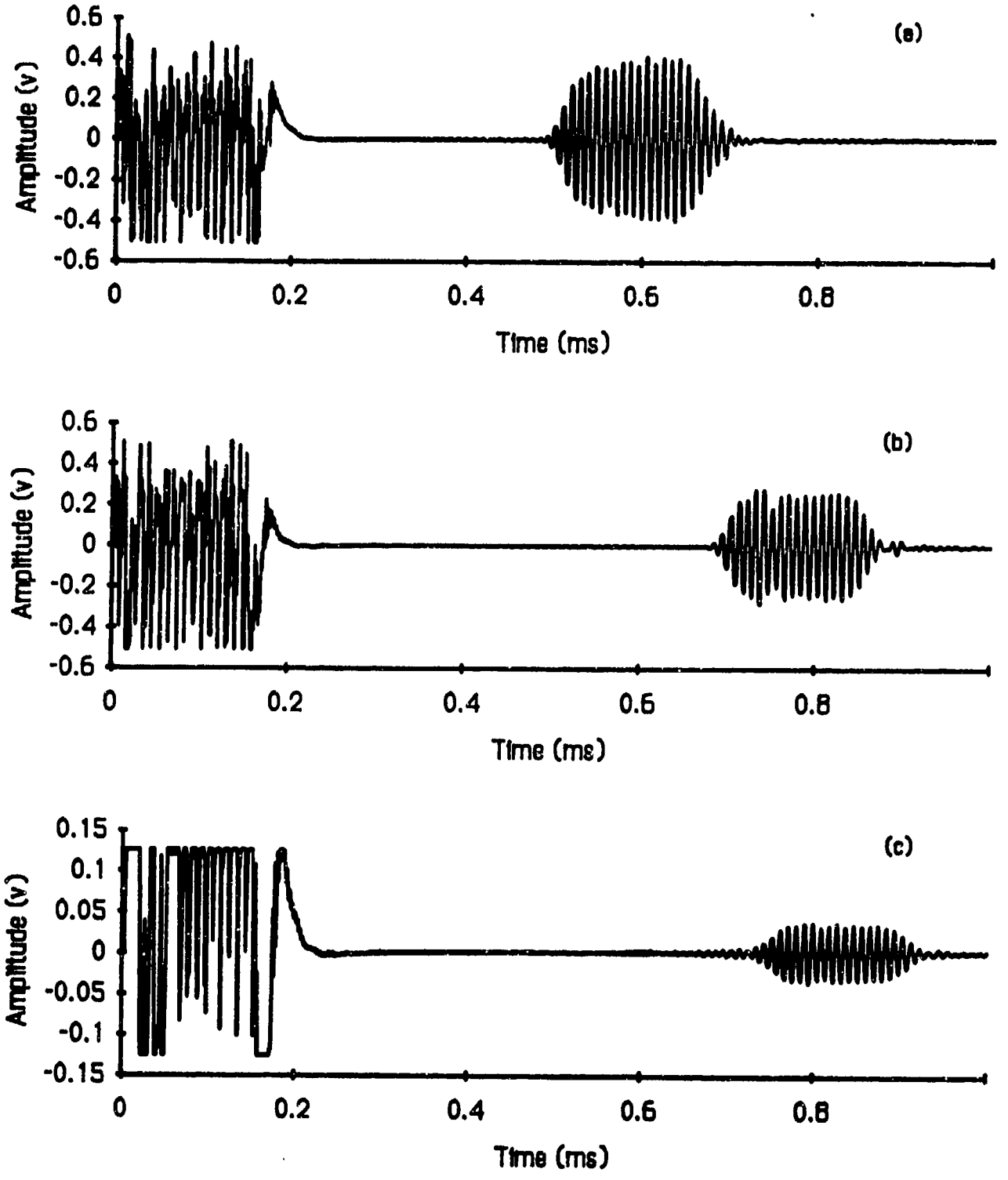

Figure 27 -- Hydrophone records for 106 kHz flexural-wave tone burst on a plate.

The wavefield that meets those boundary conditions in the presence of a plate corresponds to that of a harmonic moment (or torque) applied at the line where the plate crosses the free surface of the water. The wavefield given by differentiation (with respect to the source coordinate) of the Green's function for a line source on a fluid-loaded plate as described e.g. by Feit[25] but modified to include fluid on both sides of the plate. It is evident from Feit's analysis for excitation below the true coincidence frequency that the wavefield will consist of a superposition of an evanescent wavefield with that of a wave propagating in water from the line source. The direct wave results from nonpropagating bending of the plate localized near the line source. In the present case, localized bending at the free surfaces give rise to the transition radiation. A quantitative understanding of wavefield superposition in the water is needed before meaningful scattering experiments of the type illustrated in Fig. 22 can be completed. This wavefield appears to be a canonical problem of general interest: the radiation from a line moment. The experiment has the added complication of the finite width of the plate.

Summary of experimental results: The diffraction of evanescent waves by a barrier in air was demonstrated and the variation of signal level with barrier position is in agreement with a simple approximation that neglects the rescattering of the waves by the membrane. The experiments for flexural waves on a plate in water are more complicated due to the nature of the wavefield generated when the flexural wave packet propagates along the plate into the water. The EMAT driver for the plate waves was found to be highly-mode selective and this greatly simplifies the interpretation of the experiments. In this case the investigation of the wavefield in the water even without any scatterer present is of importance due to the contribution by nonpropagating bending of the plate at the free surface of the water.

C. Acoustical Four-Wave Mixing in Suspensions

For his Ph.D. dissertation completed in 1992, H. J. Simpson investigated a novel mechanism for the interaction of sound with sound.[T2] The new coupling mechanism relies on the slow response to the acoustic radiation pressure of pump waves by the acoustic medium, a suspension of particles in water. Three acoustic waves, two pump wave and a higher frequency probe wave, interact to produce a fourth wave. The coupling mechanism is analogous to optical four-wave mixing in photo-refractive materials.[26,27] The summary of results given below illustrates some of the nonlinear properties of this system, however the reader is referred to the dissertation for technical and theoretical details. The

suspensions studied were dilute, the volume fraction of suspended particles being typically 1.6×10^{-4}. Nevertheless, the wave generated by the interaction was not weak and it could be easily observed with a large signal-to-noise ratio for a properly aligned experiment.

Figure 28 is a diagram of the apparatus. The pump wave transducers are driven continuously and have a fixed frequency of typically 800 kHz corresponding to a resonance for multiply reflected waves within the chamber. [The losses are sufficiently small (since the transducers are backed by air) that it is only necessary to drive the upper transducer in the figure such that the second pump wave is produced by reflections from the lower transducer. The lower pump transducer is used to monitor the pump level.] The suspension consist of 25 μm diameter polymer (Latex) spheres in a saline solution such that the spheres were neutrally buoyant. In response to the radiation pressure of the standing wave some of the spheres migrate toward pressure modes of the standing wave. The amount of enrichment of the local number density of spheres is limited by their Brownian motion. A third wave is introduced in the form of a high frequency (2 - 10 MHz) probe wave. An outgoing fourth wave is produced at the same frequency as the probe wave when the following Bragg condition is met

$$k\Lambda \cos\theta = 2\pi m, \quad m = 1, 2, 3 \ldots \tag{15}$$

where θ is the angle of incidence (for the probe wave) and reflection (for the outgoing wave), Λ is the wavelength of the of the pump wave such that $d = \Lambda/2 = 0.98$ mm is the separation between enriched layers, and $k = 2\pi f/c_0 = 2\pi/\lambda_{probe}$ is the wavenumber of the probe wave. The suspension is confined by acoustically transparent walls of Mylar such that the pump and probe transducers both of water . The apparatus is aligned such that $\theta = 41°$. The probe signal consists of gated tone bursts that are sufficiently long to simulate steady-state Bragg scattering but they are short enough for the radiation pressure of the probe wave to have no significant effect. The absolute amplitude reflection coefficient $|R|$ was obtained with an appropriate calibration achieved by rotating the receiver transducer so as to directly view the transmitted probe wave. Figure 29 gives a diagram of the principal systems used in the experiment.

Figure 30 shows the received tone bursts corresponding to Bragg orders at probe frequencies f of 3.27 and 4.35 MHz. For comparison a weaker 3.77 MHz received signal is shown that is representative of the situation where the Bragg condition is not satisfied. Figure 31 shows a response surface obtained by scanning f and measuring $|R|$. The peak amplitude P of the pump standing wave is also varied beginning with P = 162 Pa and increasing to 9350 Pa. The Bragg peaks are manifested clearly as the parallel rows on this surface.

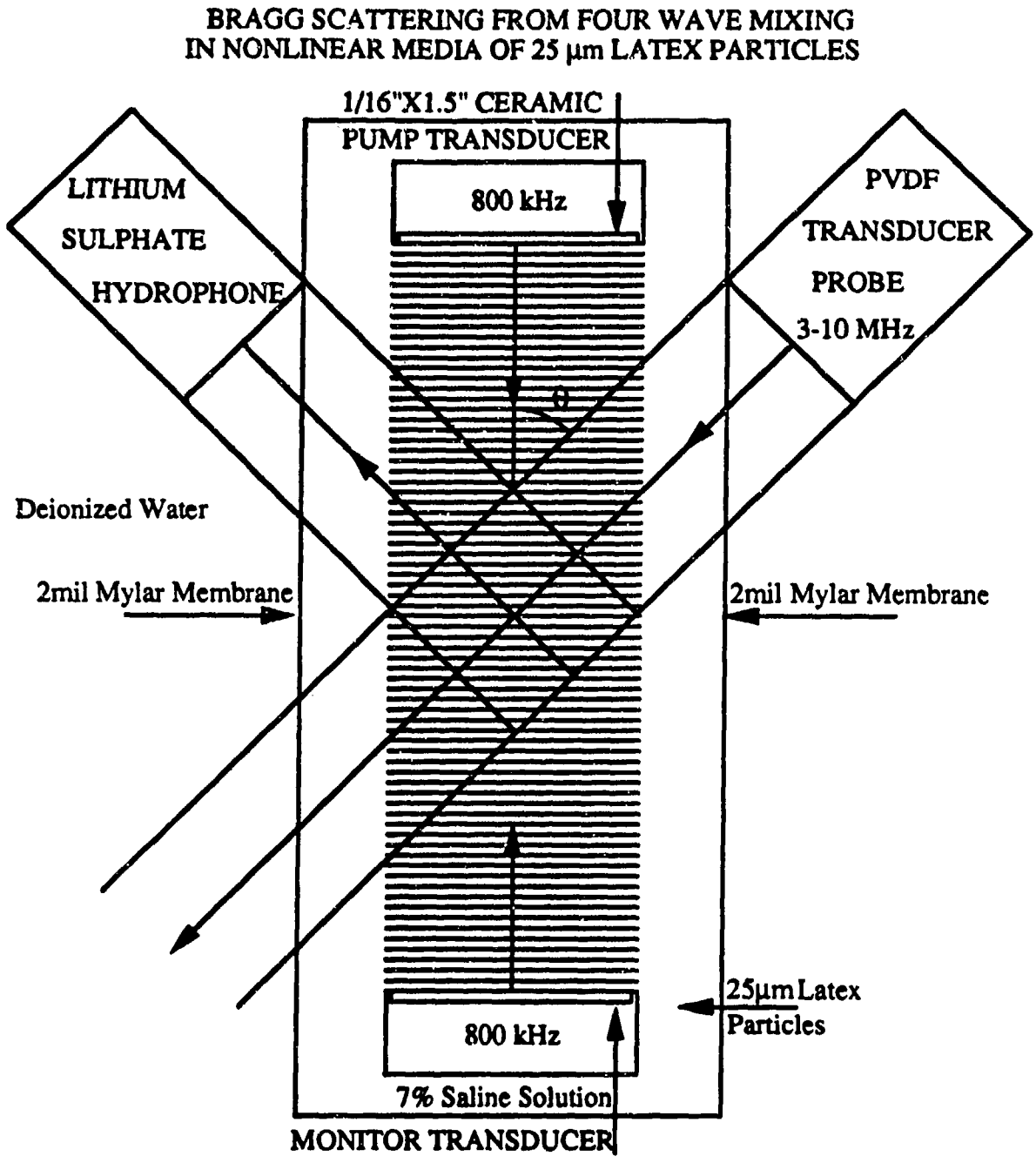

Figure 28 -- A schematic of the experimental setup used to study Bragg scattering from a grating of latex particles. The cell contains a 7% Saline solution used to make the 25 μm latex particles neutrally buoyant, and is enclosed on the sides of the cell with 2 mil Mylar to allow probing of the formed grating with the PVDF transducer. The scattered wavefield is then scanned with the Lithium Sulfate hydrophone.

The development of a theory which was capable of explaining quantitatively the observed values of |R| will now be summarized.[T2] Initially the case of an equilibrium grating will be examined for a fixed pump amplitude P and the situation of an unbounded grating. As a consequence of the small volume fraction of spheres the grating could be treated as collection of noninteracting particles in a spatially oscillating potential well U(z) resulting from the single particle radiation pressure of the standing wave. The local particle number density $n_p(z) = A \exp(- U(z)/k_B T)$ where k_B is Boltzman's constant, T is the absolute temperature, and A is a constant coefficient determined from conservation of the total number of spheres. The coordinate z is parallel to the pump wave vector and perpendicular to each pressure nodal surface of the standing wave. Then the effective variation of sound speed c(z) is calculated using a standard mixture rule that simplifies in the present case where the mass density of the particles and host liquids are the same. The problem becomes one of determining the Bragg scattering from a specified periodic variation c(z). Two approaches are used.

In the first approach the local variation in c(z) is approximated as the profile of an Epstein layer for each spatial cycle. That approach has the advantage that the reflection coefficient R_R for such a single layer is known at all frequencies. It has the limitation that the Epstein layer best approximates the calculated local c(z) oscillations at large pump amplitudes. An additional approximation is made that is analogous to a Born approximation in quantum scattering theory. This is to take the probe beam amplitude as uniform throughout the medium. (Scattering of reflected waves off of other layers is also neglected.) The resulting multiple layer reflection coefficient is approximated as

$$|R(k,\theta)| = \nu N_l \left| R_R(k,\theta) \left[\frac{\sin\left(N_l\, kd\cos\theta\right)}{N_l \sin\left(kd\cos\theta\right)} \right] \right| \qquad (16)$$

where N_l is the total number of reflecting layers crossed by the incident probe beam and $\nu \approx 1/3$ is an aperture coefficient that is calculated geometrically from the volume of overlap between the probe beam and the cylindrical volume viewed by the probe receiver.[T2]

In the second approach the acoustical refractive index $[c_0/c(z)]$, where c_0 is constant, is expressed by a spatial Fourier series. Then analytical results from optics[28] are used for Bragg scattering by a volume grating with specified Fourier coefficients. It is necessary for the Bragg condition, Eq. (15), to be satisfied.

Prior to comparison with experimental results it is appropriate to compare the two theoretical approaches by restricting attention to frequencies f that meet the Bragg condition, Eq. (15). Figure 32 shows that the Epstein layer approximation (dashed curve)

The General Component Configuration for Acoustical FWM

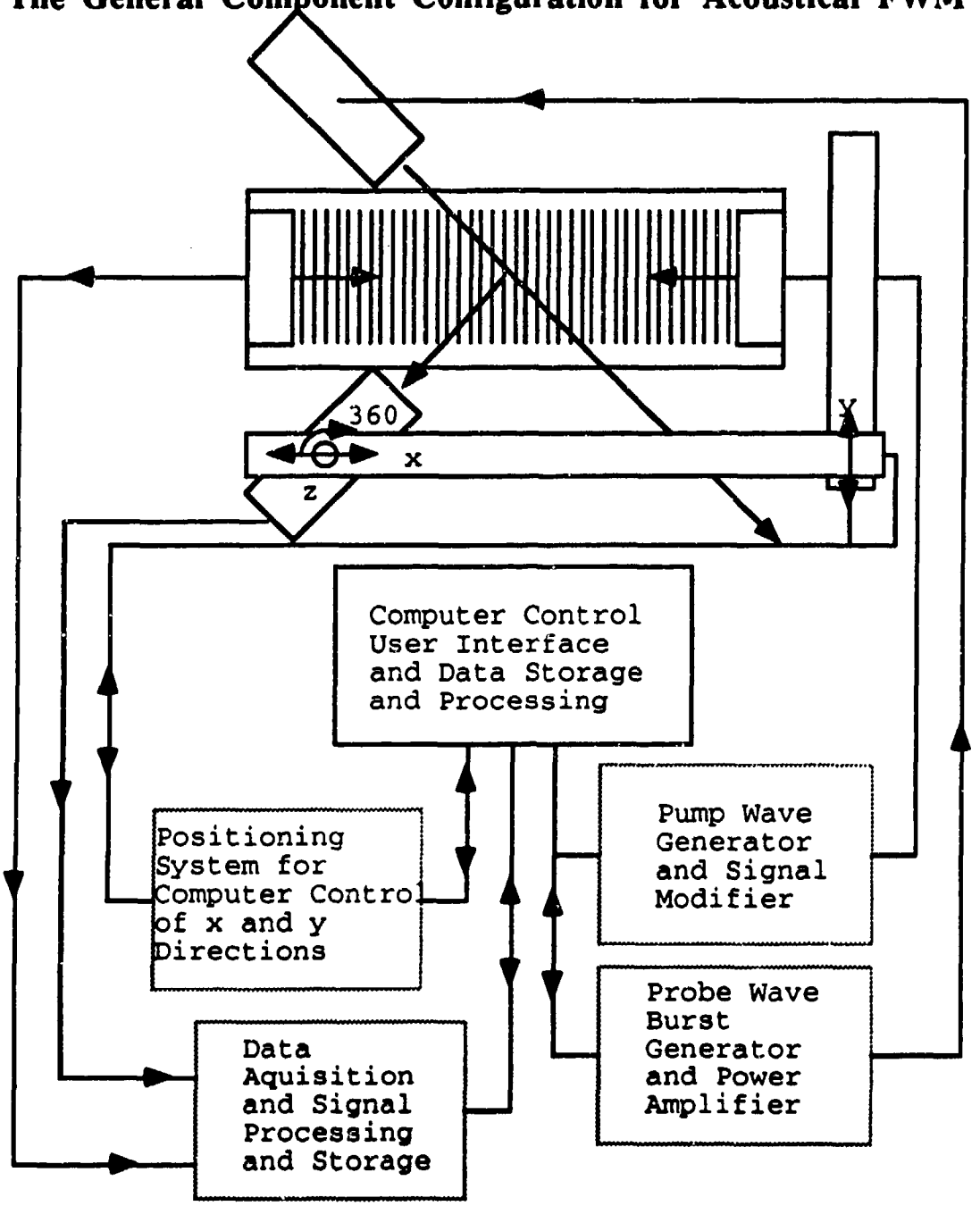

Figure 29 -- Component used to generate, control and measure bulk four-wave mixing. An XT Clone was used to control the rest of the equipment via IEEE488 and RS232 interfaces. Two sets of function generators and power amplifiers were used to drive the pump and probe transducers, and various low noise signal processing equipment was used to measure the standing wavefield and scattered probe wavefield.

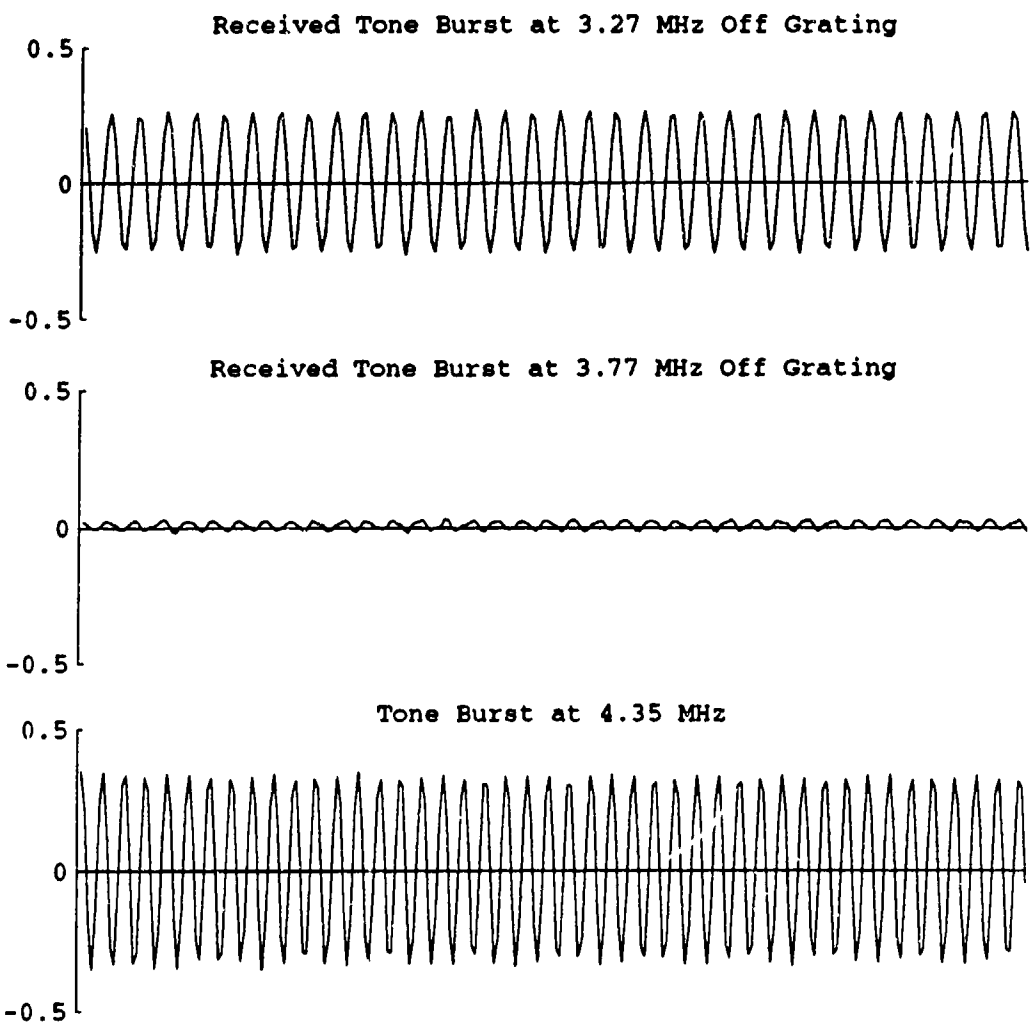

Figure 30 -- Sampled scattered tone burst at various frequencies on and off the Bragg condition. The RMS voltage of the viewed time trace is obtain using an algorithm within the digital oscilloscope. The same algorithm is used to measure the pump voltages. The top time trace shows the scattered response for a frequency that satisfies the Bragg condition. Thus for the geometry of the system and the frequency of the probe wavefield, constructive interference occurs for the reflection from the ensonified layers. For a slightly higher frequency, as shown in the middle time trace, the Bragg condition is no longer satisfied. The bottom time trace shows the next frequency that satisfies the Bragg condition.

Experimental Normalized Reflection Coefficient as Frequency and Pressure are Varied

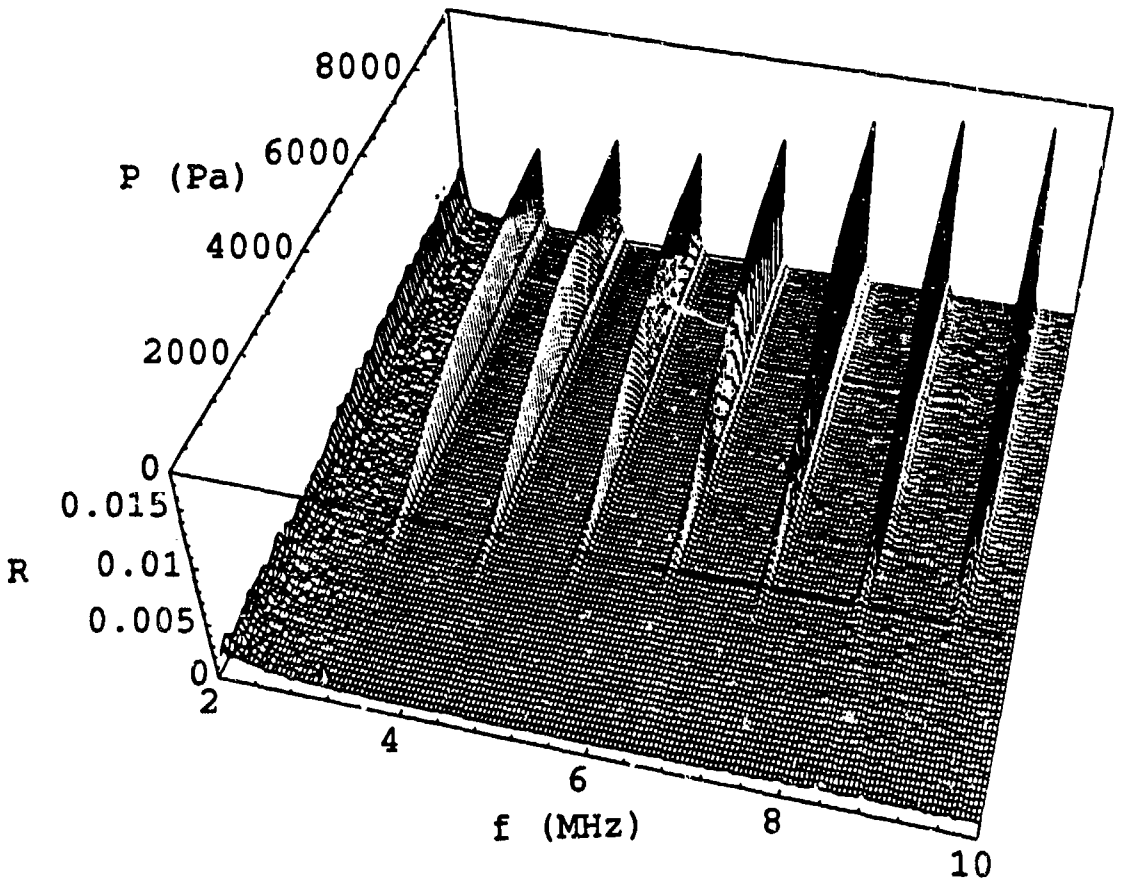

Figure 31 -- Experimental reflection coefficient plotted as the pump amplitude and the probe frequency are varied. The pump pressure is incremented from 162 Pa to 9350 Pa by 102 Pa, where the pressure is maintained constant for 2 minutes. After the 2 minutes, the frequency response of the grating is measured and the pump pressure is then incremented tot he next value.

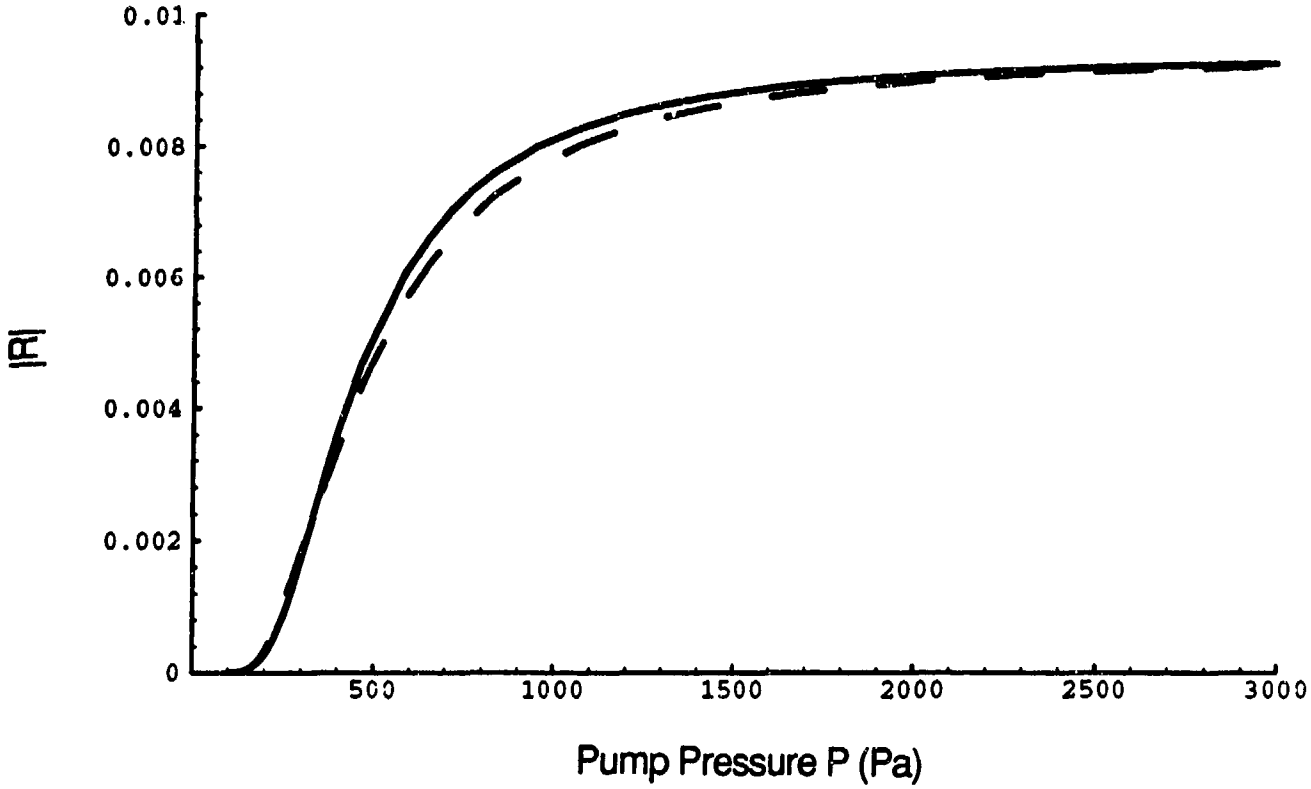

Figure 32 -- Theoretical reflectivity |R| at the 4th Bragg order for an equilibrium particle suspension plotted as a function of pump pressure P. The dashed curve approximates each pressure node as an Epstein layer while the solid curve use a more exact Fourier method.

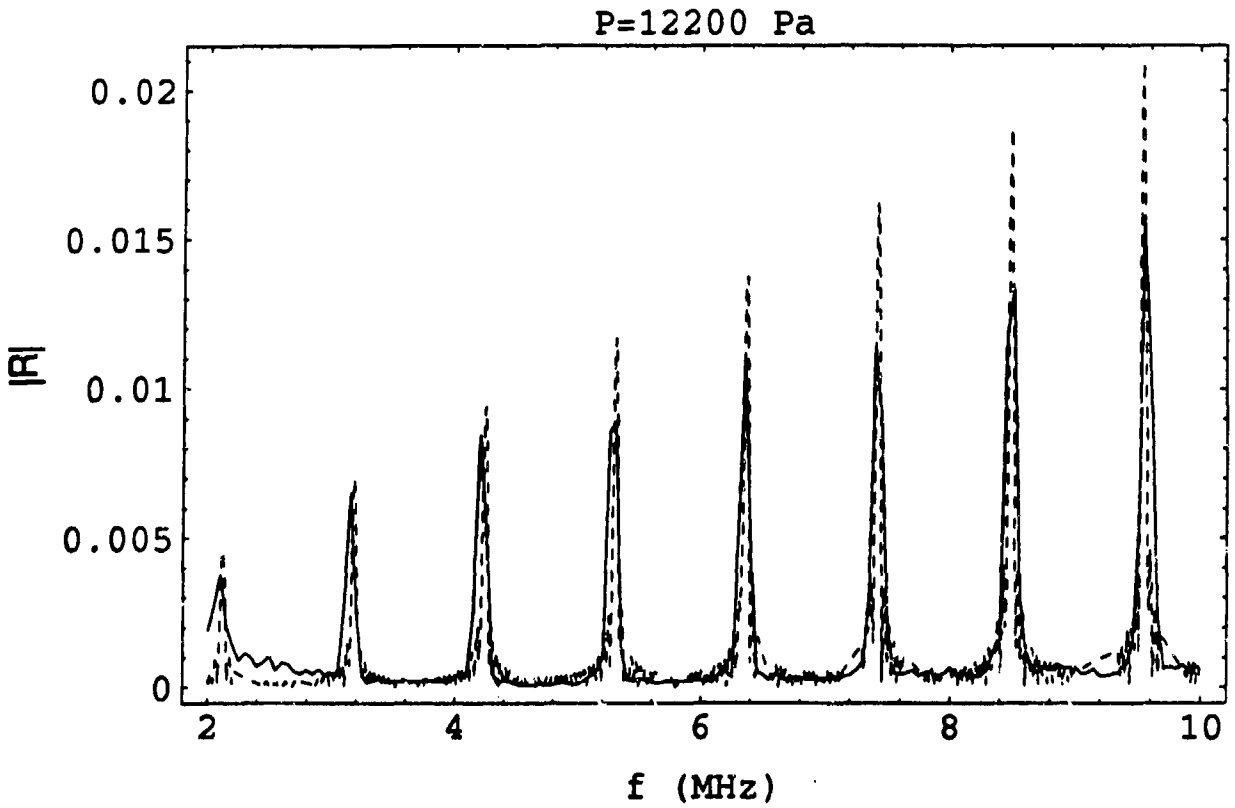

Figure 33 -- The solid curve is the measured reflectivity of the suspension as a function of the probe frequency f. The dashed curve is the theoretical reflectivity using the Epstein layer approximation for the pump pressure P = 12200 Pa.

is remarkably close to the presumably more exact method grating based on the Fourier coefficients.[29] The plot corresponds to the m = 4 Bragg peak at f = 4.44 MHz for conditions representative of the experiment. At low pump amplitudes P the grating reflectance |R| is small because the variations in |U(z)| are << k_BT and the migration of particles to pressure nodes is weak. As P is increased, |R| grows and saturates at close to the same value for both theories. Saturation is associated with the condition $|\Delta U| >> k_BT$ such that the thermal spread of particles along each pressure node is small.[T2] Unfortunately, it is not possible to observe in equilibrium the rise of |R| below approximately 5000 Pa because the time for particles to migrate to the pressure nodes is prohibitively long due to the viscous drag on the particles. Thus neither curve of Fig. 32 actually reproduces the corresponding fixed f slice through Fig. 31 at low amplitudes where the grating has not reached equilibrium.

For the reasons noted above a quantitative test of the equilibrium theory for the conditions of our apparatus must be carried out at large pump amplitudes where |R| has nearly saturated and the different approximations are in good agreement. Consequently, it is sufficient to examine the dependence of |R| on the probe frequency f at fixed angle θ and pump pressure P. Figure 33 shows a representative example of such a comparison between experiment (solid curve) and the approximate theory (dashed curve) given by |R| from Eq. (16). No adjustable scaling parameters were used in the comparison. While the measured peak amplitudes are slightly below the predicted amplitudes, the width of the observed Bragg lines are slightly wider than the predicted ones. This may be a consequence of a plausible lack of perfect spatial periodicity assumed in the theory. It is evident by inspection that the areas of the measured and calculated Bragg lines are similar.[30] The approximate linearity of the predicted peak amplitude with probe frequency f is a result of the single Epstein layer reflectivity $|R_R|$ in Eq. (16) being linear in f for a thin layer.[T2] When the Bragg condition is met, Eq. (16) shows that |R| exceeds $|R_R|$ by a factor $vN_l >> 1$ and from Fig. 33 is seen to be as large as 0.01.

A theory for the time dependence of the grating reflectivity during initial grating formation was also developed and confirmed with experiments.[T2] The situation considered is the initial build up of the grating from an homogeneous suspension when the pump amplitude P is stepped from zero to a constant value. The theory accounts for the initial viscosity-limited migration of spheres to the antinode but not the approach to equilibrium. The scattering theory is based on a time-dependent expansion of the spatial Fourier coefficients and (like the solid curve in Fig. 32) is restricted to probe frequencies f meeting the Bragg condition. Figure 34 show the comparison between the theory (smooth curves) and the experiment (noisy curves) for different values of P. The larger P, the more rapidly

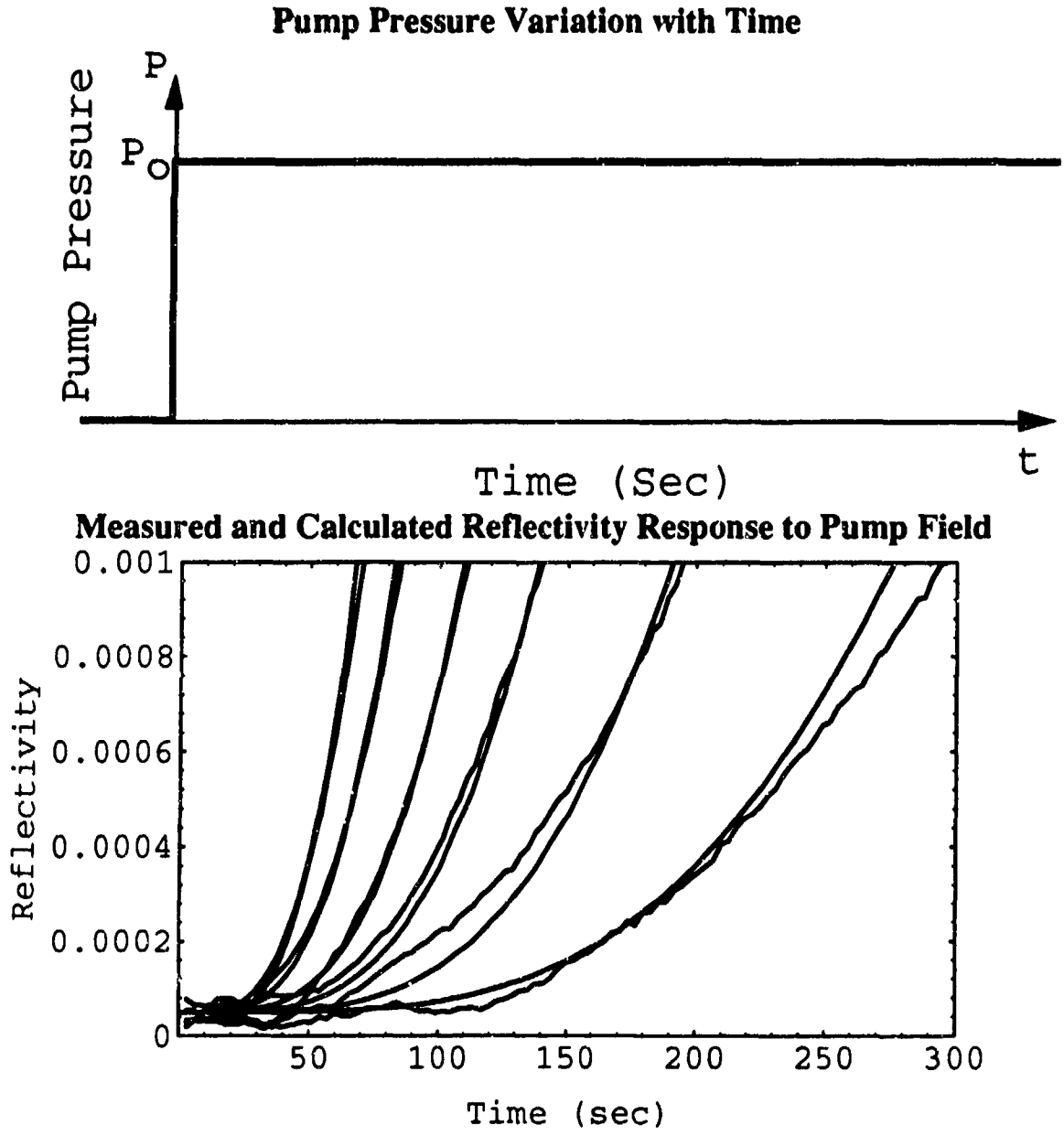

Figure 34 -- Sudden turn on of pump pressure field and measured diffraction efficiency of the forming grating. The curves are the measured and calculated reflection coefficients for the transient grating at times after the introduction of a standing wavefield. Experimentally, the scattered amplitude is measured every 3 seconds and the reflection coefficient is calculated. The pump pressure amplitudes used to calculate the reflection coefficients are 21500 Pa, 19400 Pa, 16900 Pa, 15000 Pa, 12800 Pa and 10700 Pa in order from left to right.

|R| increases with time. The experiments were limited to the fourth Bragg order (m = 4 in Eq. (15)) that for the condition of this experiment gave a probe frequency f = 4.24 MHz. Inspection of Fig. 34 suggests a general but not perfect agreement between the experiment and the theory. The experiment demonstrates the ability to measure much weaker four-wave mixing processes than for the example shown in Fig. 33.

In summary, a new class of acoustical four-wave mixing process has been demonstrated along with approximate theories for the signal strength. The process considered is nonlinear in that if either pump wave is removed there is no signal as indicated by the negligible observed signal at zero time in Fig. 34. A potential application of this process is an all acoustical probe of suspensions since the steady-state (Fig. 33) and time dependent responses (Fig. 34) depend on different suspension properties. In addition to particle size, host viscosity, and volume fraction, the acoustics signal may prove useful for probing specific condensed matter processes. For example, if the volume fraction was increased by a factor of 150 from the conditions observed, the interaction between particles should affect the signal since it would no longer be possible for the particles to migrate to layer along the pressure nodes without coming into contact.[T2] For suspended particles much smaller than the wavelengths of the pump and probe waves, the Bragg scattering should depend only weakly on the particle shape. Other media that should exhibit acoustical four-wave mixing include emulsions and microemulsions.[31]

It is noteworthy that after these experiments were started an experiment was published by Sato et al.[32] that also made use of the response of a suspension to radiation pressure to produce a scattered acoustic wave. That experiment had a more complicated geometry than ours (Fig. 28 and 29) and it made use of additional "fixing" standing acoustic wave to inhibit particle migration during readout by the probe wave. Another difference is that the pump waves were off during readout. Simpson's experiments and analysis clarifies the physical mechanisms and interpretation[T2] of the experiments by Sato et al.

Chapter 6 of Simpson's dissertation describes experimental and analytical results pertaining to a novel mechanism for the three-wave interaction of sound-with-sound at a free surface. That work was carried out early in Simpson's research work with the support of ONR Grant N00014-85-C-0141. It follows from an earlier line of research on the properties of a localized nonlinear layer.

D. Supplemental Scattering Research

In addition to the principal topics of scattering research described in Sections A and B, supplemental topics were examined with the partial support of this grant. The investigations mostly concerned examples of intermediate difficulty that served to reinforce approaches taken on primary research objectives. Most cases involve extensions of research previously supported by ONR Physics Acoustics Core Program Contract N00014-85-C-0141. Perhaps the most important accomplishment in this category was the completion of a survey of geometrically based methods in scattering emphasizing the shape of wavefronts.[B2] Figure 35 shows the table of contents.

1. Reflection by Fluid Shells and Novel Background for Elastic Shells.

Previous research by Kargl and Marston,[5,6] gave a novel ray representation for the contribution to the backscattering due to the multiple internal reflections within an empty spherical fluid shell. The result was found to be in good agreement with novel exact calculations based on a partial-wave series (PWS). At low ka the phase of the scattering in similar to that of a perfectly soft sphere while for large ka (except near longitudinal resonances, Eq. (9)), the phase becomes that of a rigid sphere. Consequently the theoretical case of a vacuum filled spherical shell is a candidate for a general "background" contribution to "isolate" the elastic response of shells. An investigation was carried out by Zhang of how this background serves to isolate the prompt contribution to the high-frequency enhancement of an elastic shell for the case of tone burst.[T1] Computations (Appendix E of Ref. T1.) demonstrate that with this background the prompt elastic contribution appears to be isolated from other contributions for the specific case of a 4% thick aluminum shell considered. Zhang[T1] also found from computations of the backscattering of tone bursts by fluid shells that certain features for ka close to the longitudinal resonance, Eq. (9), were well explained by the ray model of Kargl and Marston.[5] In related work, Marston[B1,B2,M6] extended the previous ray analysis[6] to multiple internal reflections within an empty fluid cylinder. With assistance from Sun, comparisons were made with the exact backscattering as given by a PWS for the empty fluid cylinder. The level of agreement is similar to that shown previously for spheres (Ref. 6) and the comparison has been published in summary form.[B1,B2] Comparison with the sphere case reveals certain geometrical differences in the backscattering contributions by reverberations. The calculation justified the use of the specular echo amplitude to calibrate the backscattering measurement shown in Fig. 16.

2. Focused Backscattering by Liquid-Filled Spherical Reflectors.

— 1 —

Geometrical and Catastrophe Optics Methods in Scattering

PHILIP L. MARSTON

Department of Physics, Washington State University, Pullman, Washington

Figure 35 -- Table of contents of Publication B2 from *Physical Acoustics* Vol. 21.

A previous ray analysis by Marston and Langley of backscattering by fluid spheres described an amplitude enhancement associated with axial focusing or glory scattering.[33] The confirmation by comparison with the partial wave series (PWS) had been carried out for spheres with an acoustical refractive index $N = c/c_{fluid} < 1$. In the present work the analysis and comparison was extended by Marston and Sun to the important practical case of a two-chord glory ray for N between $\sqrt{2}$ and 2. This is the ray that is relevant to focused spherical reflectors used by some acousticians for sonar calibration or for the enhancement of target strength for thin shells filled with a liquid. The comparison confirms the ray analysis for the situation where shell effects are neglected.[B2] The special case of the limit $N = 2$ was also analyzed and confirmed. In that limit the outgoing wavefront has a different shape and the analysis of the focused scattering is different. Both cases are summarized in the survey chapter (section 4.8 of publication B2) to illustrate relationships between wavefront geometry and scattering.

3. Diffraction Catastrophes

In research support by Contract N00014-85-C-0141, Frederickson completed a Ph.D. dissertation on transverse cusp caustics produced by the reflection of sound from a curved metal surface in water.[34] Unlike the work on scattering by shells discussed in Section A, the elastic response of Frederickson's metal surface was unimportant to the formation of the caustic: caustic formation was principally a result of the shape of the reflector. During the final year of present grant, aspects of Frederickson's results were put in a form suitable for publication.[J5]

In research also supported by Contract N00014-85-C-0141, Kaduchak photographed and studied the conditions for the formation of a novel caustic in the backscattering of light by a penetrable spheroid. (The experiment was performed with an acoustically levitated water drop.) Preliminary results were sent to J. F. Nye of Bristol who confirmed[35] a previous conjecture by Marston[36] that the caustic classification was that of an E_6 catastrophe. After taking up a Ph.D. project on scattering by shells,[J7] Kaduchak returned to this project briefly to examine his experimental results with the aid of Nye's analysis.[I5] The research serves to explore the relationship between scattering geometry and caustic classification for a complicated situation not previously considered.

4. Response of Shear Layers Separating from a Circular Cylinder to Small-Amplitude Rotational Oscillations.

J. Filler completed a Ph.D. dissertation on this topic with support from the previous ONR contract (N00014-85-C-0141).[37] Subsequently in 1990 while providing engineering

support to the water tank facility used in scattering experiments (Section V), he put the shear layer research in publishable form.[J2] The experiment demonstrated a novel fluid-structure interaction associated with flow past an oscillating cylinder. The reader is referred to publication J2 or to a review of the results by Griffin.[38]

V. ACOUSTICAL RADIATION AND SCATTERING FACILITY

With the proposal for this research came a commitment by Washington State University (WSU) to provide laboratory space suitable for the water tank facility needed for the research described in Section IV A, B, and C. The needed space was remodeled at the expense of WSU in 1990 while the grant facilitated the procurement of a 6500 gallon (12 ft. diameter × 8 ft. deep) redwood tank. A second 3000 gallon (8 ft. diameter × 8 ft. deep) wooden tank was also installed and the grant was the principal source of support for positioning equipment purchased for use in these tanks. WSU provided a platform to facilitate access by people and equipment to space above the tanks. (The remodeled laboratory space was also used for most of the research on four-wave mixing described in Sec. IV C.) The large wooden tanks were essential to the work and several students and other staff contributed to the facility development and testing including J. R. Filler, D. H. Hughes, G. Kaduchak, T. J. Matula, S. P. Parry, and H. J. Simpson. The summary here illustrates how the facility was used in the supported research. The facility has remained in operation for additional research on radiation and scattering.

Figures 36(a) and (b) are photographs of the facility. Shown in Fig. 36(a) are the adjacent wooden tanks with the larger of the two tanks situated on the right side. The stairway to the platform above the tanks is also visible. The tanks are supported by pumping and water filtration systems that are operated continuously except while data is actually being acquired. Figure 37 illustrates how the large tank was used to acquire the backscattering data shown in Figs. 6-9 where the frequencies used ranged from 220 to 430 kHz. The large tank was needed for the experiments to prevent reflections from the walls, top, and bottom from interfering with the signal of interest. The repetition rate is kept sufficiently low that reverberations have a negligible amplitude at the time of the next ping.

The smaller of the wooden tanks shown on the left of Fig. 36(a) was needed so that the radiation and scattering experiment could be set up and aligned separately. Figure 25 illustrates how the 8 ft diameter tank is used in acoustic radiation experiments. Visible in Fig. 36(b) is the two-dimensional positioning system that is supported above the tank, the EMAT driver (on the left), and the curved aluminum plate that travels down into the water.

(a)

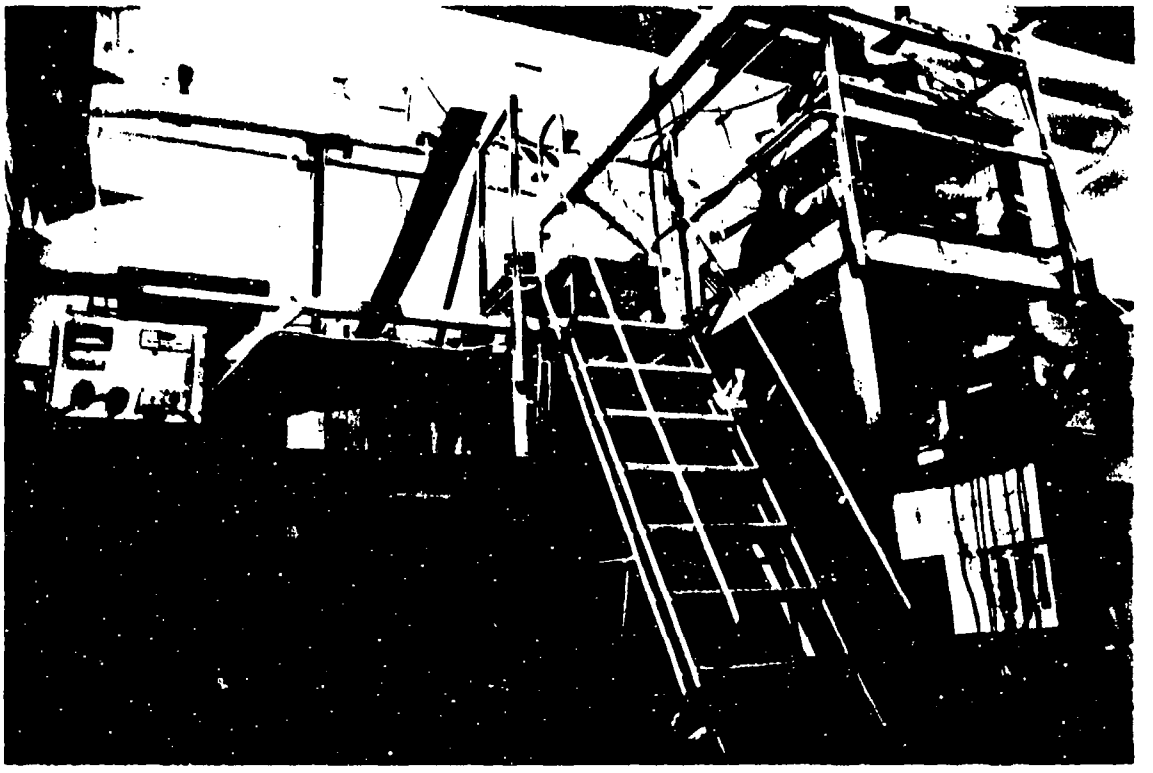

(b)

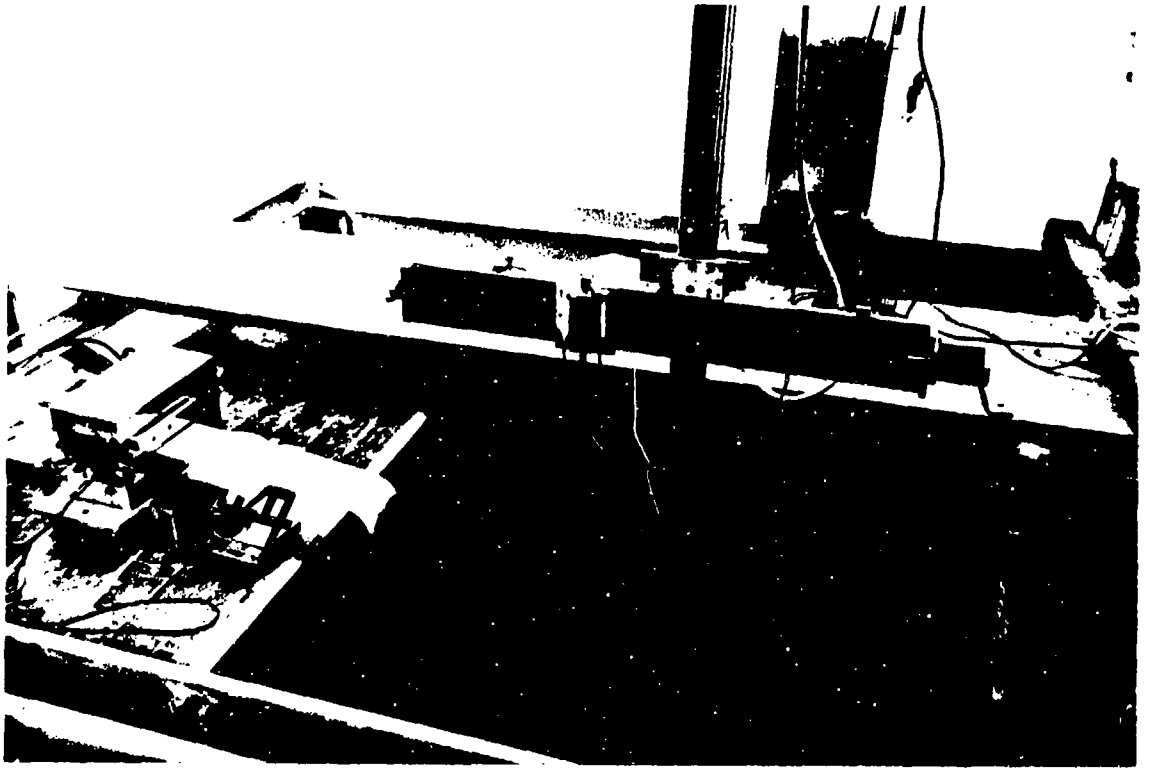

Figure 36 -- (a) Water tank facility for radiation and scattering experiments in water.
(b) Set-up for measuring radiation from flexural wave tone bursts on plates.

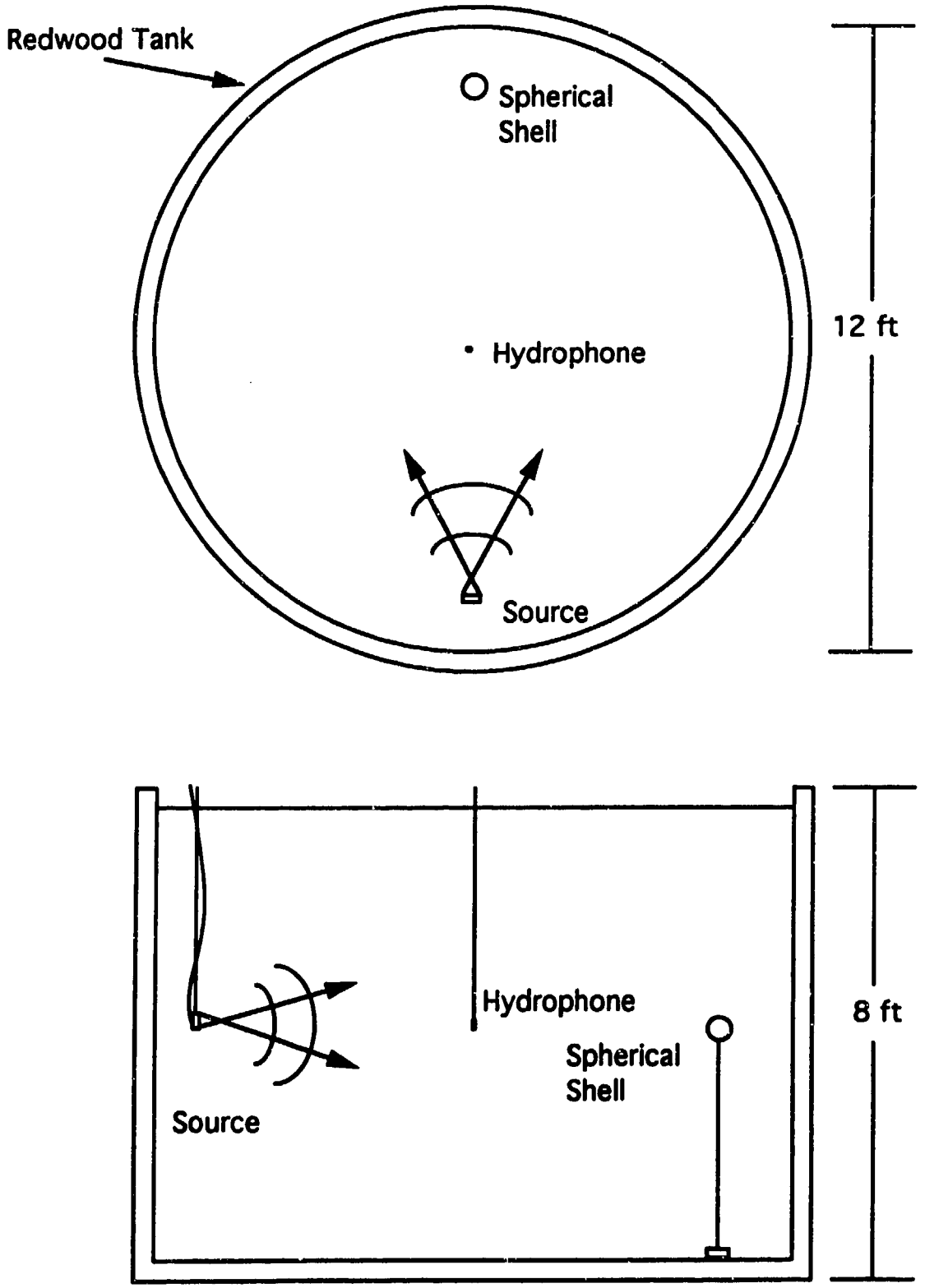

Figure 37 -- Experiment in the large tank for studying the midfrequency of the backscattering by a shell.

VI. REFERENCES

1. P. L. Marston, "GTD for backscattering from elastic spheres and cylinders in water and the coupling of surface elastic waves with the acoustic field," J. Acoust. Soc. Am. **83**, 25-37 (1988); A summary is given in the following abstracts in J. Acoust. Soc. Am. Suppl. **81**, 14 (1987); **82**, 89 (1987); and **83**, 94 (1988).

2. S. G. Kargl and P. L. Marston, "Observations and modeling of the backscattering of short tone bursts from a spherical shell: Lamb wave echoes, glory, and axial reverberations," J. Acoust. Soc. Am. **85**, 1014-1028 (1989); J. Acoust. Soc. Am. Suppl. (abstract) **81**, 14 (1987).

3. K. L. Williams and P. L. Marston, "Backscattering from an elastic sphere: Sommerfeld-Watson transformation and experimental confirmation," J. Acoust. Soc. Am. **78**, 1093-1102 (1985).

4. S. G. Kargl and P. L. Marston, "Ray synthesis of Lamb wave contributions to the total scattering cross section for an elastic spherical shell," J. Acoust. Soc. Am. **88**, 1103-1113 (1990).

5. S. G. Kargl, "Quantitative ray methods for scattering of sound by spherical shells," Ph.D. Dissertation, Washington State University (1990). Report N00014-85-C-0141-TR10; DTIC report number A240255.

6. S. G. Kargl and P. L. Marston, "Longitudinal resonances in the form function for backscattering from a spherical shell: Fluid shell case," J. Acoust. Soc. Am. **88**, 1114-1122 (1990).

7. J. M. Ho and L. B. Felsen, "Nonconventional traveling wave formulations and ray acoustic reductions for source-excited fluid-loaded thin elastic spherical shells," J. Acoust. Soc. Am. **88**, 2389-2414 (1990).

8. L. B. Felsen, J. M. Ho, and I. T. Lu, "Three-dimensional Green's function for fluid-loaded thin elastic cylindrical shell: Alternative representations and ray acoustic forms." J. Acoust. Soc. Am. **87**, 554-569 (1990); erratum **89**, 1463-1464 (1991).

9. M. F. Osborne and S. D. Hart, "Transmission, reflection, and guiding of an exponential pulse by a steel plate in water. I. Theory," J. Acoust. Soc. Am. **17**, 1-18 (1945).

10. W. M. Ewing, W. S. Jardetzky, and F. Press, *Elastic Waves in Layered Media* (McGraw-Hill, 1957) pp. 288-293.

11. P. S. Dubbelday, "Application of a new complex root-finding technique to the dispersion relations for elastic waves in a fluid-loaded plate," SIAM J. Appl. Math. **43**, 1127-1139 (1983).

12. G. S. Sammelmann, D. H. Trivett, and R. H. Hackman, "The acoustic scattering by a submerged, spherical shell. I: The bifurcation of the dispersion curve for the spherical antisymmetric Lamb wave," J. Acoust. Soc. Am. **85**, 114-124 (1989); "The acoustic scattering by a submerged, spherical shell. III: Pole trajectories in the complex-*ka* plane," J. Acoust. Soc. Am. **90**, 2705-2717 (1991).

13. G. C. Gaunaurd and M. F. Werby, "Lamb and creeping waves around submerged spherical shells resonantly excited by sound scattering. II: Further applications," J. Acoust. Soc. Am. **89**, 1656-1667 (1991); "Sound scattered by resonantly excited, fluid-loaded, elastic spherical shells," J. Acoust. Soc. Am. **90**, 2536-2550 (1991).

14. M. F. Werby, "The acoustical background for a submerged elastic shell," J. Acoust. Soc. Am. **90**, 3279-3287 (1991).

15. N. Yen, L. R. Dragonette, and S. K. Numrich, "Time-frequency analysis of acoustic scattering from elastic objects," J. Acoust. Soc. Am. **87**, 2359-2370 (1990).

16. A. H. Nuttall, *Signal Processing Studies*, Naval Underwater Systems Center (1989).

17. D. H. Hughes, Ph.D. dissertation, in preparation.

18. P. L. Marston, S. G. Kargl, and K. L. Williams, "Rayleigh, Lamb, and whispering gallery wave contributions to backscattering from smooth elastic objects in water described by a generalization of GTD," in *Elastic Wave Propagation and Ultrasonic Nondestructive Evaluation*, edited by S. K. Datta, et al. (Elsevier Science, Amsterdam, 1990) pp. 211-216.

19. D. C. Worlton, "Experimental confirmation of Lamb waves at megacycle frequencies," J. Appl. Phys. **32**, 962-971 (1961). [Note: Worlton's analysis of normal surface velocity for the case of antisymmetric Lamb waves is incorrect but that had not been discovered by us until after P2 and M4 were written.]

20. R. D. Mindlin, "Waves and vibrations in isotropic elastic plates," *in* Structural Mechanics (Pergamon, 1960).

21. A. H. Meitzler, "Backward-Wave Transmission of Stress Pulses in Elastic Cylinders and Plates," J. Acoust. Soc. Am. **38**, 835-843 (1965).

22. G. S. Sammelmann and R. H. Hackman, "The acoustic scattering by a submerged, spherical shell. II: The high-frequency region and the thickness quasiresonance," J. Acoust. Soc. Am. **89**, 2096-2103 (1991).

23. B. W. Maxfield and C. M. Fortunko, "The design and use of electromagnetic acoustic wave transducers (EMATs)," Materials Evaluation **41**, 1394-1408 (1983); B. W. Maxfield, A. Kuramoto, and J. K. Hulbert, "Evaluating EMAT Designs for Selected Applications," Materials Evaluation **45**, 1166-1183 (1987).

24. L. B. Felsen, "Evanescent Waves," J. Opt. Soc. Am. **66**, 751-760 (1976).

25. D. Feit and Y. N. Liu, "The nearfield response of a line driven fluid-loaded plate," J. Acoust. Soc. Am. **78**, 763-766 (1985).

26. J. Feinberg, "Photorefractive nonlinear optics," Physics Today **41**, 46-52 (Oct. 1988).

27. P. W. Smith and A. Ashkin, "Four-wave mixing in an artificial Kerr medium," Opt. Lett. **6**, 284-286 (1981); "Use of a liquid suspension of dielectric spheres as an artificial Kerr medium," Opt. Lett. **7**, 347-349 (1982).

28. See e.g.: R. Magnusson and T. K. Gaylord, "Diffraction efficiencies of thick phase gratings with arbitrary grating shape," J. Opt. Soc. Am. **86**, 806-809 (1978); H. Kogelnik, "Coupled wave theory for thick hologram gratings," Bell Syst. Tech. J. **48**, 2909-2974 (1969).

29. The Fourier expression is given by Eq. (11) on p 223 in Chapter 5 of Simpson's dissertation (Ref. T2) where due to an error of transcription the factor of two in the numerator should be omitted. This correction does not affect the plots in Chapter 4 nor the conclusions of the dissertation.

30. As described in Simpson's dissertation several comparisons analogous to Fig. 33 were carried out in which the initial volume fraction of particles was shifted slightly from the directly measured value to give an improved fit. This shift was not done in Fig. 33 and turns out to be unnecessary. The reason it was needed in the dissertation is traceable to a constant factor in the computed |R| caused by a computer error that had the effect of shifting the aperture factor v from the analytical value. As evident from Fig. 33 the conclusions are not changed when the correct computation is used as is shown here.

31. Figure 5.1 on page 225 of Simpson's dissertation shows the banding of an emulsion of oil in water in an ultrasonic field.

32. T. Sato, H. Katoaka, T. Nakayama, and Y. Yamakoshi, "Ultrasonic phase conjugator using microparticle suspended cell and its application," in *Acoustical Imaging* Vol. 19 (Plenum Press, N. Y., 1990).

33. P. L. Marston and D. S. Langley, "Glory- and rainbow-enhanced acoustic backscattering from fluid spheres: Models for diffracted axial focusing," J. Acoust. Soc. Am. **73**, 1464-1475 (1983).

34. C. K. Frederickson, "Wavefields Near Transverse Cusp Caustics Produced by Reflecting Ultrasonic Transients and Tone Bursts from Curved Surfaces," Ph.D. dissertation, Department of Physics, Washington State University (1991). Report N00014-85-C-0141-TR11; DTIC number A240641.

35. J. F. Nye, "Rainbows from ellipsoidal water drops," Proc. R. Soc. Lond. A **438**, 397-417 (1992).

36. P. L. Marston, renewal proposal for Contract N00014-85-C-0141 submitted in 1987.

37. J. R. Filler, "Response of the shear layer separating from a circular cylinder to small amplitude rotational oscillation," Ph.D. dissertation, Washington State University (1989).

38. O. M. Griffin and M. S. Hall, "Vortex shedding lock-on and flow control in bluff body wakes," J. Fluids Eng. **113**, 526-537 (1991).

FINAL TECHNICAL REPORT DISTRIBUTION, UNCLASSIFIED GRANT

Scientific Officer Code: 1112 — 3 copies
Logan E. Hargrove
Office of Naval Research
800 North Quincy Street
Arlington, Virginia 22217-5000

Administrative Grants Officer — 1 copy
Office of Naval Research
Resident Representative N63374
Administrative Contracting Officer
Univ. of Washington, Univ. District
Bldg., Rm 410, 1107 NE 45th Street
Seattle, WA 98105-4631

Director, Naval Research Laboratory — 1 copy
Attn: Code 2627
Washington, DC 20375

Defense Technical Information Center — 2 copies
Building 5, Cameron Station
Alexandria, Virginia 22314

Supplemental distribution to research participants — (1 copy each)

Dept. of Physics
Washington State University
Pullman, Washington 99164-2814

ATTN: D. H. Hughes
G. Kaduchak
T. J. Matula

L. G. Zhang
Dept. of Electrical Engineering and Computer Science
Washington State University
Pullman, Washington 99164-2752

H. J. Simpson
Naval Research Lab., Code 5136
Overlook Ave.
Washington, DC 20375

N. H. Sun
EXP Group Inc.
44063 Fremont Blvd.
Fremont, CA 94538-6045

J. R. Filler
Dept. of Civil Engineering
University of Idaho
Moscow, Idaho 83843

S. P. Parry
Nuclear Physics Lab., Box 446
University of Colorado
Boulder, Colorado 80309-0446

Additional Supplemental Distribution as per direction of Office of Naval Research will be listed separately.